The Abdus Salam
International Centre for Theoretical Physics

United Nations
Educational, Scientific and
Cultural Organization

IAEA
International Atomic Energy Agency

1956-10

Targeted Training Activity: Seasonal Predictability in Tropical Regions to be followed by Workshop on Multi-scale Predictions of the Asian and African Summer Monsoon

4 - 15 August 2008

Predictability and Extended Range Prediction of Indian Summer Monsoon ISOs

Goswami B.N.

Indian Institute of Tropical Meteorology
Ministry of Science & Technology. Government of India
Dr.Homi Bhabha Road, Ncl Post Office, Pashan, 411 008 Pune
INDIA

Predictability and Extended Range Prediction of Indian Summer Monsoon ISOs

B. N. Goswami

Indian Institute of Tropical Meteorology (IITM)

Outline

- Space-time characteristics of Monsoon ISOs
- Monsoon ISOs : Building Block of Monsoon Systems
- Predictability of Monsoon ISOs
- Extended range prediction Monsoon ISOs : Recent Developments

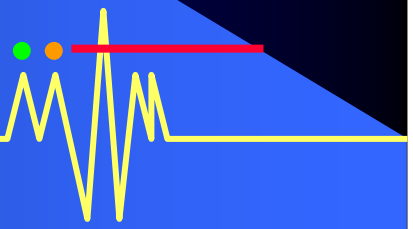

Long term mean

JJA precipitation and

DJF precipitation

Monsoon ?

Wet- summer

Dry - winter

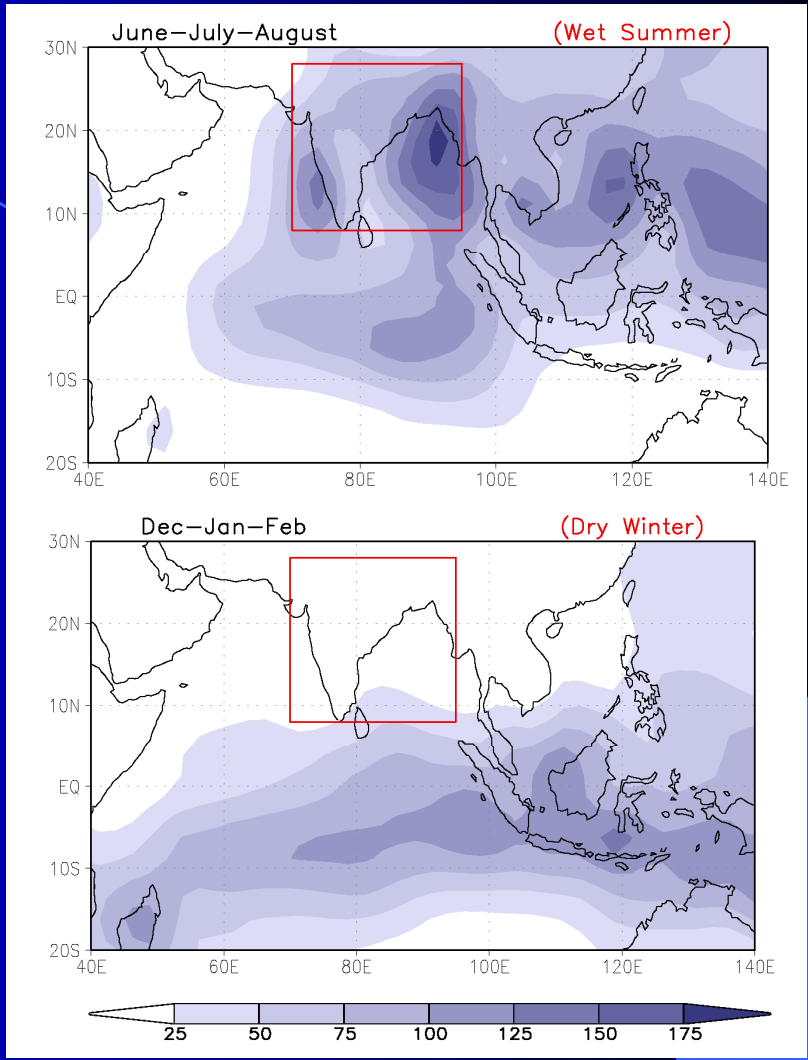

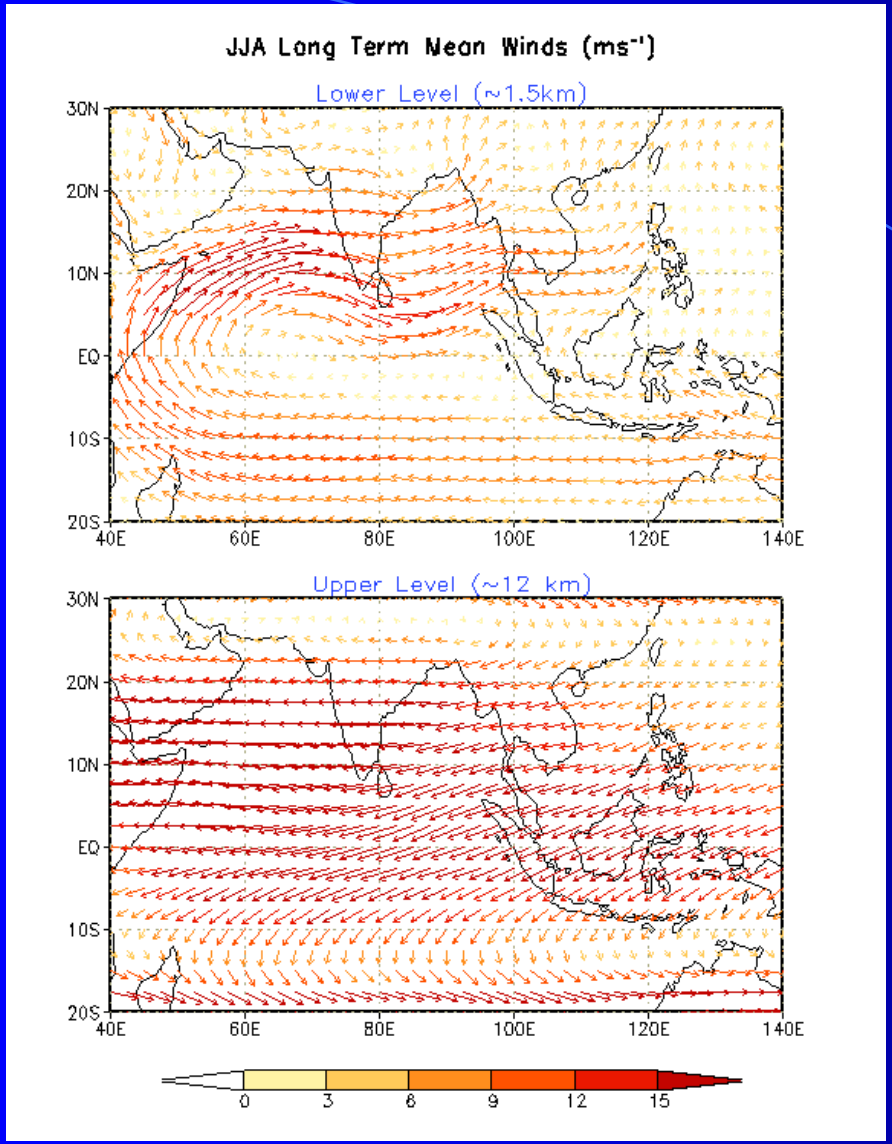

Characteristic features of summer monsoon circulation

Low level, cross-equatorial flow, south-westerlies, westerly jet in Arabian sea

Deep Baroclinic vertical structure

Upper level easterlies, Monsoon Easterly Jet

All India Rainfall

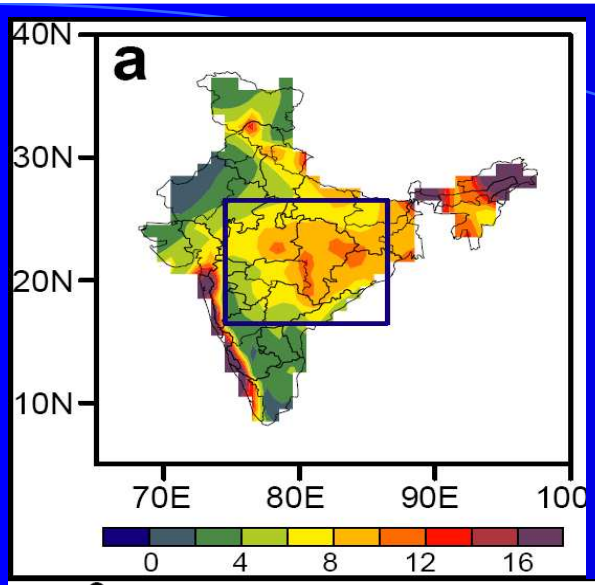

JJAS Mean

AIR Mean : 86 cm

AIR S.D. : 8.6 cm

Interannual Variability

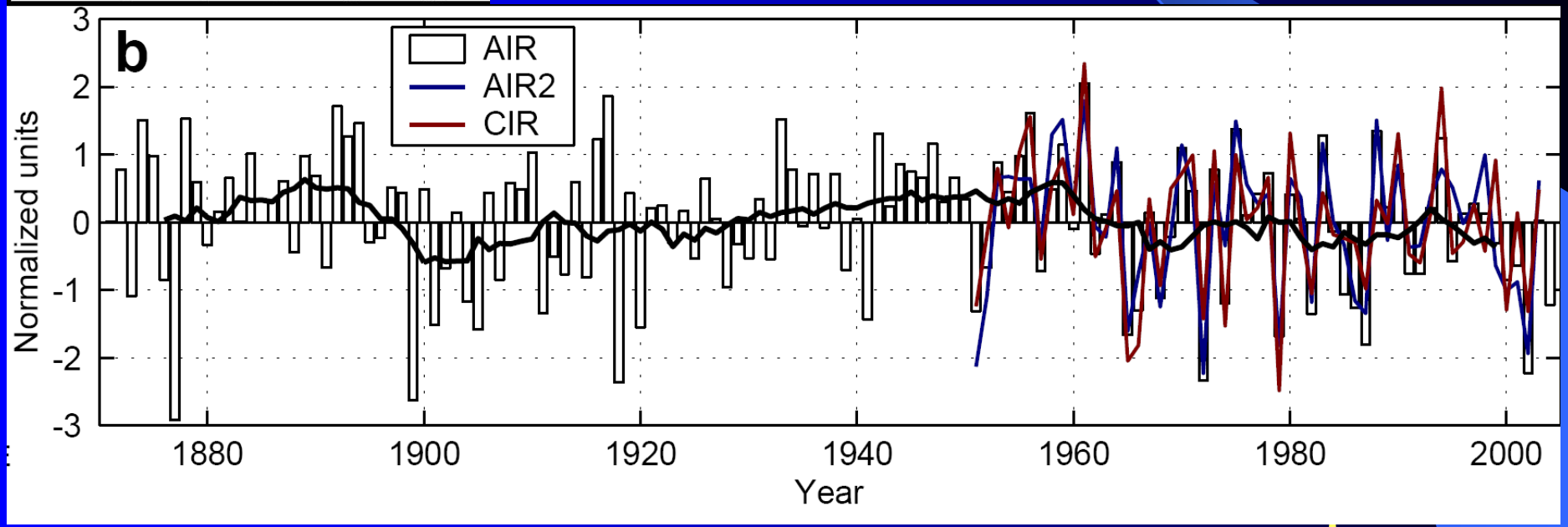

Active-break spells (cycles)

Daily rainfall (mm/day) over central India for three years, 1972, 1986 and 1988

The smooth curve shows long term mean.

Red shows above normal or wet spells while blue shows below normal or dry spells

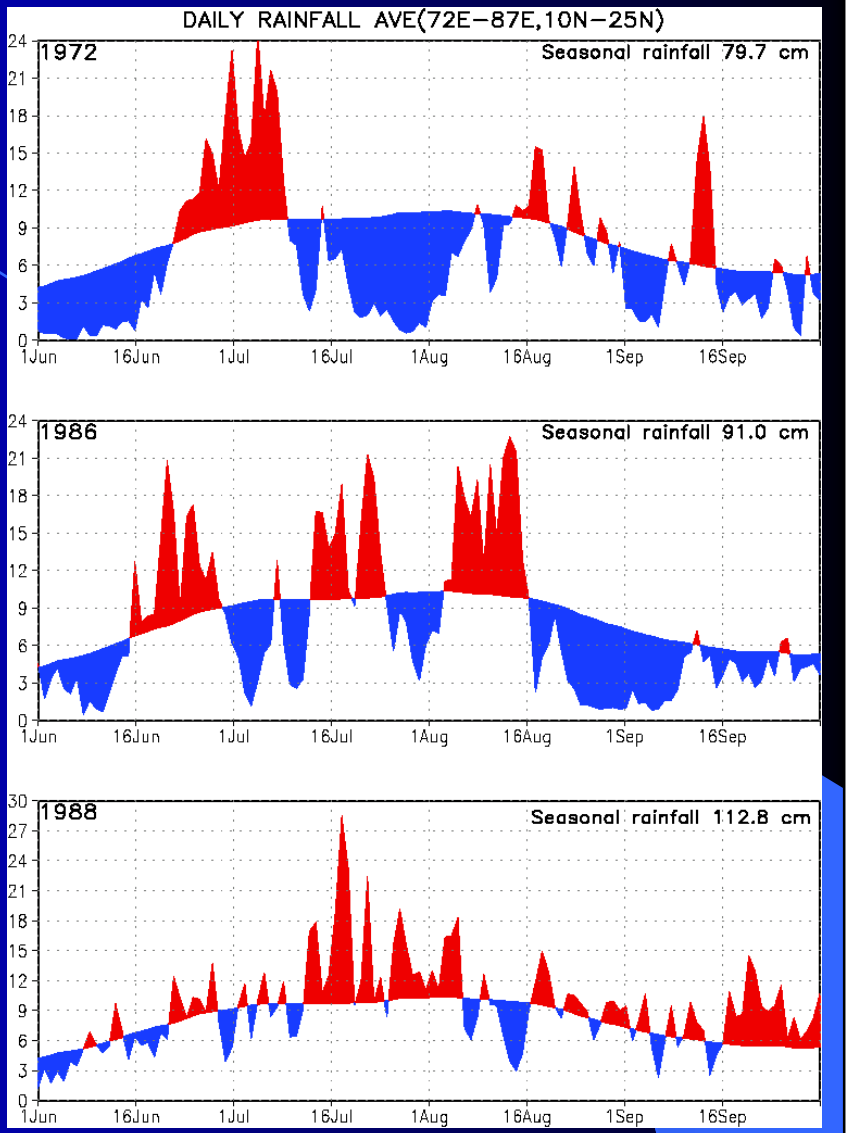

Monsoon Intraseasonal Oscillations

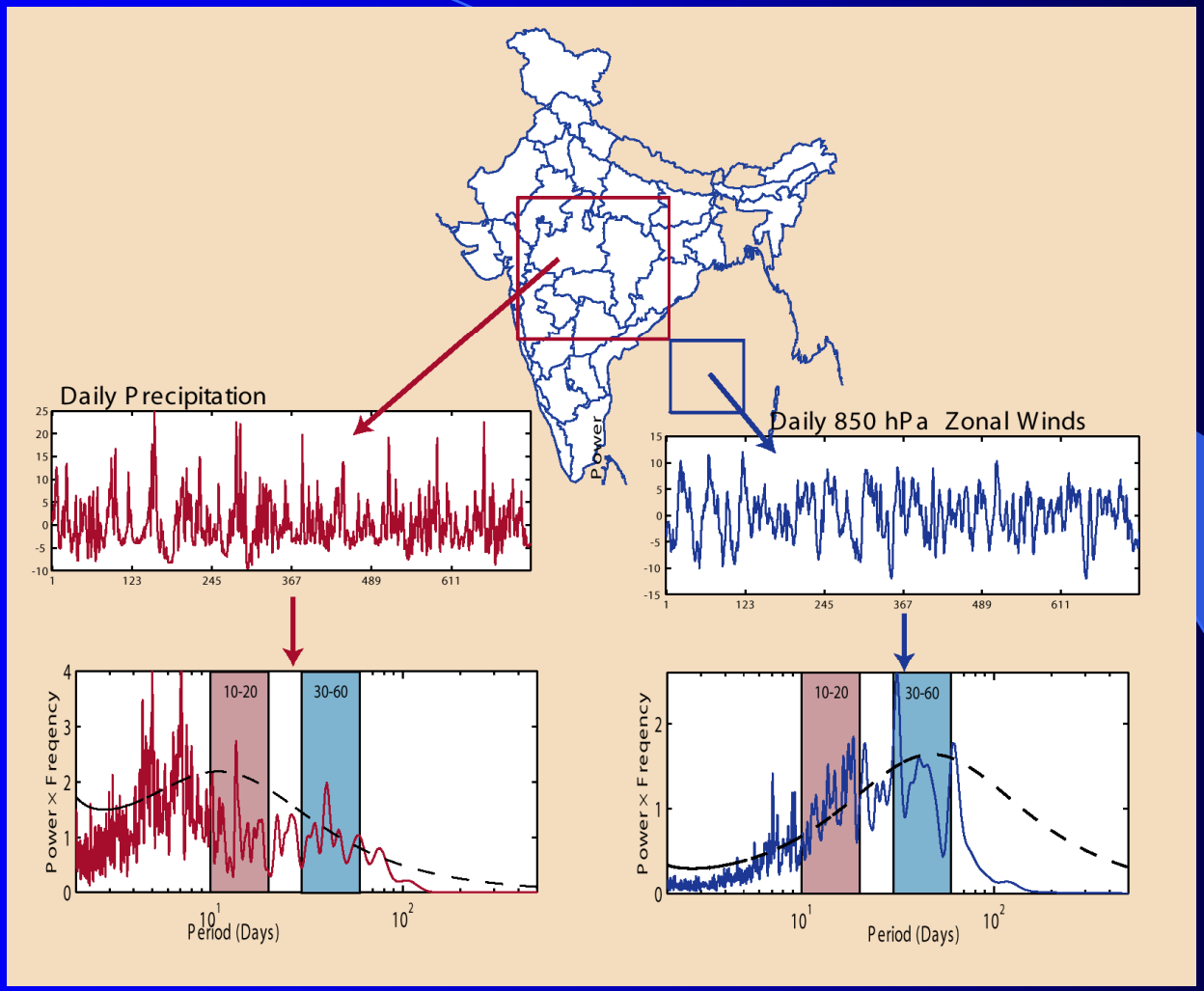

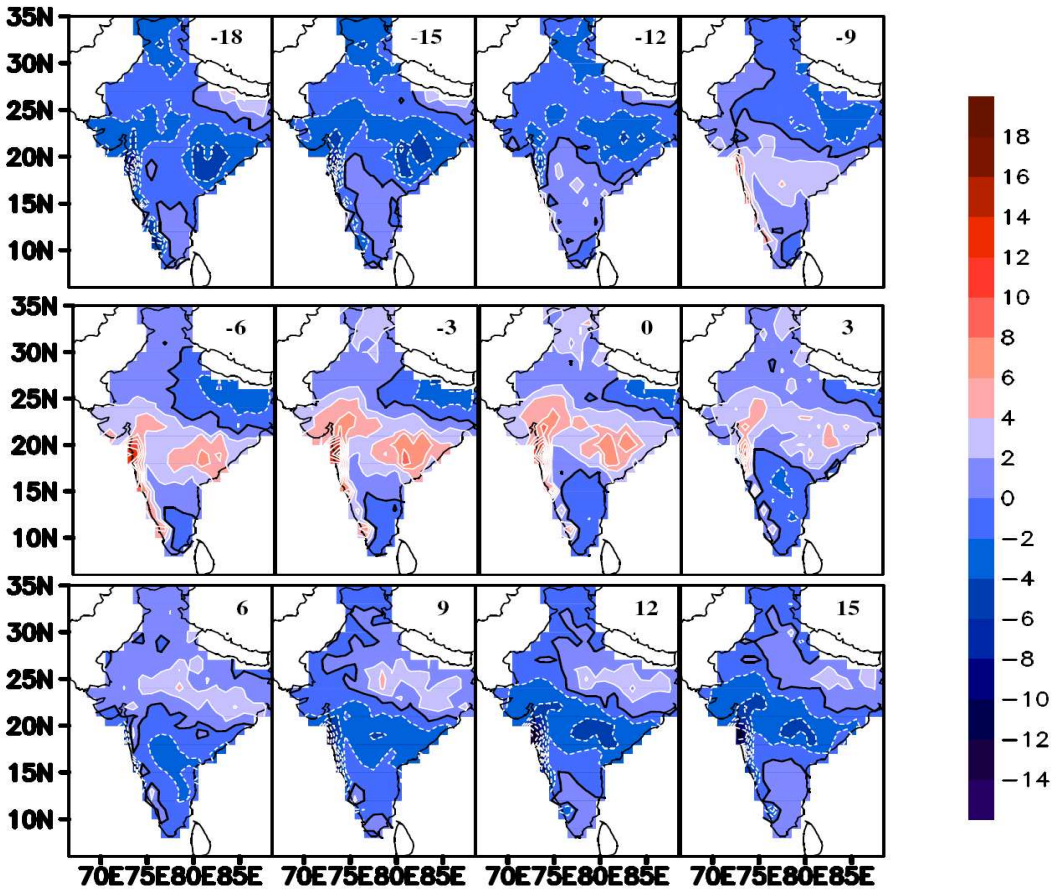

S3. (a) Lagged phase composites of 20-70 day filtered rainfall anomalies (mm/day) between May - October with respect to active phase of monsoon ISO identified from a reference series averaged over central India (72°E- 85°E, 15°N - 25°N). Composites from 18 day lag to 15 day lead are shown for the pre75 period. Lag or lead day is indicated at the top right corner of each panel.

Relationship between Monsoon ISOs and monsoon onset

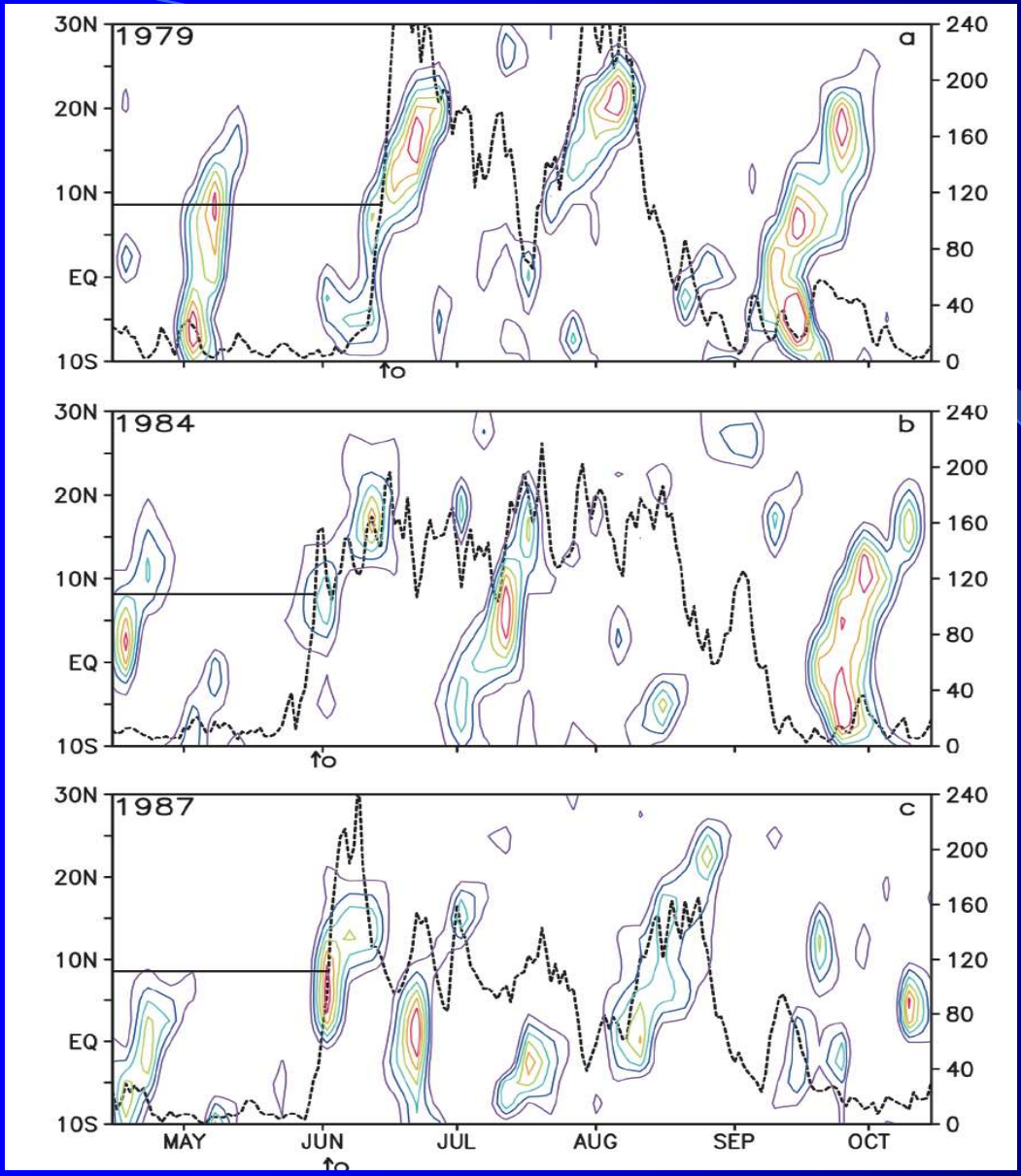

Onset

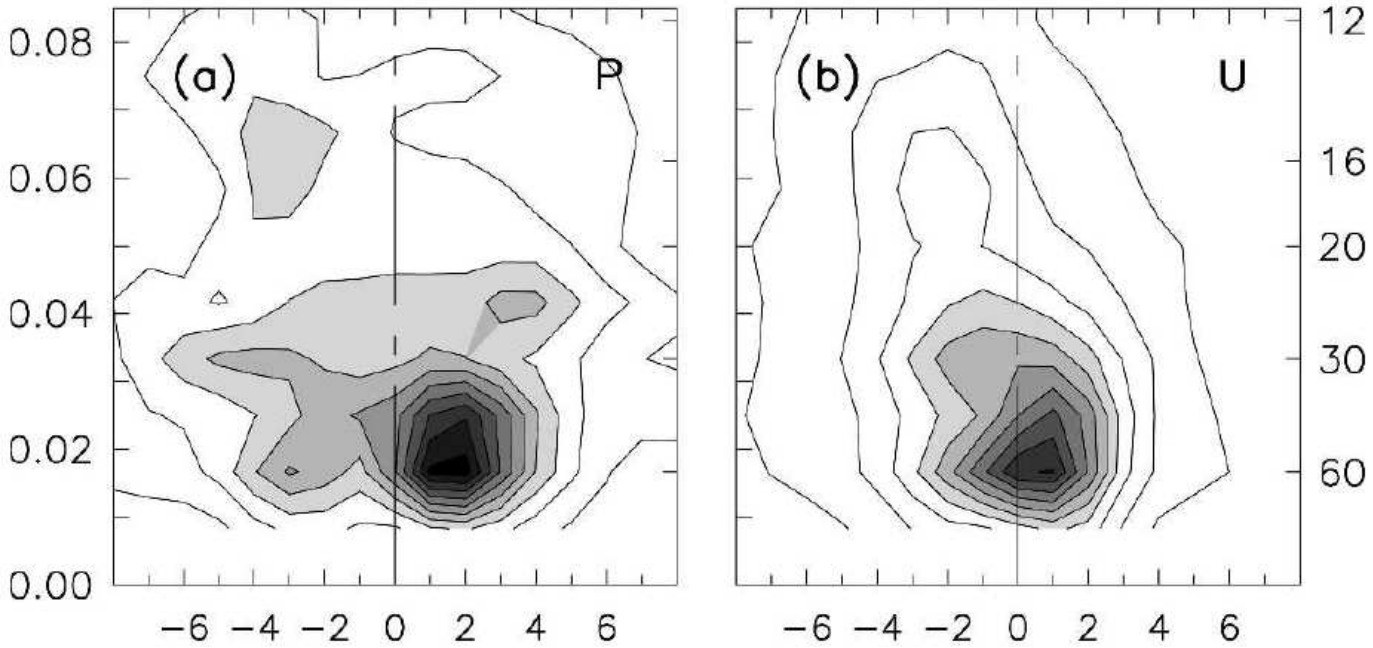

FIG. 2. Wavenumber–frequency spectral power of observed precipitation and 850-hPa zonal winds anomalies averaged over the latitude band 5°–25°N. The *y* axis left ordinate is frequency (in cycles per day, cpd) and right ordinate is period (days), while the *x* axis represents zonal wavenumber. The minimum contour and contour interval is 0.5; contours greater than 2.0 are shaded.

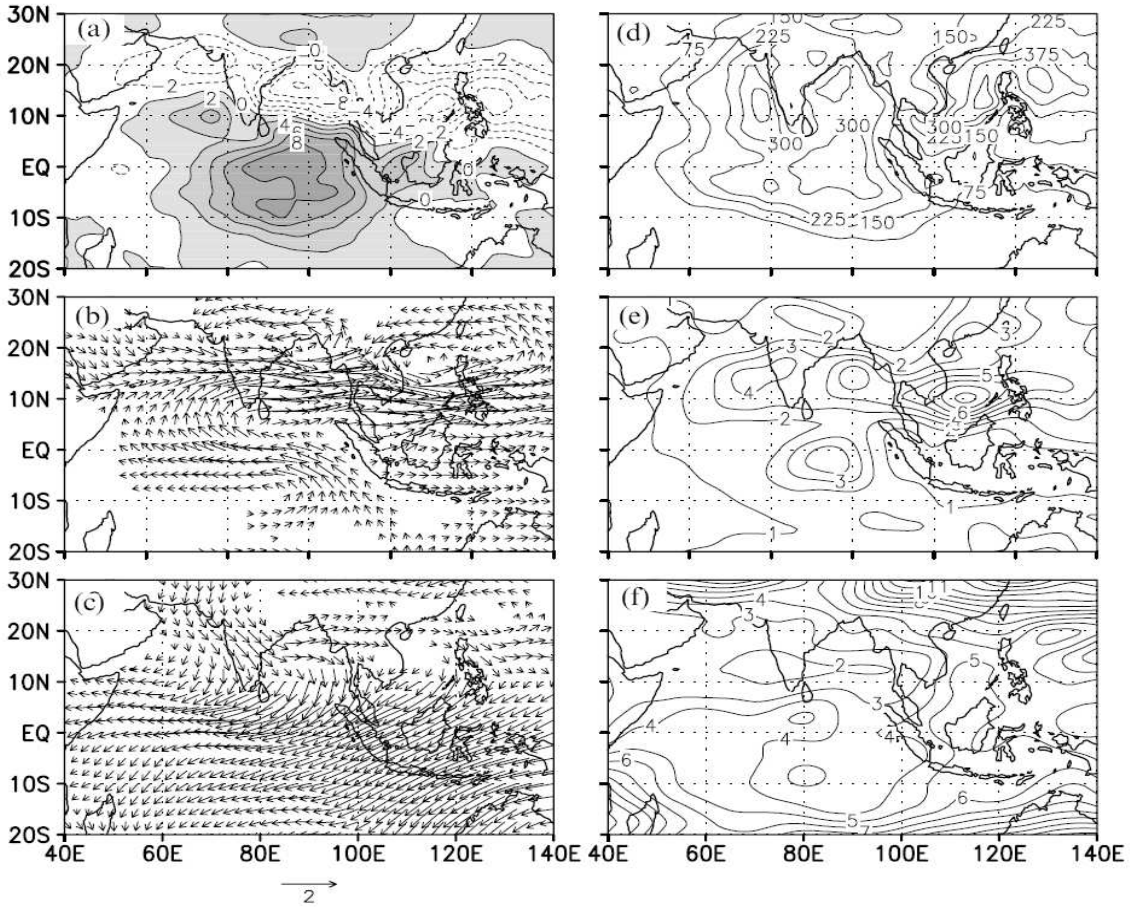

Figure 2.10. Spatial structure and amplitude of the 30–60-day mode. Regressed 30–60-day filtered anomalies of (a) OLR (in $W m^{-2}$), (b) 850-hPa winds, and (c) 200-hPa winds (in $m s^{-1}$) with respect to a reference time series of 30–60-day filtered zonal winds averaged over 85°E–90°E and 5°N–10°N with 0 lag. Only regressed wind anomalies significant at 95% confidence level are plotted, with a mean variance of 30–60-day filtered (d) OLR (in $W^2 m^{-4}$), (e) 850-hPa, and (f) 200-hPa zonal winds (in $m^2 s^{-2}$), based on 20 (1979–1998) summers (1 June–30 September).

What makes the TCZ oscillate with 30-60 day periodicity?

Goswami and Shukla (1984, JAS) proposed a convective-radiative-dynamical feedback to explain this temporal scale selection

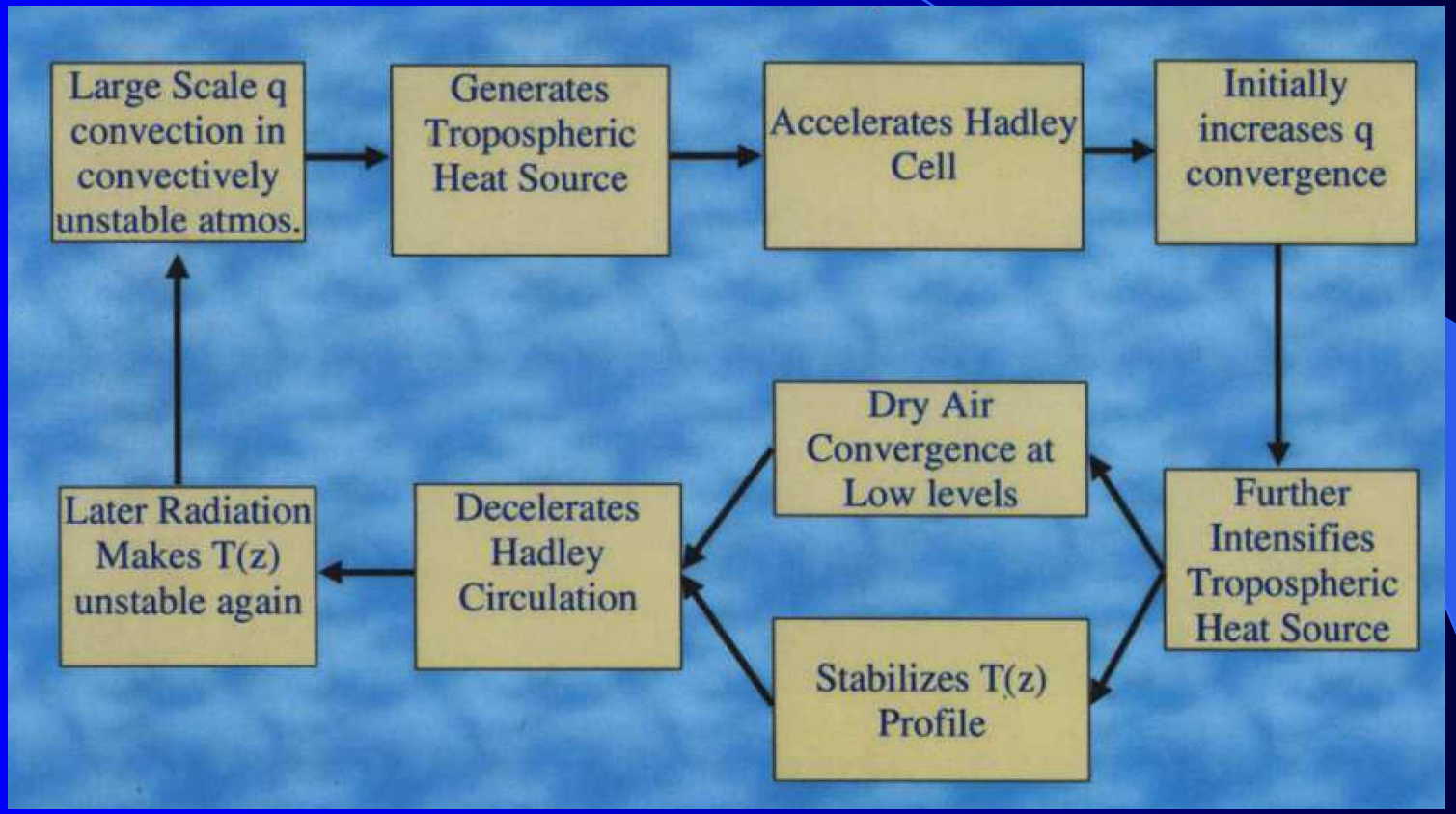

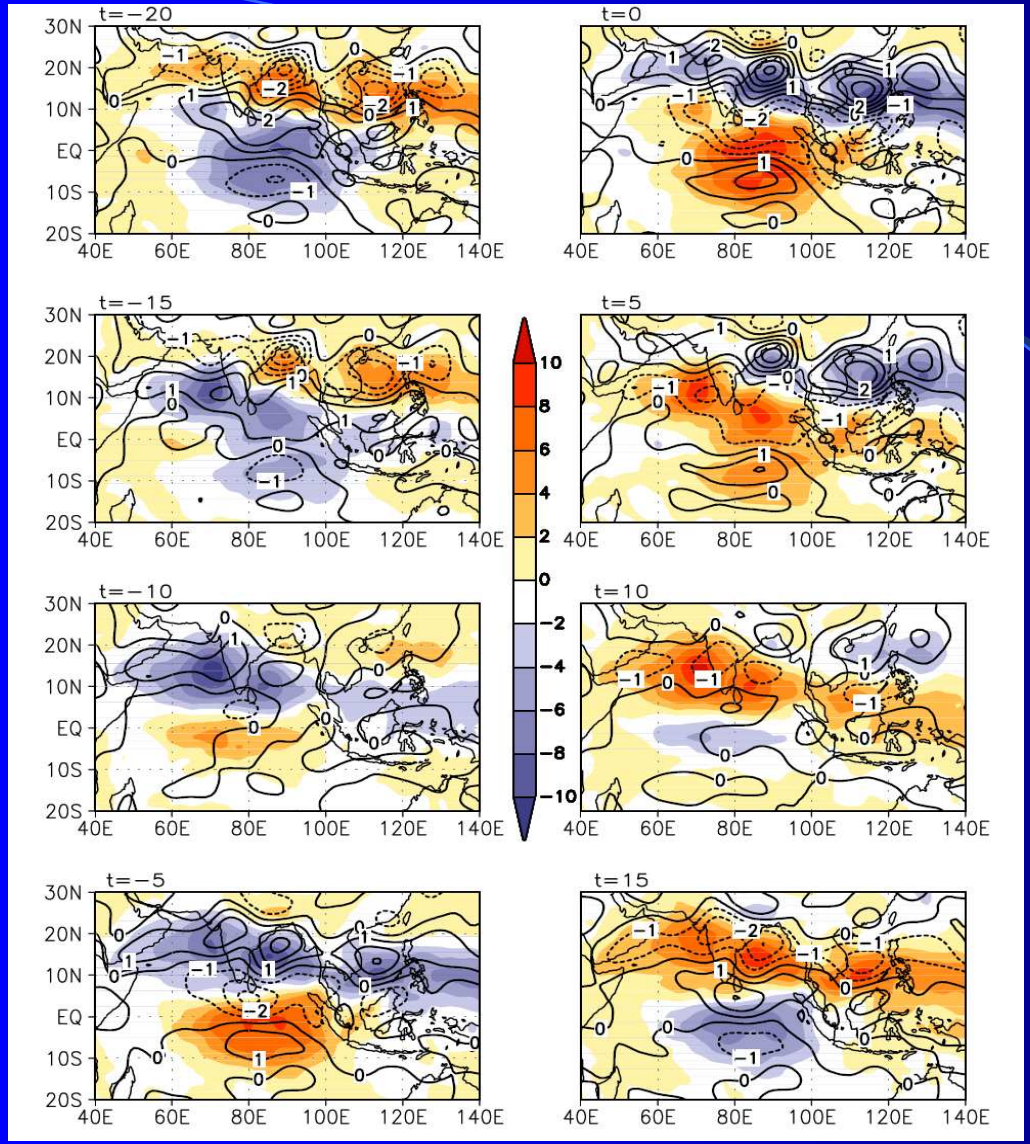

What is responsible for the northward propagation?

Regressed OLR (shaded) and 850 hPa relative vorticity (contour) w.r.t a reference time series of 10-90 day filtered OLR

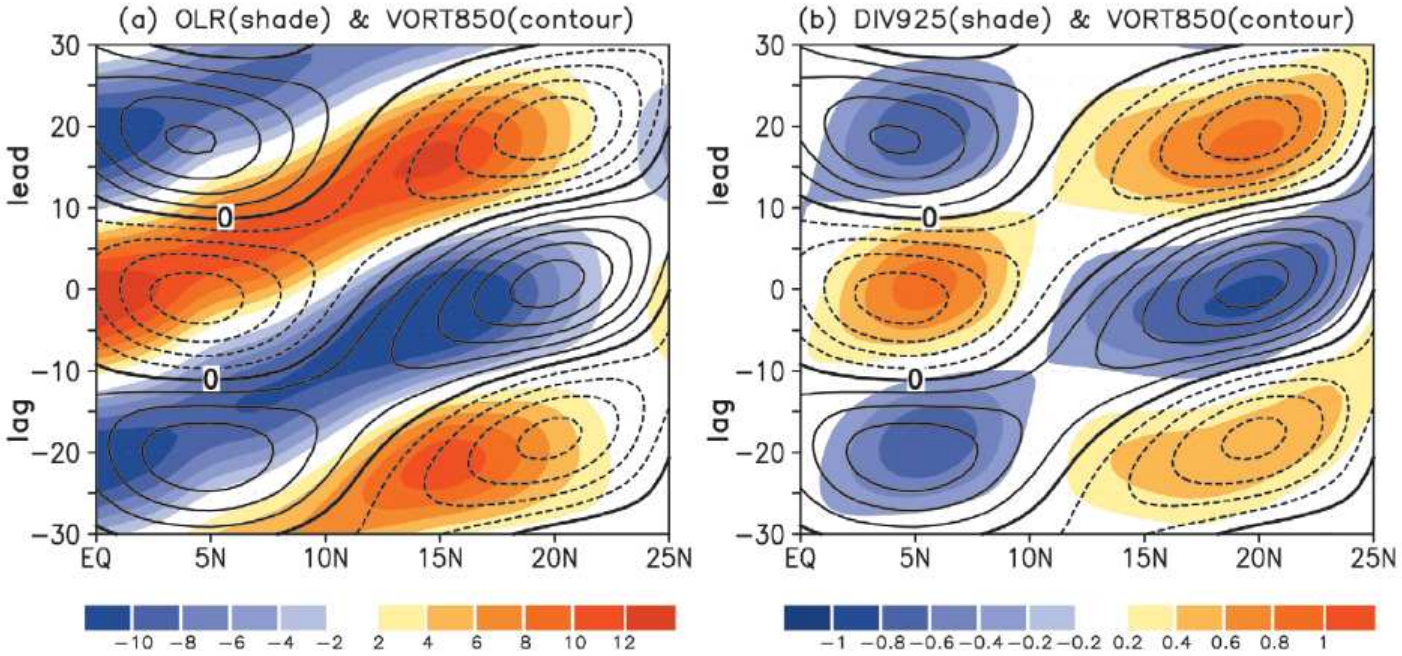

Figure 2.15. (a) Regressed 30–60-day filtered anomalies of OLR (shaded; $W\,m^{-2}$) and 850-hPa relative vorticity (contour, positive solid and negative dashed, contour interval $1 \times 10^{-6}\,s^{-1}$) with respect to the reference time series described in Figure 2.10 averaged over 80°E–90°E. (b) Regressed 30–60-day filtered anomalies of 850-hPa relative vorticity (contour, positive solid and negative dashed, contour interval $1 \times 10^{-6}\,s^{-1}$) and divergence at 925 hPa (shaded; $10^{-6}\,s^{-1}$) with respect to the same reference time series.

What is responsible for making the low level moisture convergence north of the heat source?

Jiang , Wang and Li (2004, J. Climate, 17, 1022-1039)

- They show that response of a heat source in the presence easterly mean flow leads to cyclonic barotropic vorticity centered slightly to the north of the heat source.
- It drives frictional convergence in the boundary layer north of the heat source.
- Near the equator, positive meridional gradient of low level mean humidity leads to anomalous moisture convergence north of the heat source.

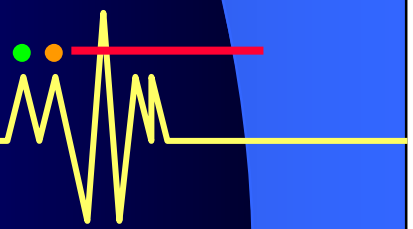

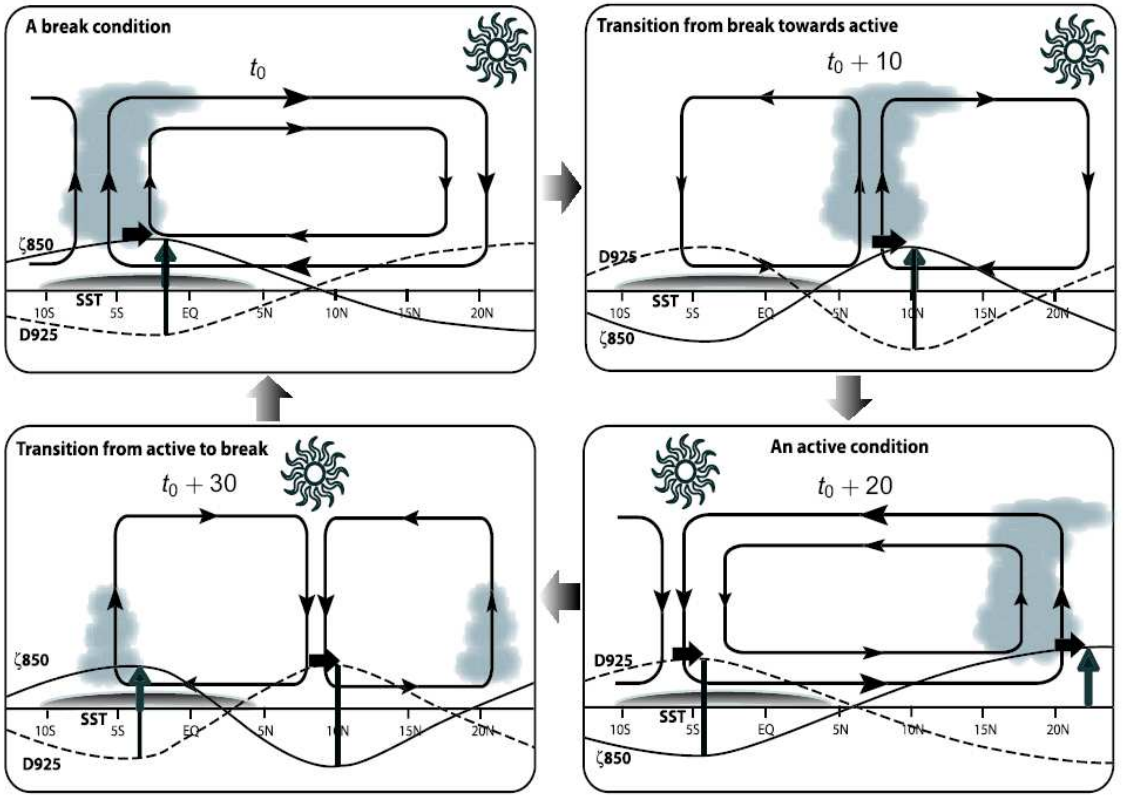

Figure 2.16. A schematic representation of the evolution and northward propagation of the meridional circulation associated with the 30–60-day mode in the meridional plane. The thin arrows indicate the anomalous Hadley circulation. The thick vertical arrow indicates the location of the center of the boundary layer moisture convergence, while the thick horizontal arrow indicates the direction of poleward motion of the cloud band. The thin solid (dotted) line indicates the phase of the relative vorticity at 850 hPa (divergence at 925 hPa) with positive (negative) phase being above (below) the base line. The location of clear sky conditions is shown by the sun-like symbol.

Climatological mean JJAS P and 850 hPa winds

P and 850 hPa wind anoms during 'Active' phase

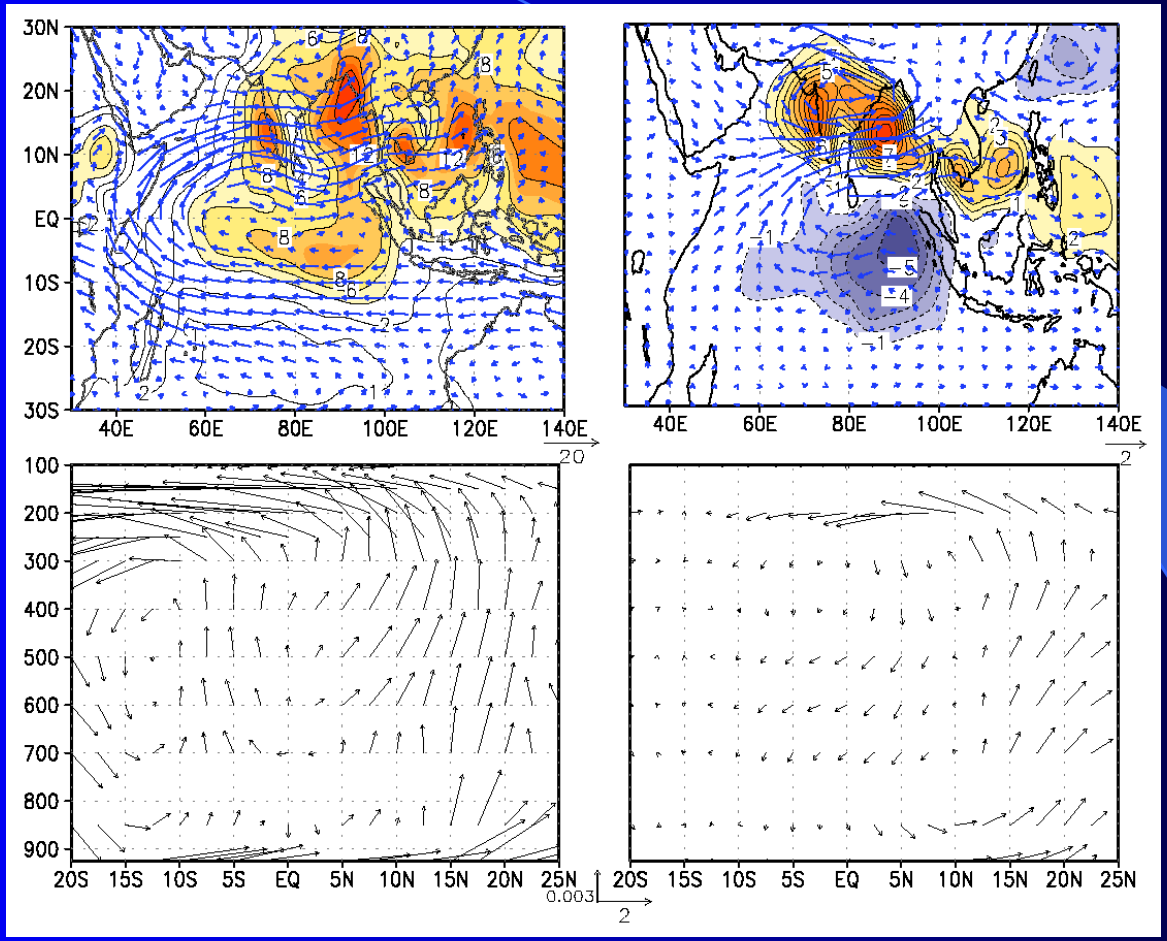

Mean monsoon Hadley circul.

70E-90E

Anom. Hadley circul. In an 'active' phase,

70E-90E

A common mode : Intraseasonal & interannual variability

Structure of dominant ISO mode

Active-Break composite of precipitation from NCEP

From 10-90 day filtered precip. Between 1 June-30 Sept., 1949-2002

Structure of dominant ISV mode

Strong-weak monsoon composite of precipitation from NCEP

From JJAS precip. Between 1949 and 2002, 6 strong and 4 weak monsoon years.

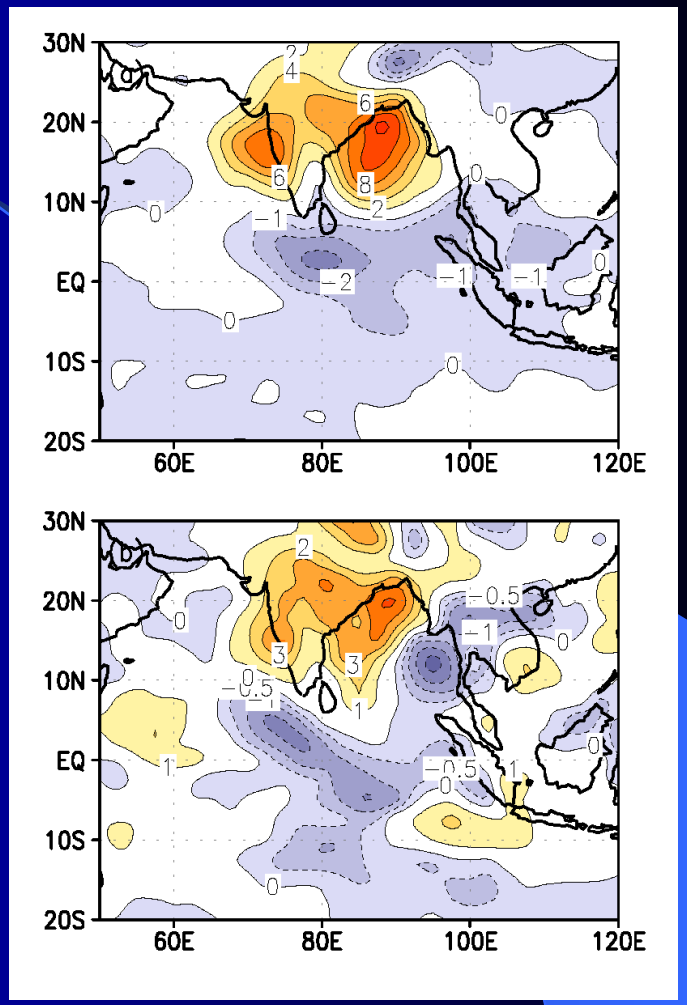

How does the ISOs influence the seasonal mean and IAV ?

- We have shown that the spatial structure of the summer ISOs have certain similarity with that of the summer seasonal mean. A common spatial mode of sub-seasonal and interannual variability.

- Seasonal mean of ISO anomaly can influence seasonal mean if frequency of occurrence of active and break phases are different.

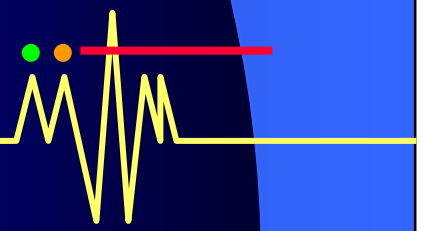

Frequency distribution of ISO anomalies of P over 70E-90E, 10N-30N

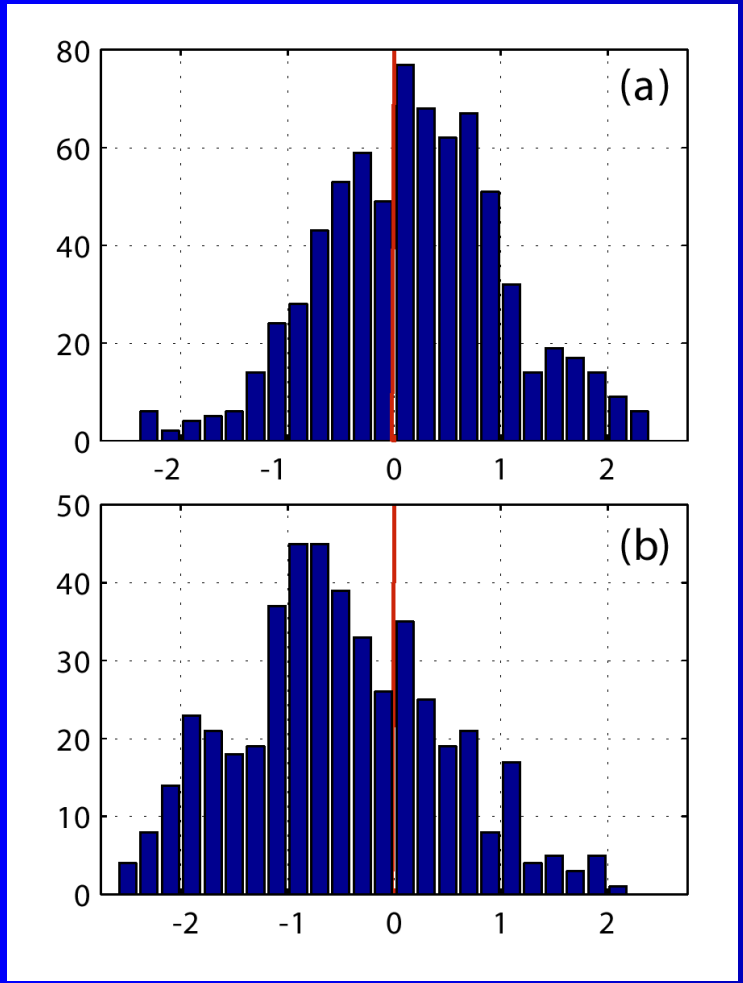

For 6 ‘strong’ Indian monsoon years

For 4 ‘weak’ Indian monsoon years

Goswami ,Wu and Yasunari, 2006, J. Climate

Seasonal mean of ISO anom. Vs interannual anomaly of seasonal mean

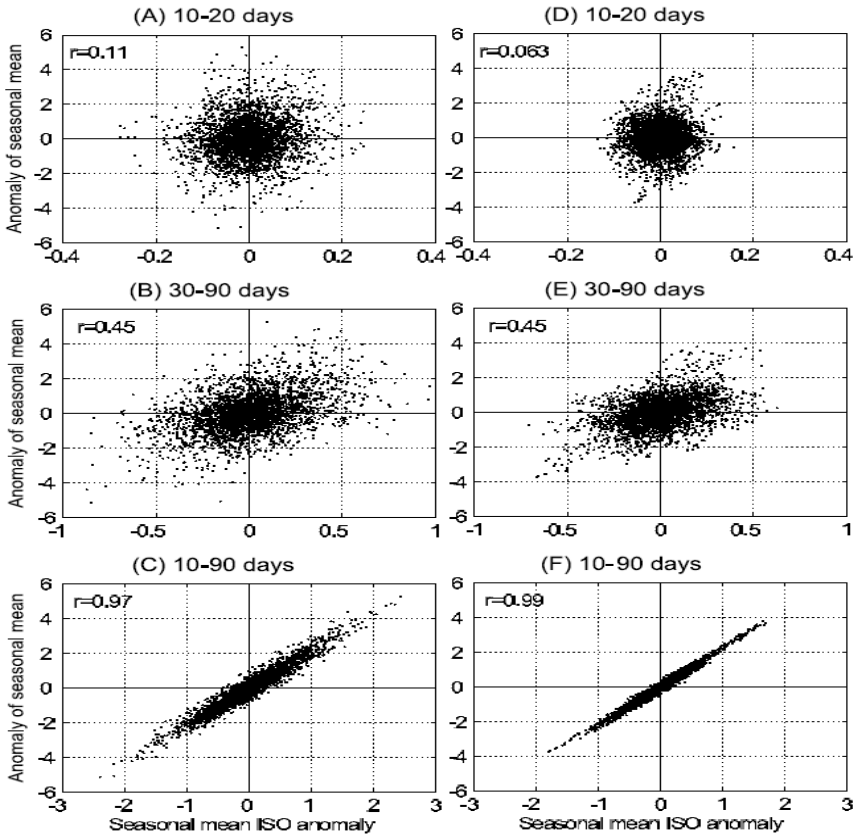

Figure 13. Scatter plot of interannual anomalies of seasonal mean versus seasonal mean of intraseasonal anomalies of precipitation (mm day^{-1}) from (a) 10–20 days band, (b) from 30–90 days band and (c) from 10–90 days band at all grid points in the domain 70°–100°E, 10°–30°N. (d, e, f) Similar to Figures 13a, 13b, and 13c, but for U850. Correlation values are given in the respective panels.

Goswami and Xavier, 2005, JGR

ISOs Modulate Monsoon Synoptic Activity

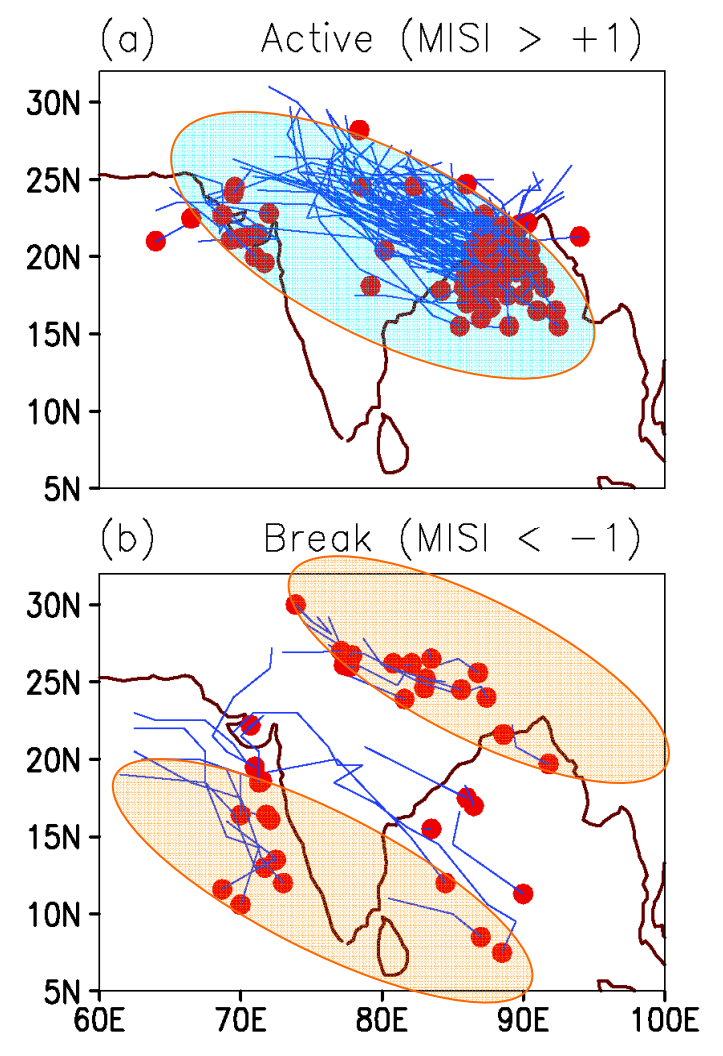

Tracks of LPS for the period 1954-1983 during extreme phases of monsoon ISO. (a) 'Active' ISO phase (MISI > +1) and (b) 'Break' ISO phase (MISI < -1). Red dots represent the genesis point and their lines show the tracks.

Goswami et al. 2003, *GRL*, 30, doi:10.1029/2002GL016734

Summer composite

850 hPa 10-20 day filtered winds and OLR for two opposite phases (a,b) of the QBM . (c) Relative vorticity (x 1.0e+6) averaged between 5S-5N as a function 15 phases

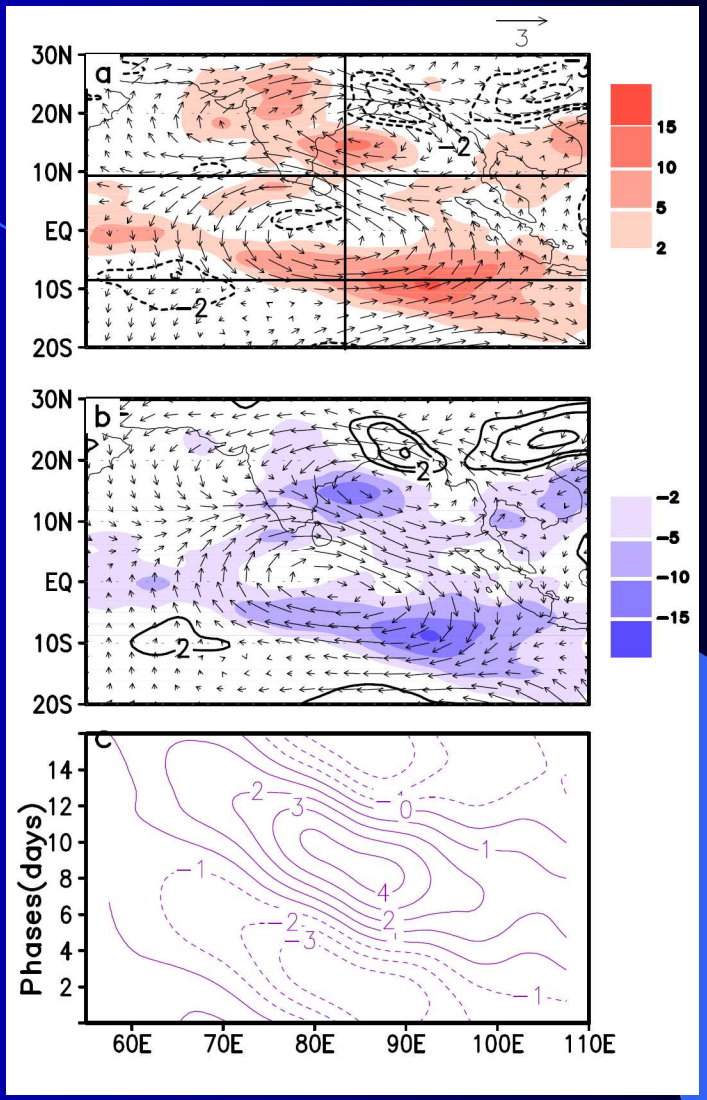

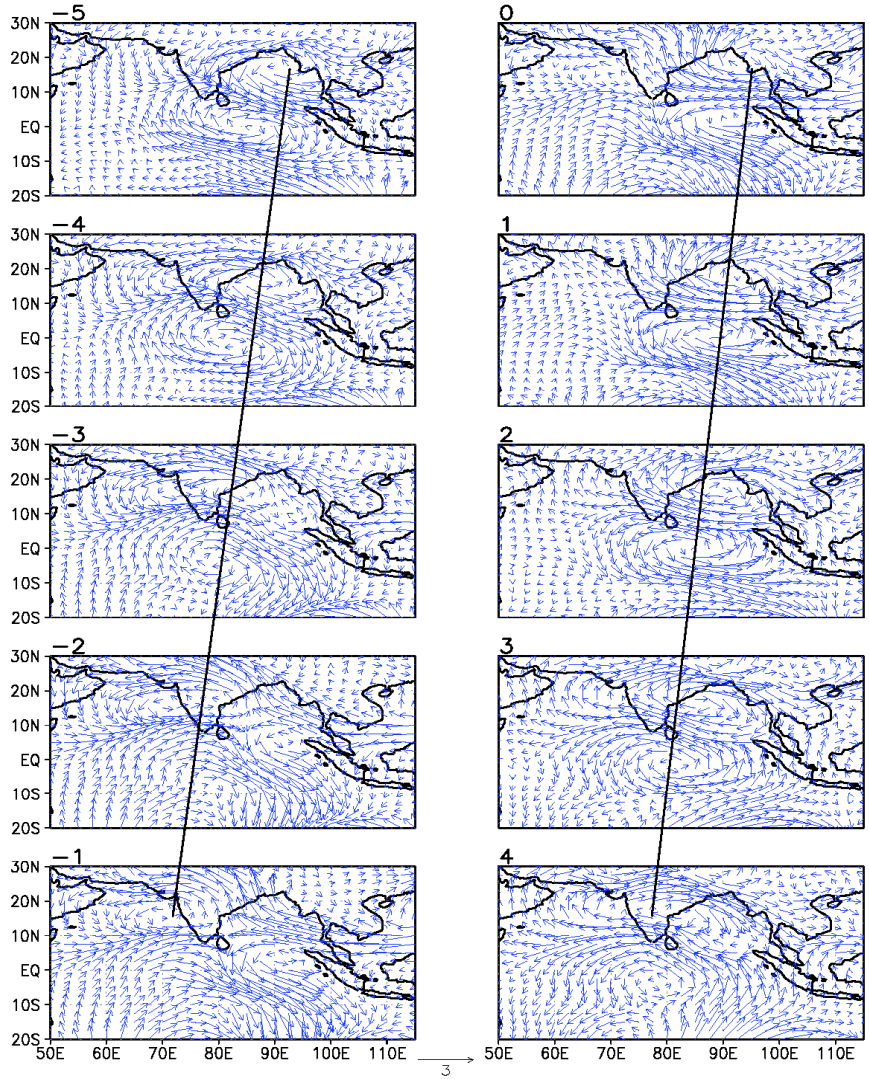

Figure 5: Composites of different phases showing generation and westward movement of vortices. The scale for wind vectors is same for all levels and shown at the bottom.

Composite structure for different phases.

Westward phase propagation of the two vortices is evident

Winter composite

850 hPa 10-20 day filtered winds and OLR for two opposite phases (a,b) of the QBM . (c) Relative vorticity (x 1.0e+6) averaged between 5S-5N as a function 15 phases

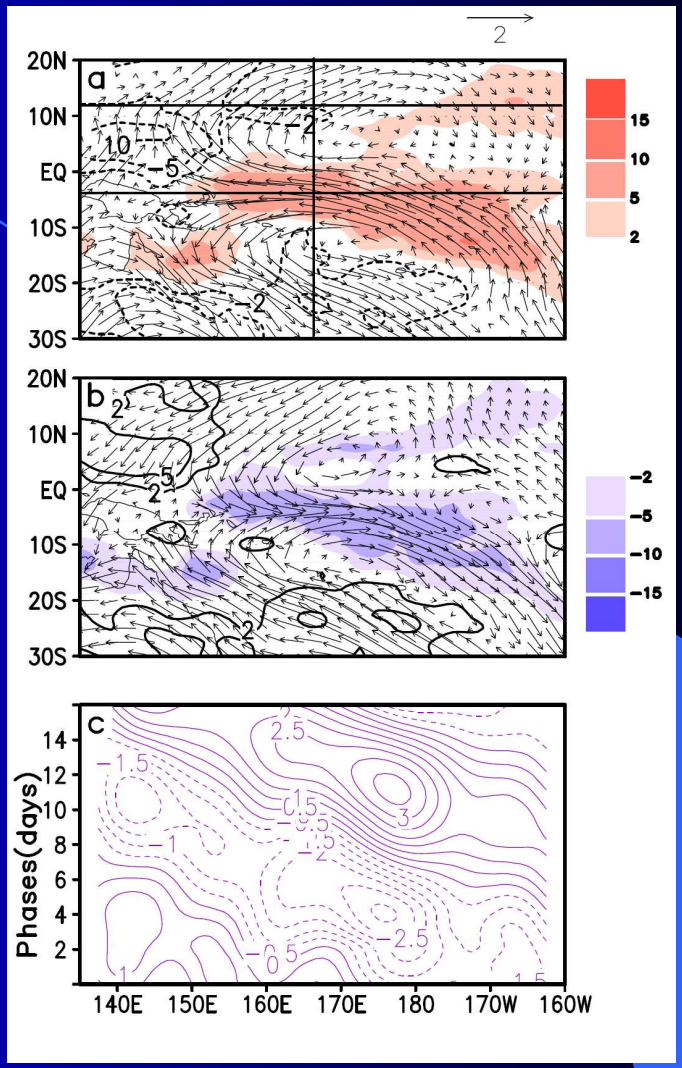

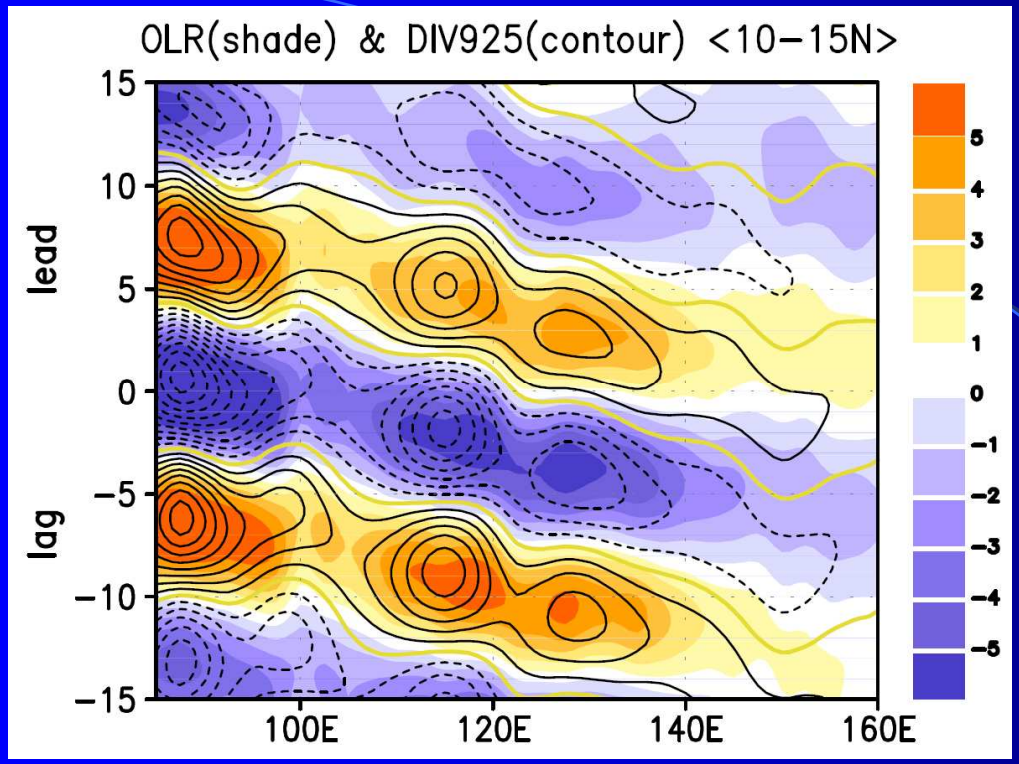

Lag-longitude plot of Regression of 10-20 day filtered OLR and 925 hPa div. on the QBM index averaged between 10N-15N.

Div. Maximum (minimum) at 925 hPa (BL) is west of the OLR maximum (minimum).

➔BL moisture convergence makes convection move westward

➔Convective coupling

Chatterjee and Goswami, 2004, QJRMS

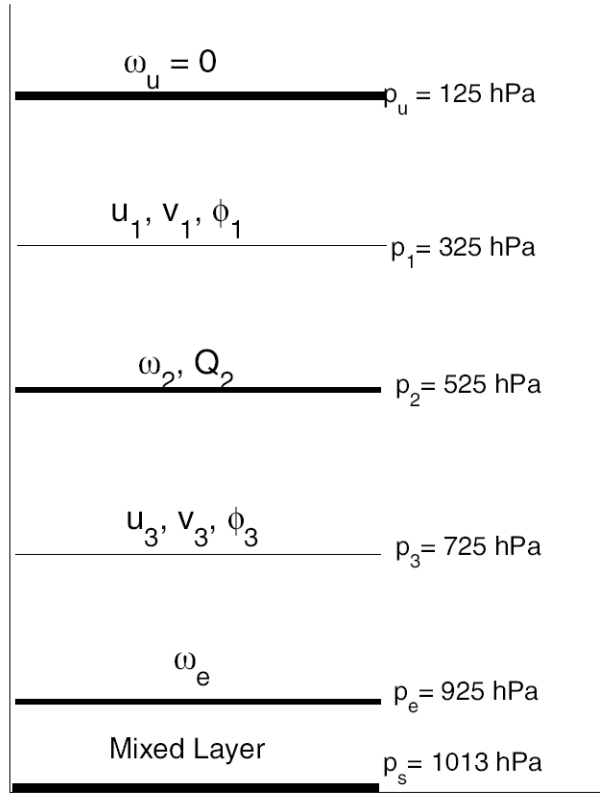

Figure 6. The vertical structure of the model.

Momentum eqns.at levels 1 and 3 while the thermodynamic energy eqn.at level 2.

Define barotropic and baroclinic components as

$$\chi_c = (\chi_3 - \chi_1)/2 \text{ and } \chi_t = (\chi_3 + \chi_1)/2,$$

Where χ represents zonal and meridional winds u and v or geopotential Φ, $\bar{U}$ represents mean background flow.

Results: The control case; No mean flow, No EWF

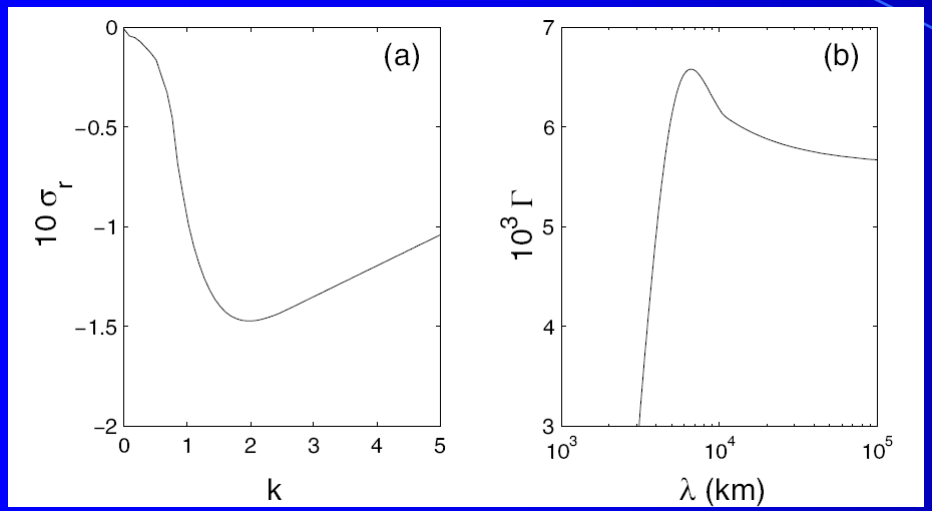

(a) Wavenumber vs real freq.

(b) Growth rate Γ vs wave length

Max Growth for k=1.33, or λ=6750 km. Period=16 days, Cp= 4.8 m/s

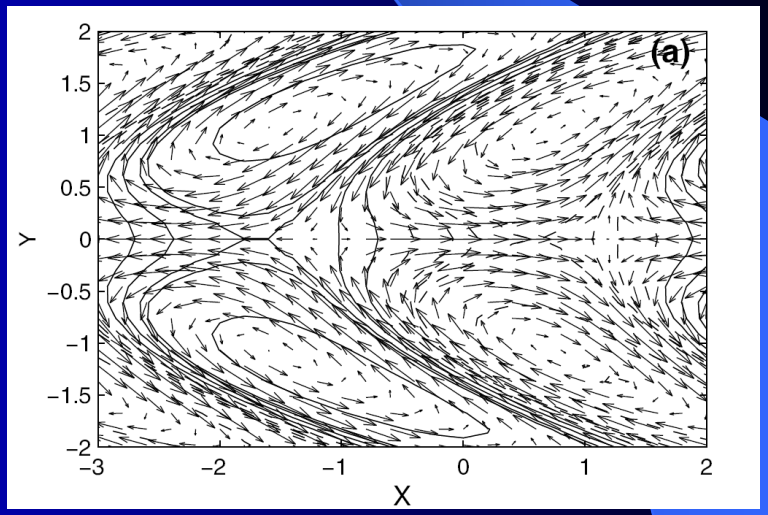

Structure of the most unstable , n = 1 Rossby mode

Vortices symmetric about the equator

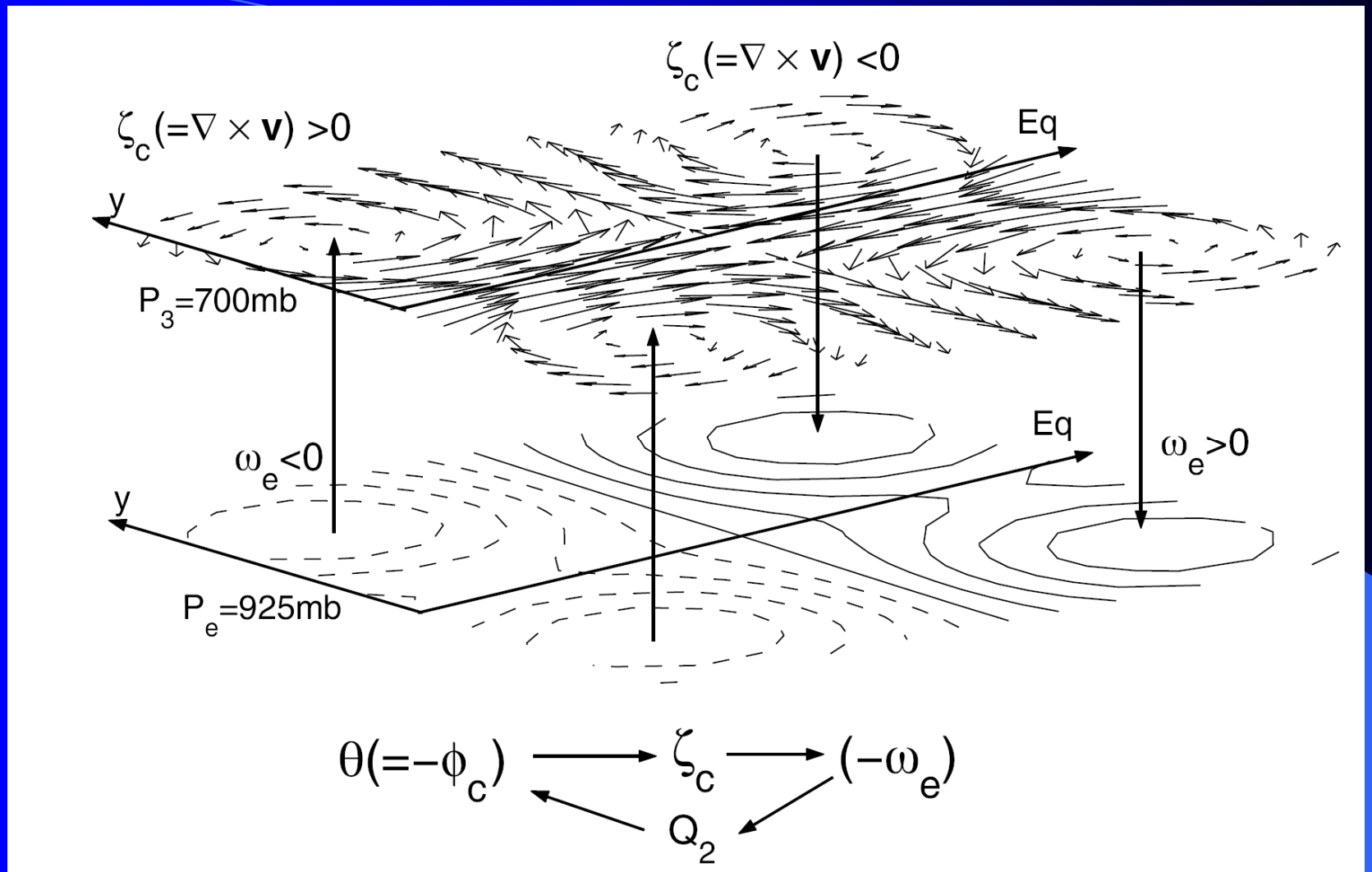

Schematic illustrating the Wave-Boundary-Layer-CISK for the unstable mode

Role of the mean background flow on the unstable mode:

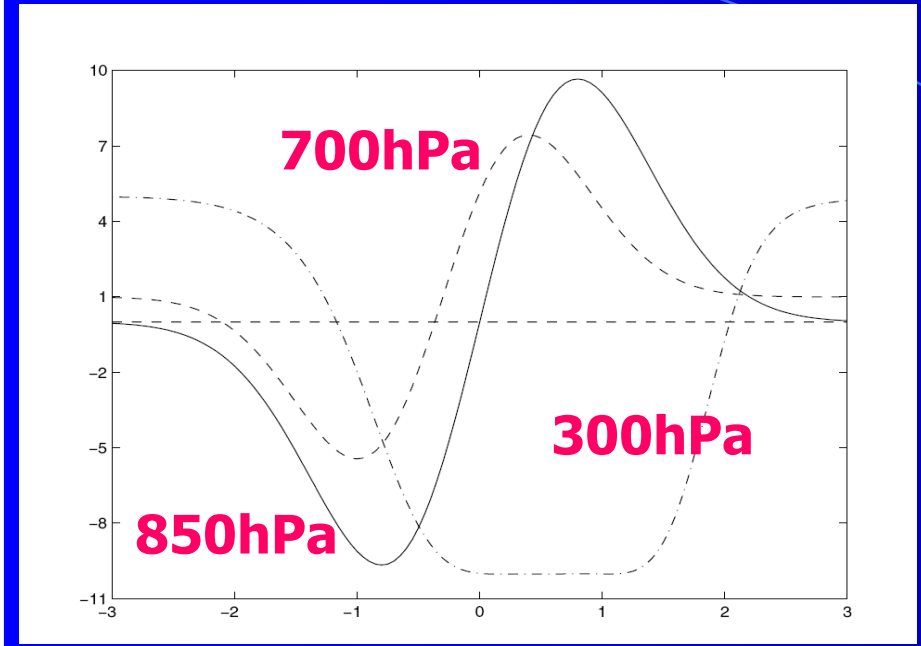

T=17 days, λ = 6020 km

Cp = 4.1 m/s

Spatial structure of the unstable mode with mean flow.

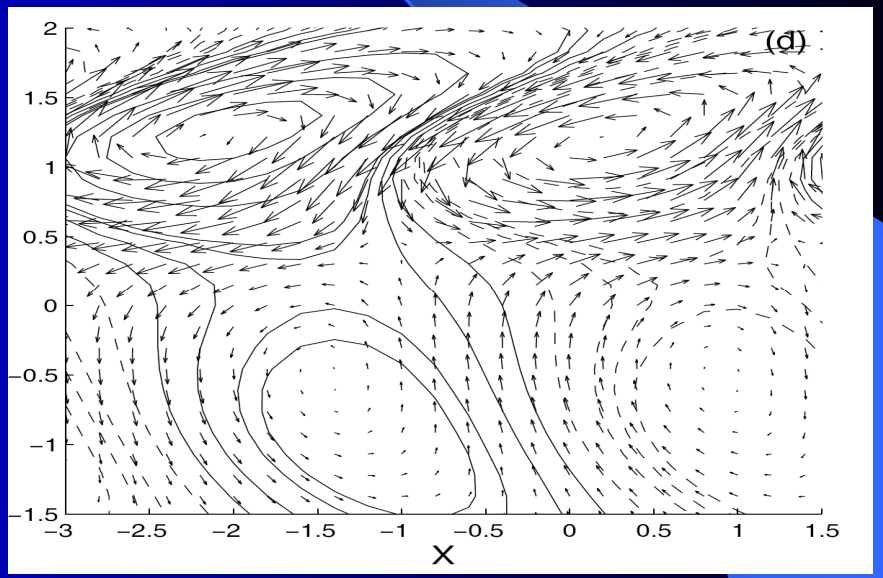

Climatological zonal winds for July averaged between 40E-120E

Vertical shear of mean winds:

Not essential for the basic instability. When included makes the structure more realistic.

Evaporation wind feedback:

Again not essential for the basic instability. When included enhances the growth rate of the unstable mode without changing the period and phase speed substantially.

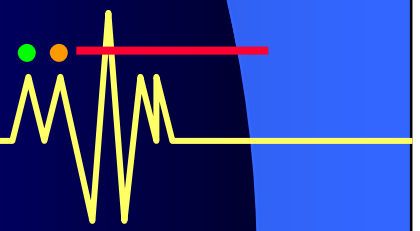

Importance of QBM in Tropical Intraseasonal Variability

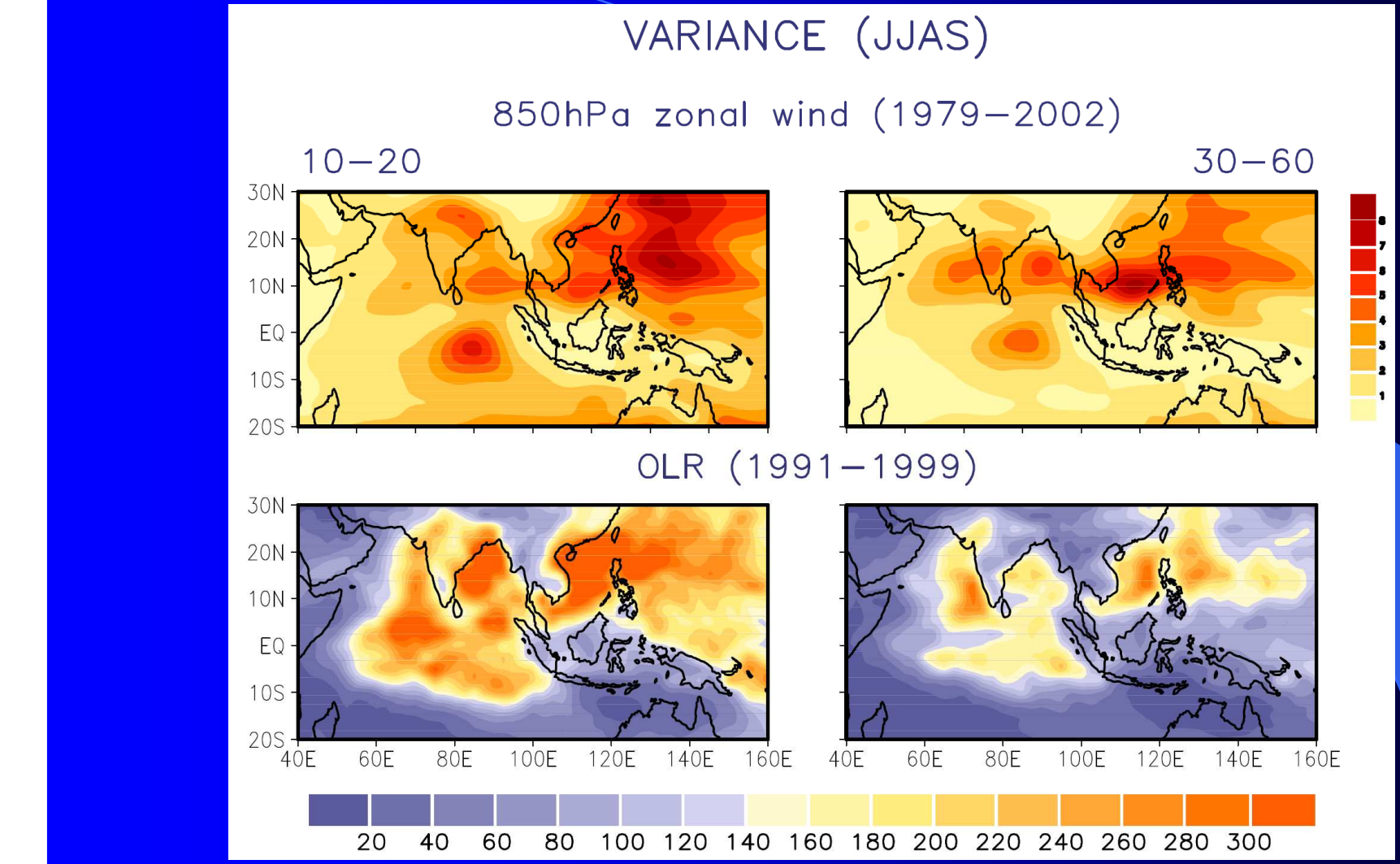

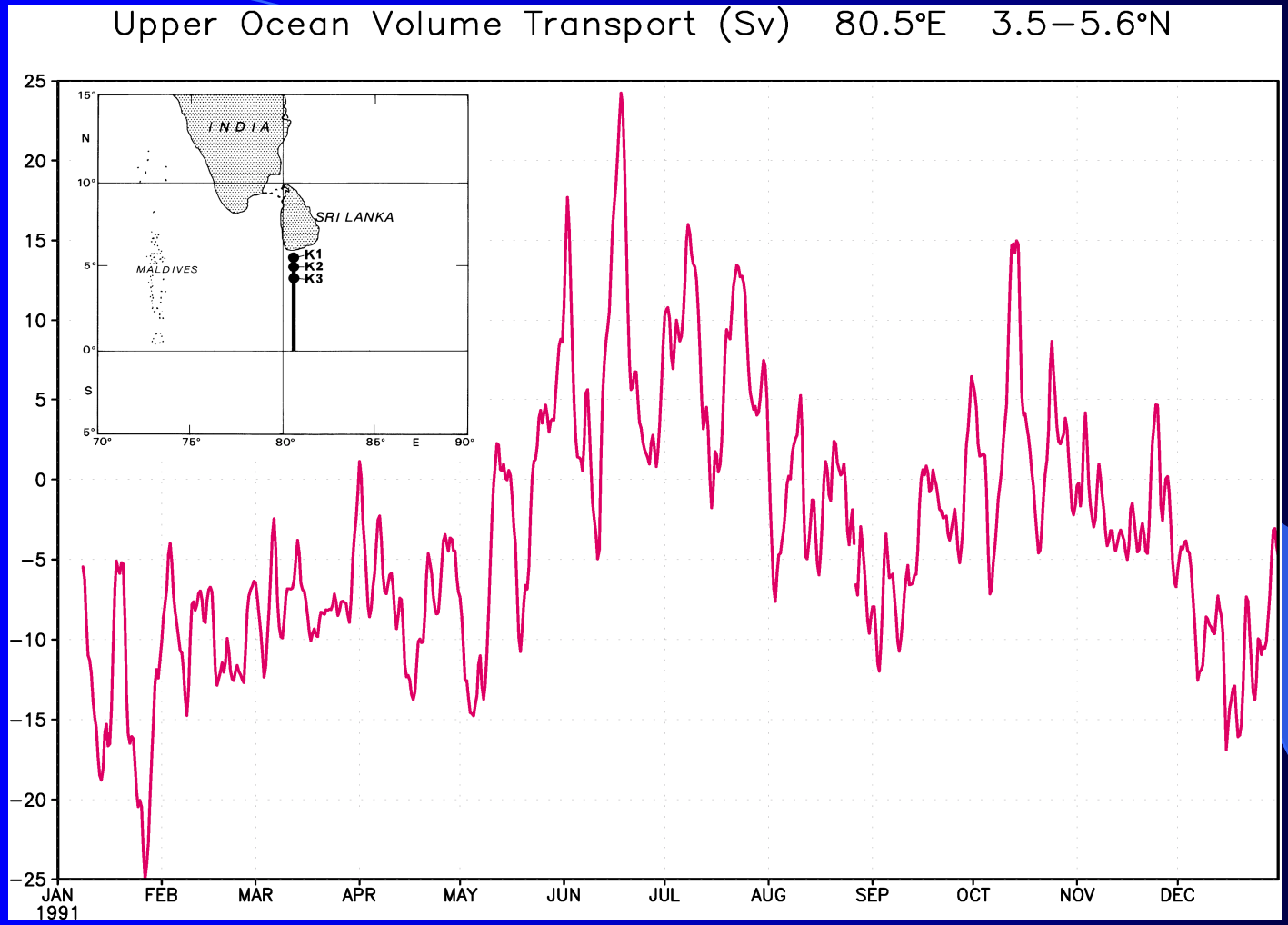

Schott et al., 1994, JGR

MERIDIONAL VELOCITY (cm s^{-1}) 90°E EQUATOR

OBSERVATION *(Masumoto, Murty et al., Presented at IOGOSS Conference, Mauritius, November 2002)*

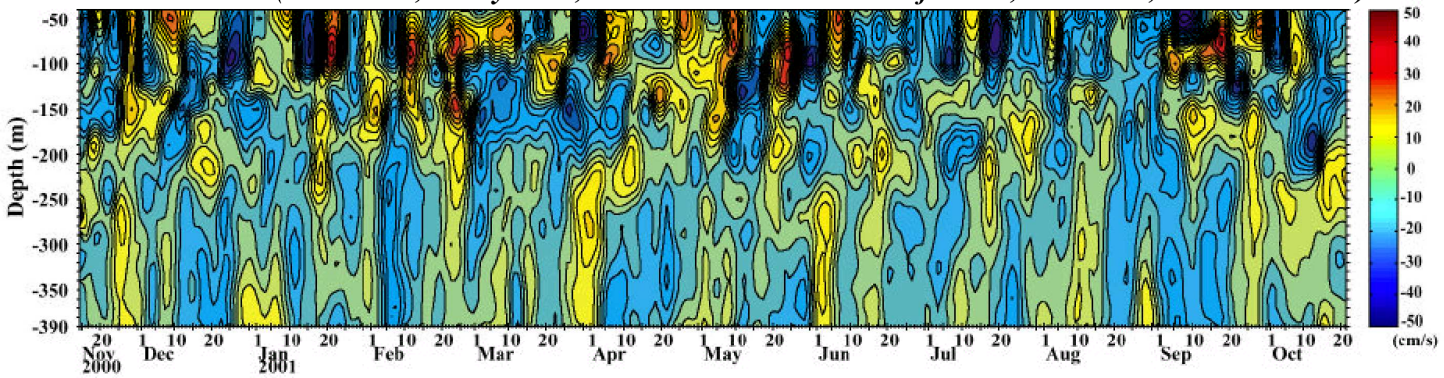

MODEL

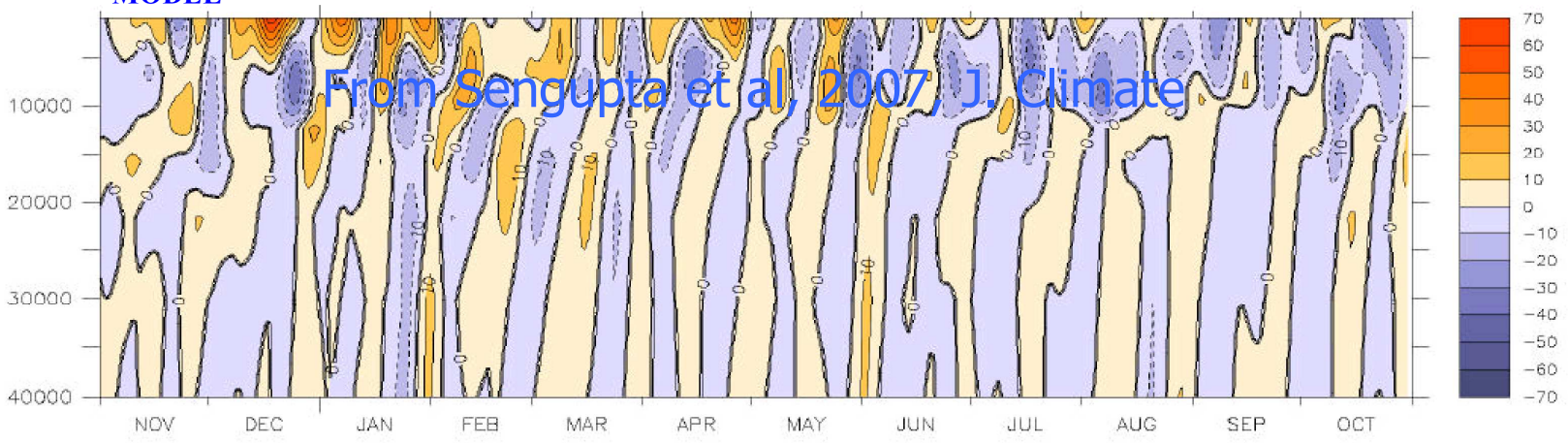

From Sengupta et al, 2007, J. Climate

v variability: mainly 14-day Yanai waves at all depths + 30-60 day ?? below ~150m

Predictability of Monsoon ISOs

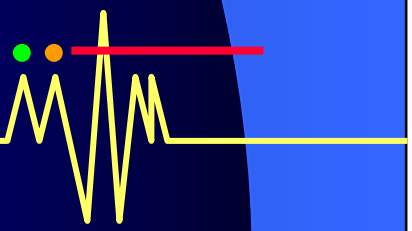

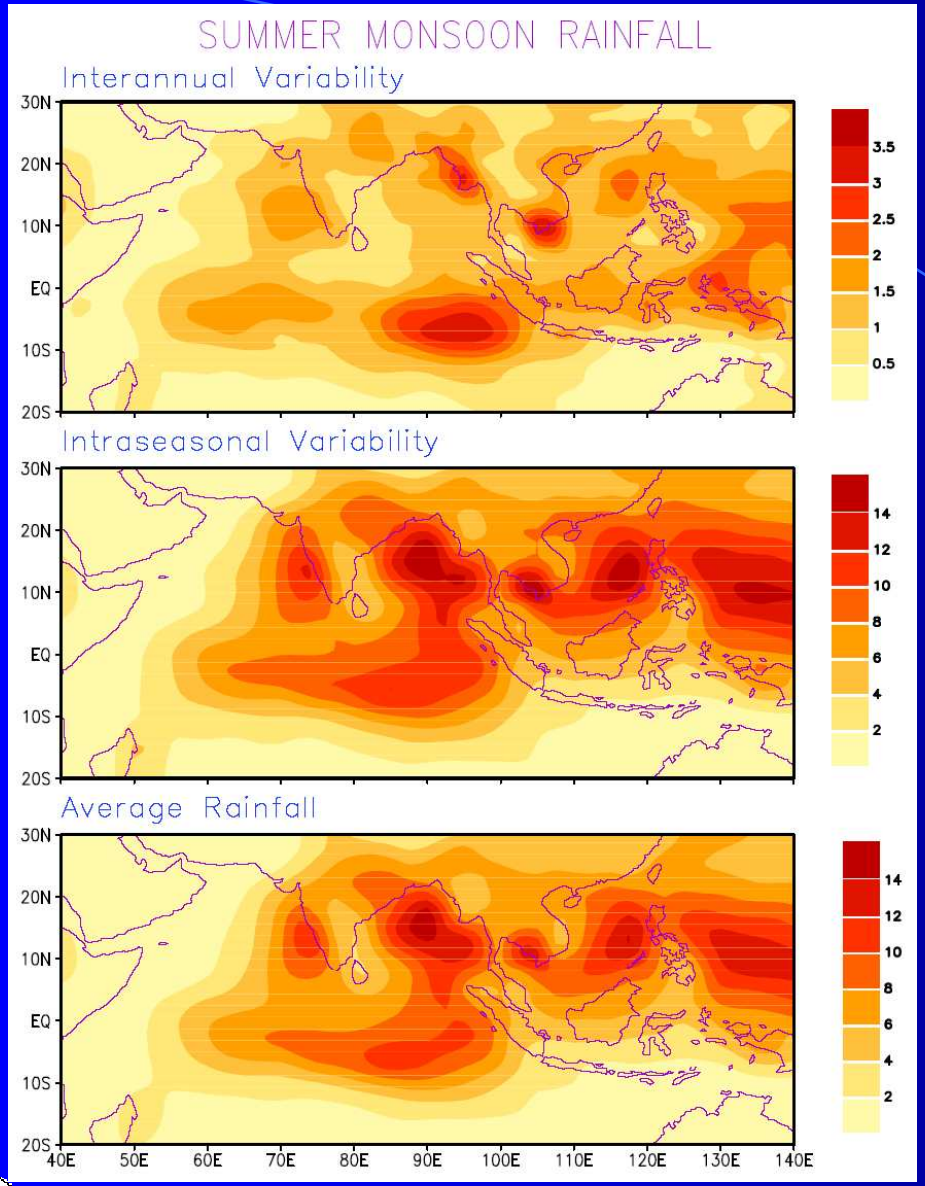

The ISO signal is much larger than signal in IAV of monsoon

Amplitude of (s.d.) of interannual variability of JJAS precipitation (mm/day) , (middle) Amplitude of intraseasonal variability (s.d. Of 10-90 day filtered anomalies during June 1 – Sept. 30) and (bottom) climatological mean JJAS precipitation (mm/day).

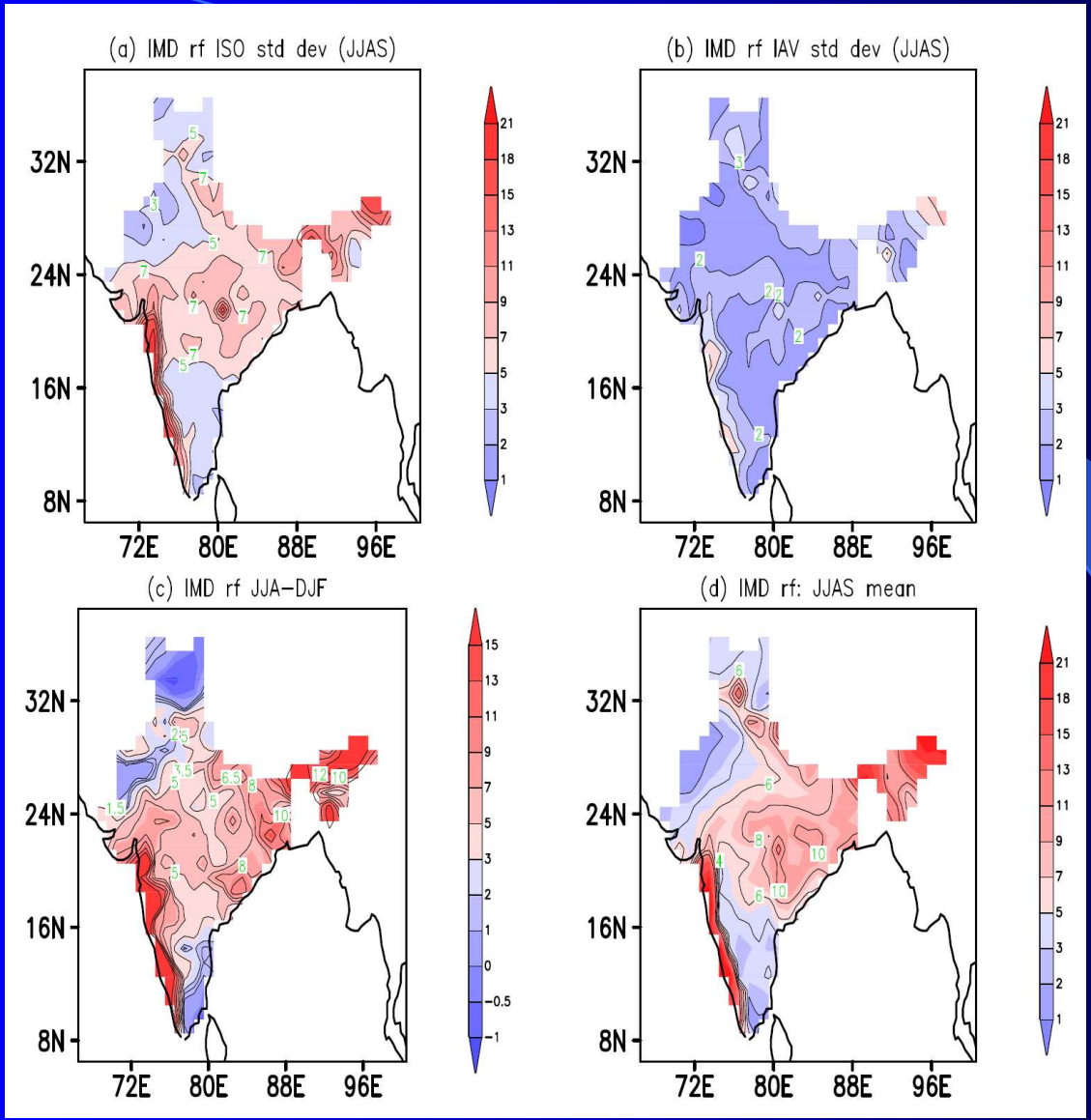
(a) IMD rf ISO std dev (JJAS)
(b) IMD rf IAV std dev (JJAS)
(c) IMD rf JJA–DJF
(d) IMD rf: JJAS mean
32N
24N
16N
8N
72E
80E
88E
96E
21
18
15
13
11
9
7
5
3
2
1
0
−0.5
−1

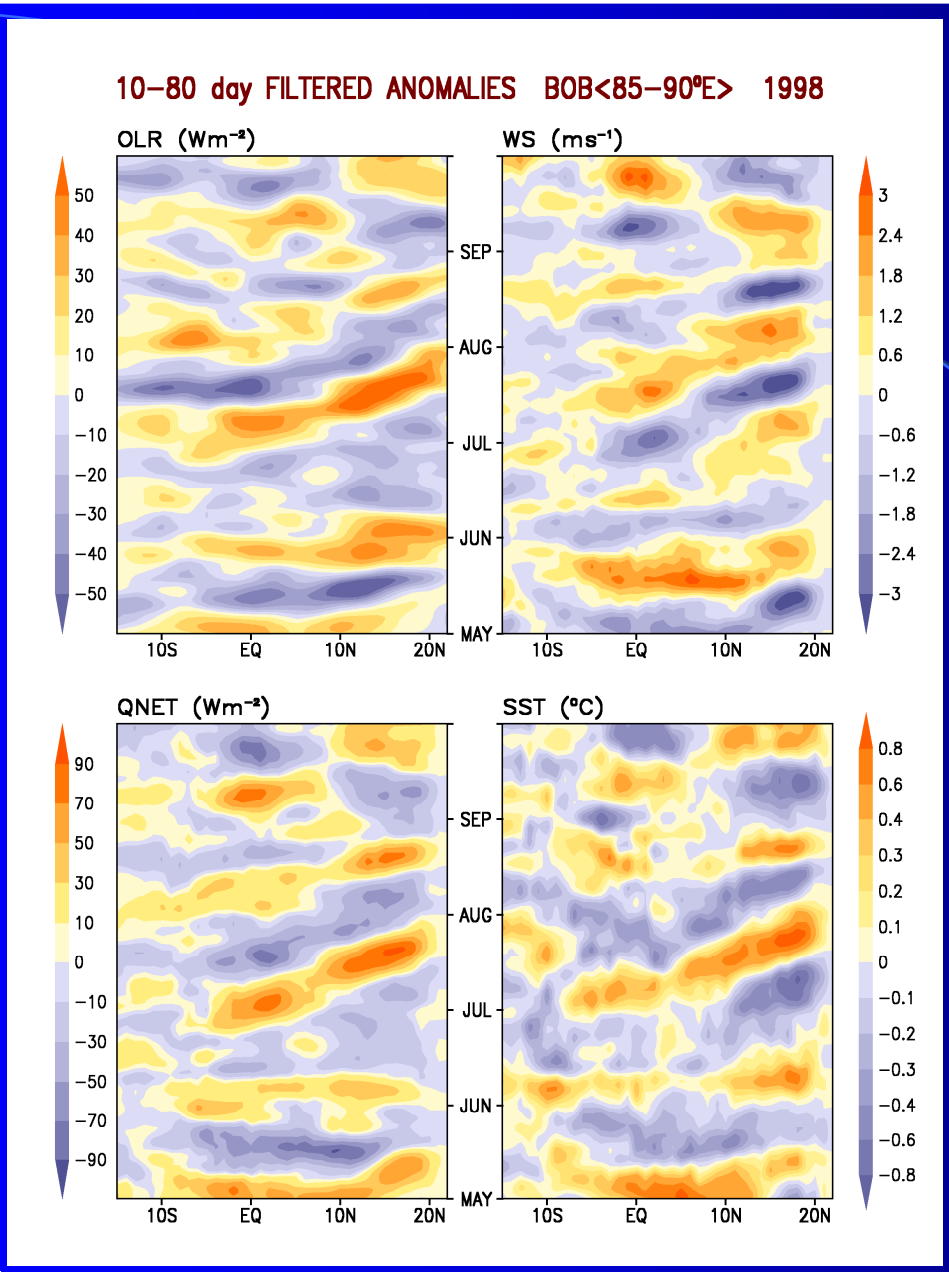

Monsoon ISOs are associated with Ocean-Atmosphere coupling

Coherent northward propagation of OLR, surface wind speed (WS), Qnet and SST during summer of 1998

Large amplitude of the ISO anomalies is noteworthy

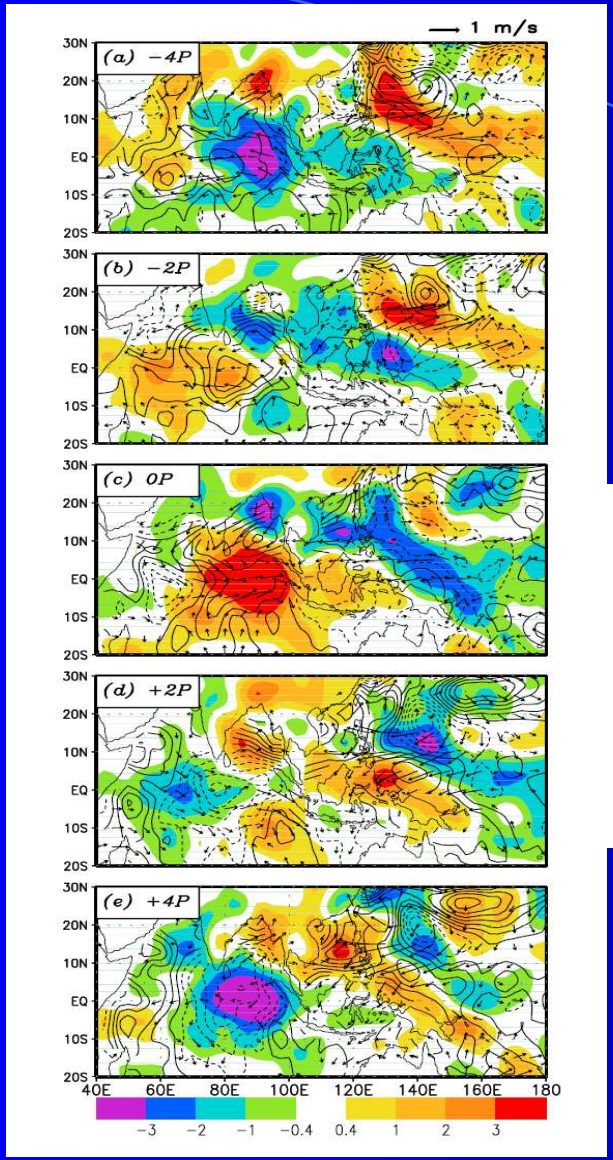

Fu et al. 2006; GRL

Figure 2. Composite space-time evolutions of rainfall (color shaded, mm day^{-1}), SST (contour interval: 0.1°C), and surface wind (m s^{-1}) anomalies of seven intraseasonal events at (a) −4 pentads, (b) −2 pentads, (c) 0 pentad, (d) +2 pentads, and (e) +4 pentads. The rainfall is from GPCP data set; SST from Aqua/AMSR_E; and surface wind from QuikSCAT.

How Predictable are the Monsoon ISOs?

- **A simple procedure is described to make such an estimate of potential predictability for active and break conditions from observations**

Goswami and Xavier, 2003, GRL

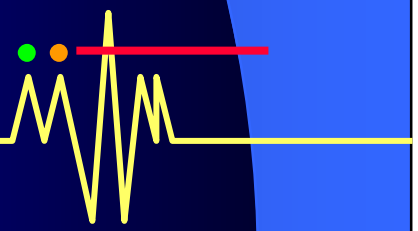

Data Used

- Daily rainfall over Indian continent from rain gauge stations (1951-2000)
- CMAP pentad data (linearly interpolated to daily values) , 1979-2001
- NCEP/NCAR Reanalysis daily winds ; 1979 – 2001
- NOAA daily OLR ; 1979-2001

10-90 day band-pass Lanczos filter is used to isolate ISO

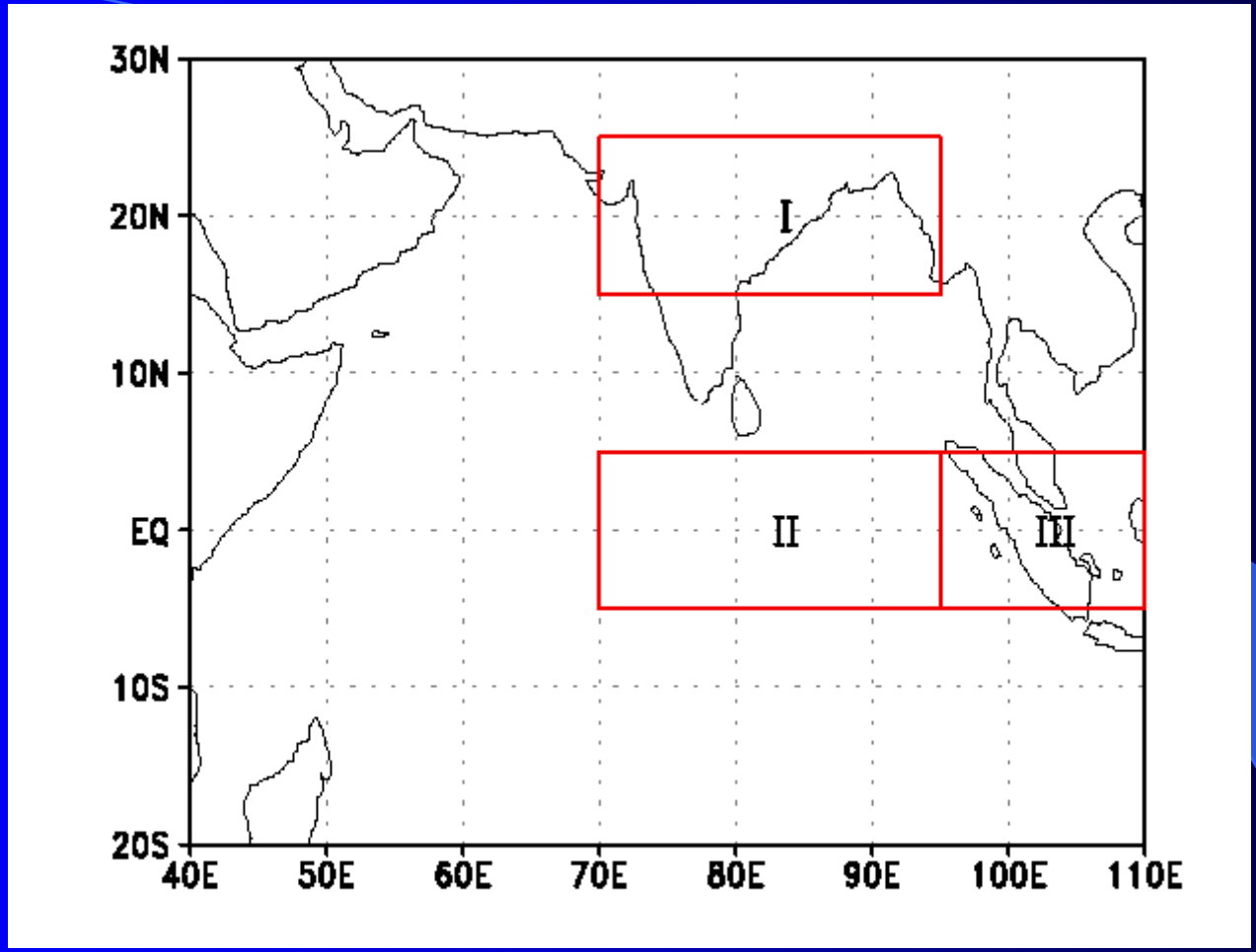

Regions over which potential predictability of precipitation is examined

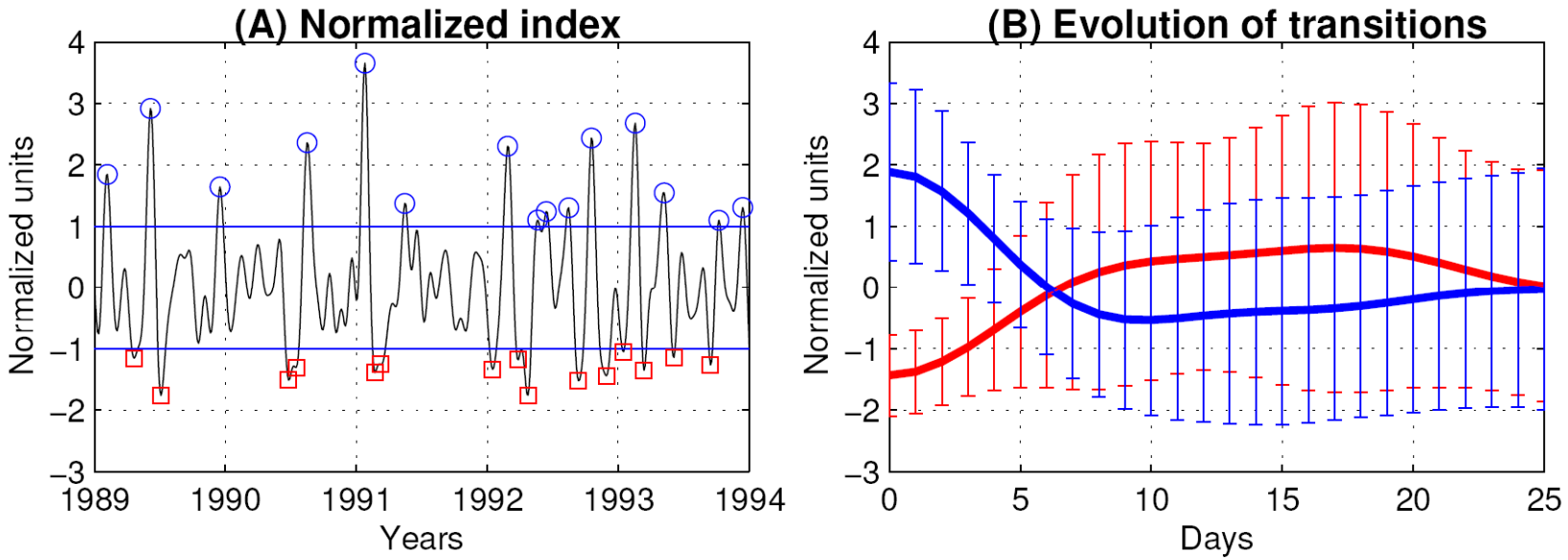

FIGURE 6.2: (A) An index of the monsoon intraseasonal variability defined as the time series of rainfall anomalies averaged over, 70°-90°E, 15°-25°N and normalized with its own standard deviation. The index is shown for a typical period of 4 years. Active phases are marked with red circles and break phases are marked with blue squares. (B) shows the evolution from active to break (in blue) and from break to active (in red). Average transitions are plotted in thick lines and the spread in transitions in terms of standard deviation of different evolutions at each lag are plotted as error bars with corresponding colors.

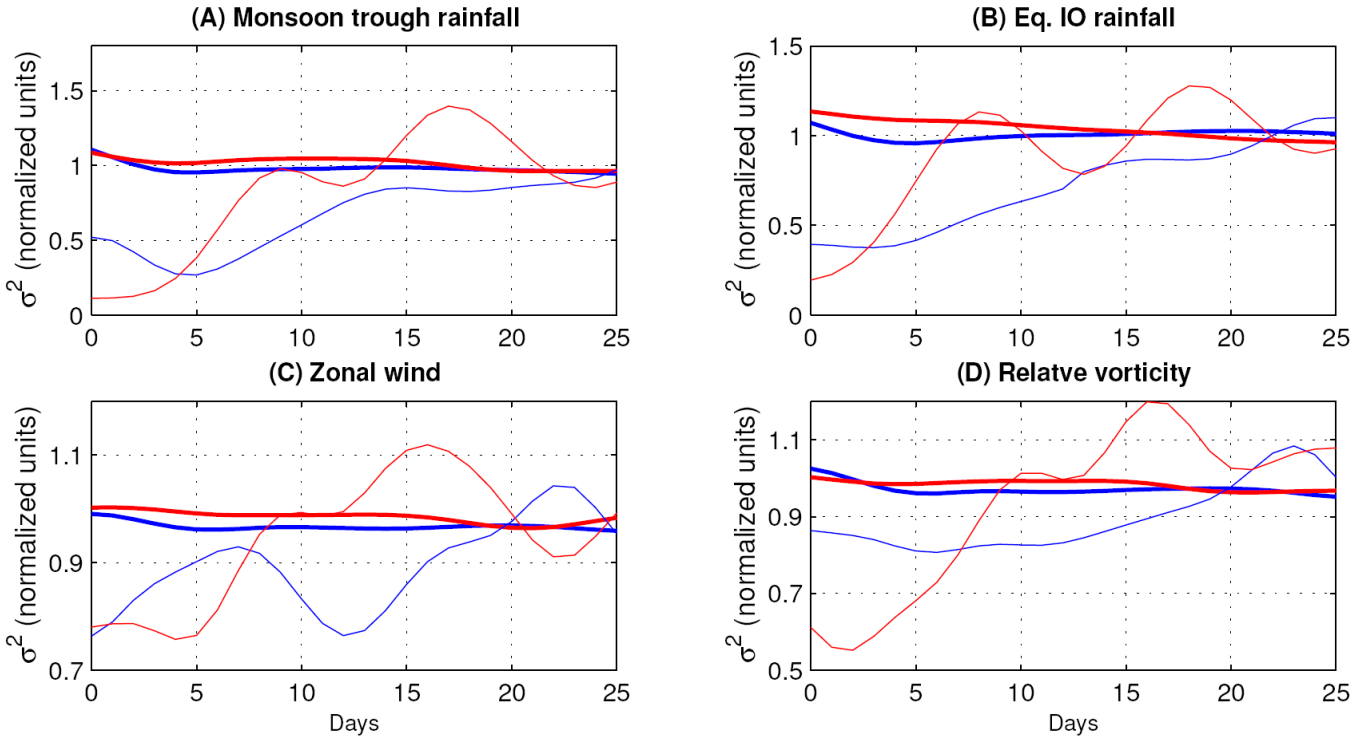

FIGURE 6.3: (A) The thick red (blue) line is the monsoon ISO 'signal' starting from troughs (peaks) of the index (Fig.6.2A). The thin red (blue) line is the standard deviation (or spread) of ensemble members as a function days from the initial date corresponding to all troughs (peaks) of the index representing transitions from break to active (active to break). (B) is same as (A) but for a precipitation index averaged over the eastern equatorial Indian Ocean (80°-100°E, 5°S-5°N). (C) same as (A) but for evolution of zonal wind at 850 hPa averaged over 80°-95°E, 12°-18°N. (D) same as (A) but for relative vorticity at 850 hPa averaged over the monsoon trough.

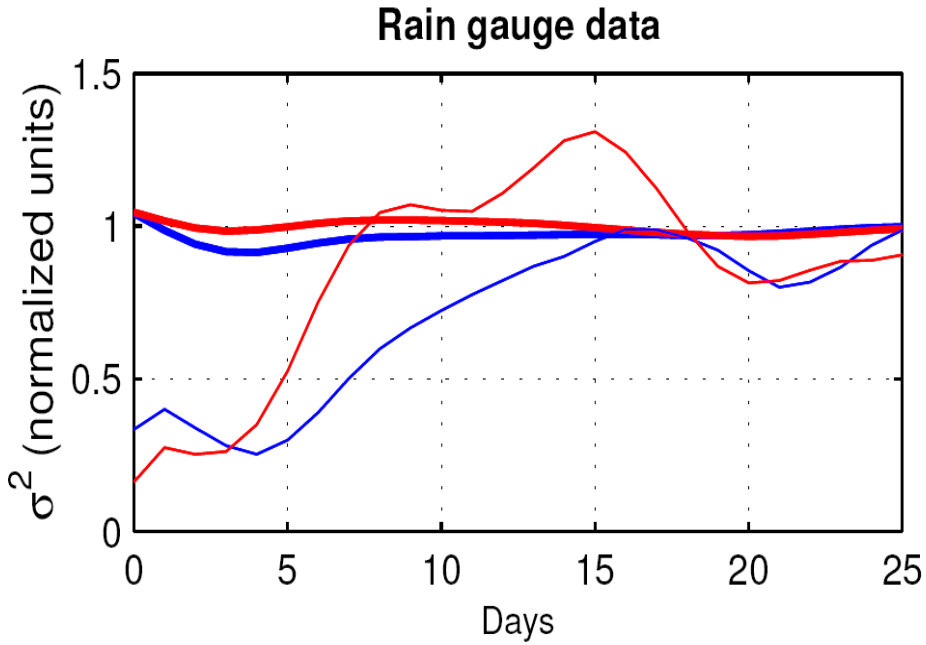

FIGURE 6.4: Same as Fig.6.3A, but for high resolution gridded daily rain gauge data (Rajeevan et al., 2006) for the JJAS season of 1951-2003, averaged over 70°-90°E, 18°-30°N.

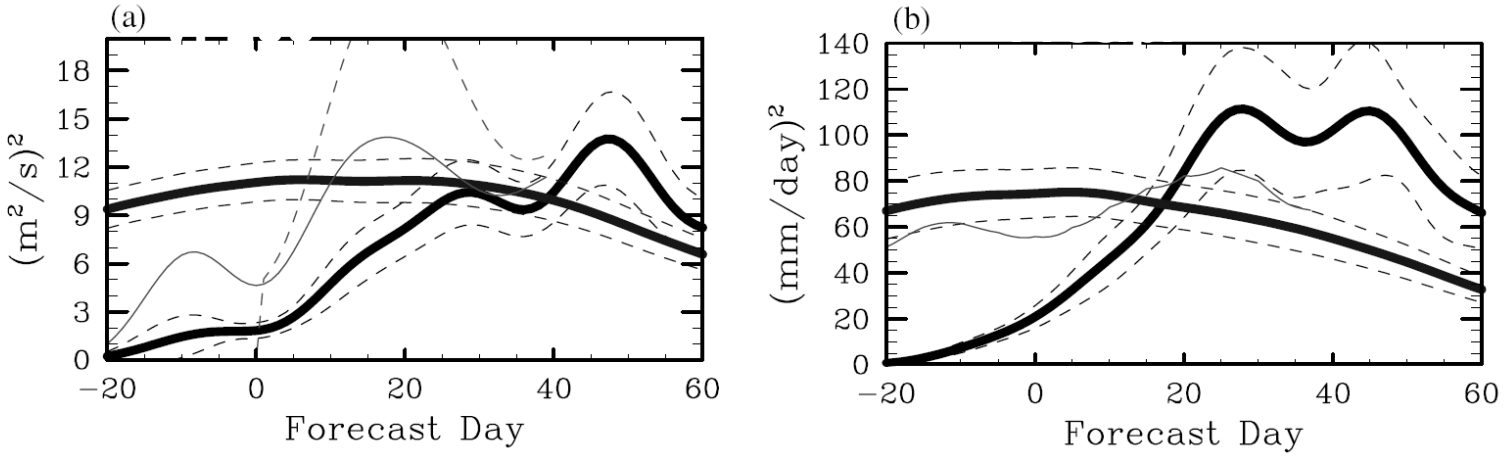

Figure 8. (a) Mean-squared forecast error (Eq. (4)) for the (30–90 day) filtered 200 hPa velocity potential (VP200) over the region 12–16°N and 117.5–122.5°E (model grid point at centre of smaller box in Figs. 10 and 11) for all the selected intraseasonal oscillation (ISO) cases ($N = 168$), shown by the thick solid black line that increases with forecast time; the mean ISO signal (Eq. (3)) is also shown, by the thick solid black line that is roughly constant with forecast time; 95% confidence limits for these two quantities using a Students t-test are given by the thin dotted lines; additionally the mean-squared forecast errors for two different types of persistence forecasts (see section 4 for more details) are given by the thin grey line. (b) As (a) but for rainfall, except that the thin grey line in this case gives the mean-squared forecast errors for an empirical forecast method based on the canonical ISO pattern depicted in Fig. 2 (see section 4 for more details). VP200 values have been scaled by 10^{-12}.

Waliser et al. 2003, QJRMS. **129**, 2897-2925

Uses GLA GCM, carried out 'identical twin' predictability experiments 84 cases selected from the amplitude of EEOF of 30-90 day filtered fields.

Conclusion: ISO Predictability

The transition from break to active conditions is intrinsically more chaotic than transitions from active to break conditions.

A fundamental property of monsoon ISOs.

Why?

Break →Active – convective instability— growth of error governed by fast conv. Instability

Active→Break – dying convection -- slow error growth due to slow oscillation

Consequence,

The potential predictability limit for monsoon breaks is about 20 days while that for monsoon active conditions is only about 10 days

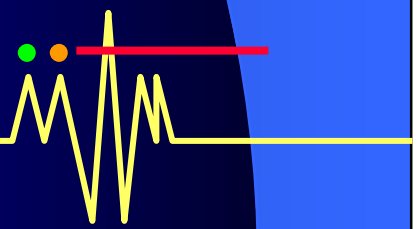

Empirical models:

Waliser et al. (1999), *J. Climate*, 12, 1918- 1939**.**

Lo and Hendon (2000), ***Mon. Wea. Rev.*****.,** **128**, 2528–2543.

Mo (2001), *Mon. Wea. Rev*. 129, 802- 817**.**

Wheeler and Weickmann (2001), *Mon. Wea. Rev*. 129, 2677- 2694

Jones C et al (2004) ***J. Climate*** **, 17,** 2078- 2095

Use empirical technique and demonstrate skilful forecasts of the MJO in OLR and 200 hPa streamfunction up to 20 days in advance. The models perform well when the MJO is active at the initial condition but not so well when it is inactive.

All these studies primarily concentrated on MJO and use 25-90 day filtered data.

We feel that same may be possible for summer monsoon ISOs although existence of higher frequencies (10-20 day) may limit it to some extent.

Webster and Hoyos (2004, BAMS) also show very good skill for predicting ISO phases using a slightly different empirical technique (wavelet banding)

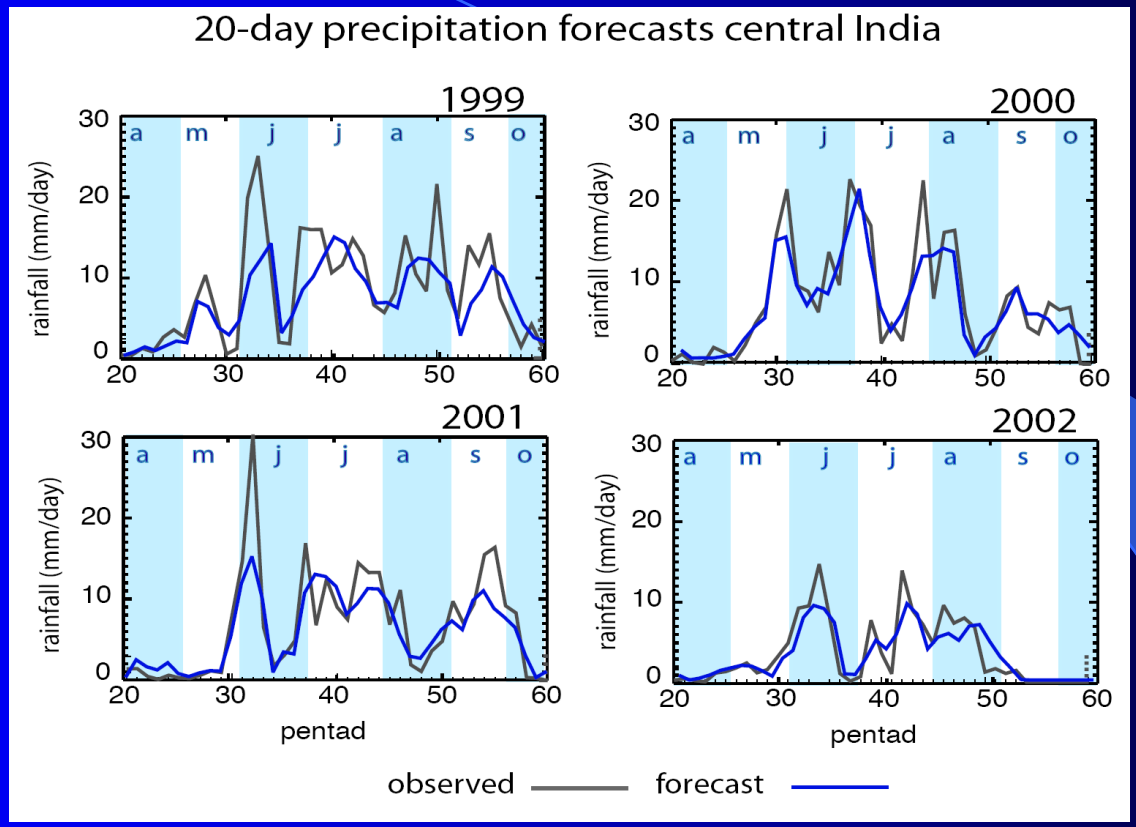

20-day forecast of precipitation over central India for the summers of 1999-2000. Blue lines indicate forecasts while the grey lines indicate verification obtained from area averaged GPI precipitation.

Our Model

- Based on first 10 EOFs of 10-90 day filtered CMAP precipitation
- Predictors: Principal components of precipitation itself and first two PCs of sea level pressure.
- Linear regression

Goswami and Xavier, 2003, GRL, vol 30, No.18

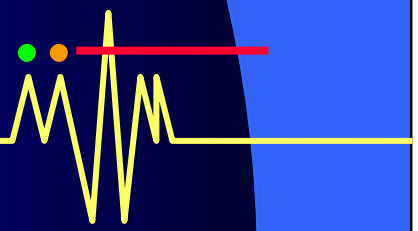

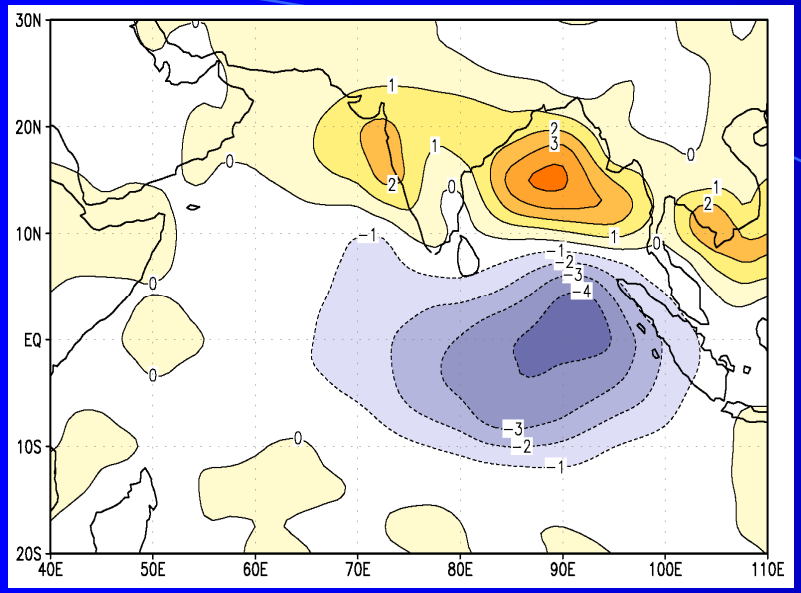

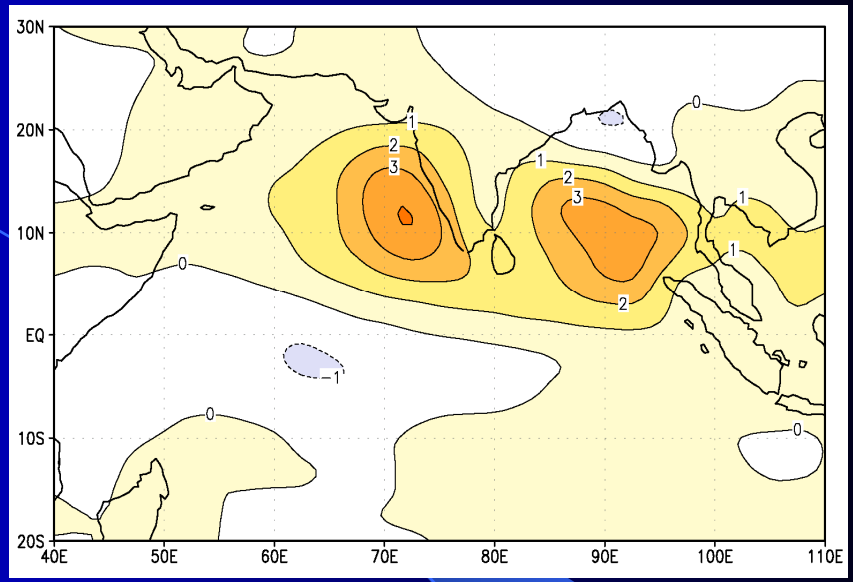

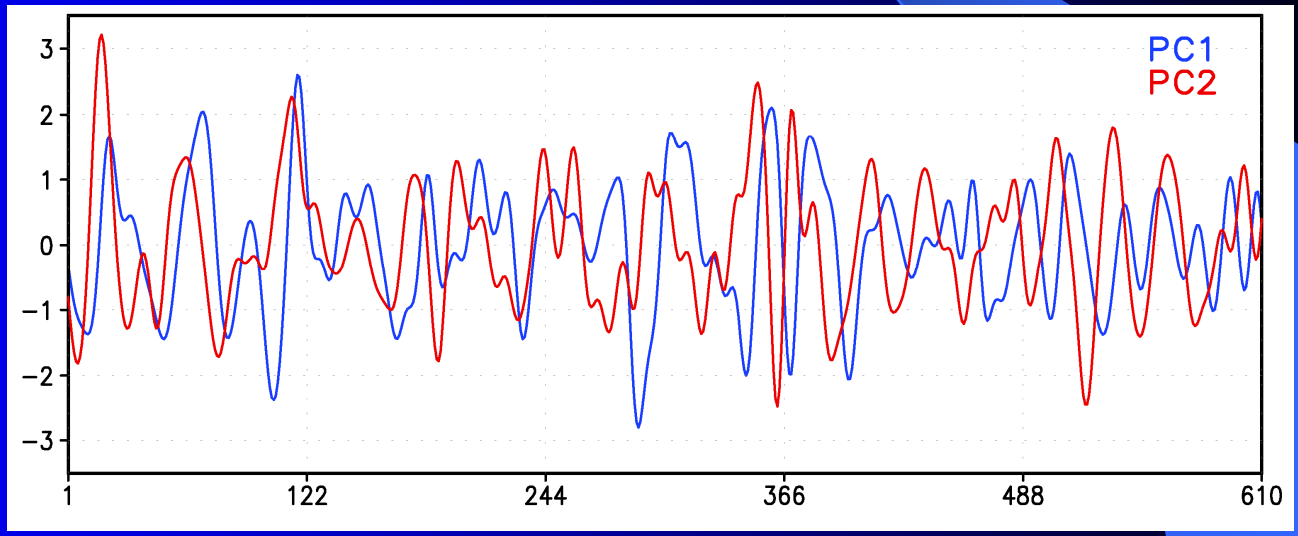

First two EOFs of CMAP pentad (interpolated to daily) rainfall for JJAS (1979-2001)

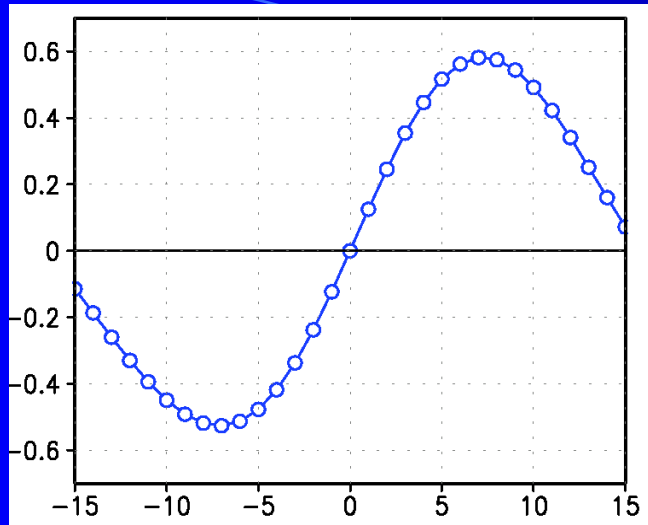

Lag correlation between PC1 and PC2

ISO Index :

$$I(t) = (PC1(t) + PC2(t+8))/2$$

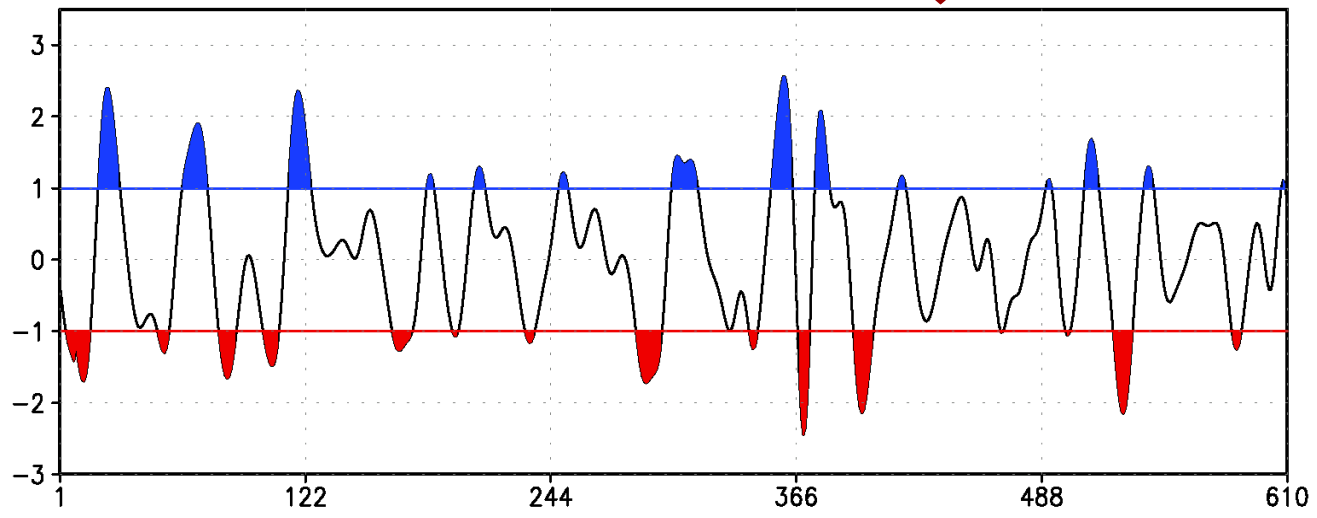

Predictors

PC1-4 of 10-90 day filtered CMAP

PC1-2 of Surface Pressure

$$PC^*(t+\tau) = \sum_{i=1}^{N} \beta_i(\tau) PC_i(t)$$

Predictants

PC1-4 of filtered rainfall

Predicted rainfall at lead time τ

$$P(x, y, t+\tau) = \sum_{i=1}^{4} PC_i^p(t+\tau) E_i^p(x, y)$$

Model developed on 1 June-30 Sept. data for 1979-1995

Model is tested on independent data for 1996-2001

15-day predictions and verifications of rain anoms ave(70E-90E)

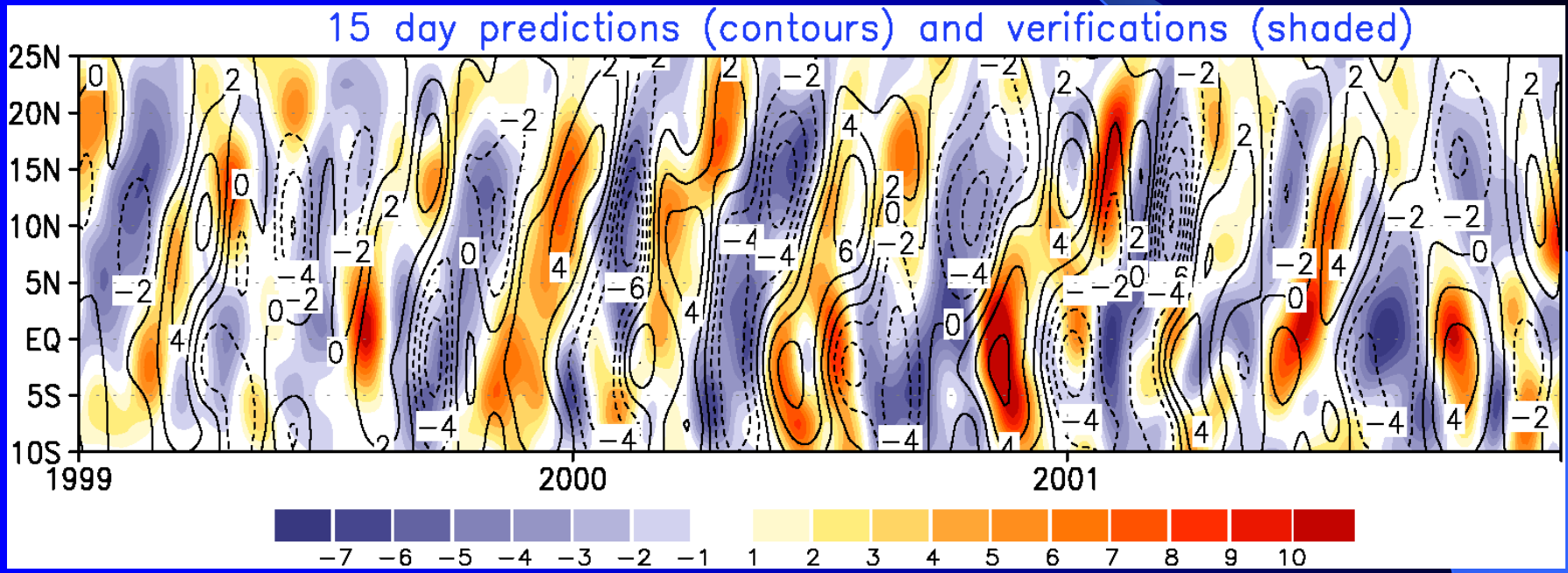

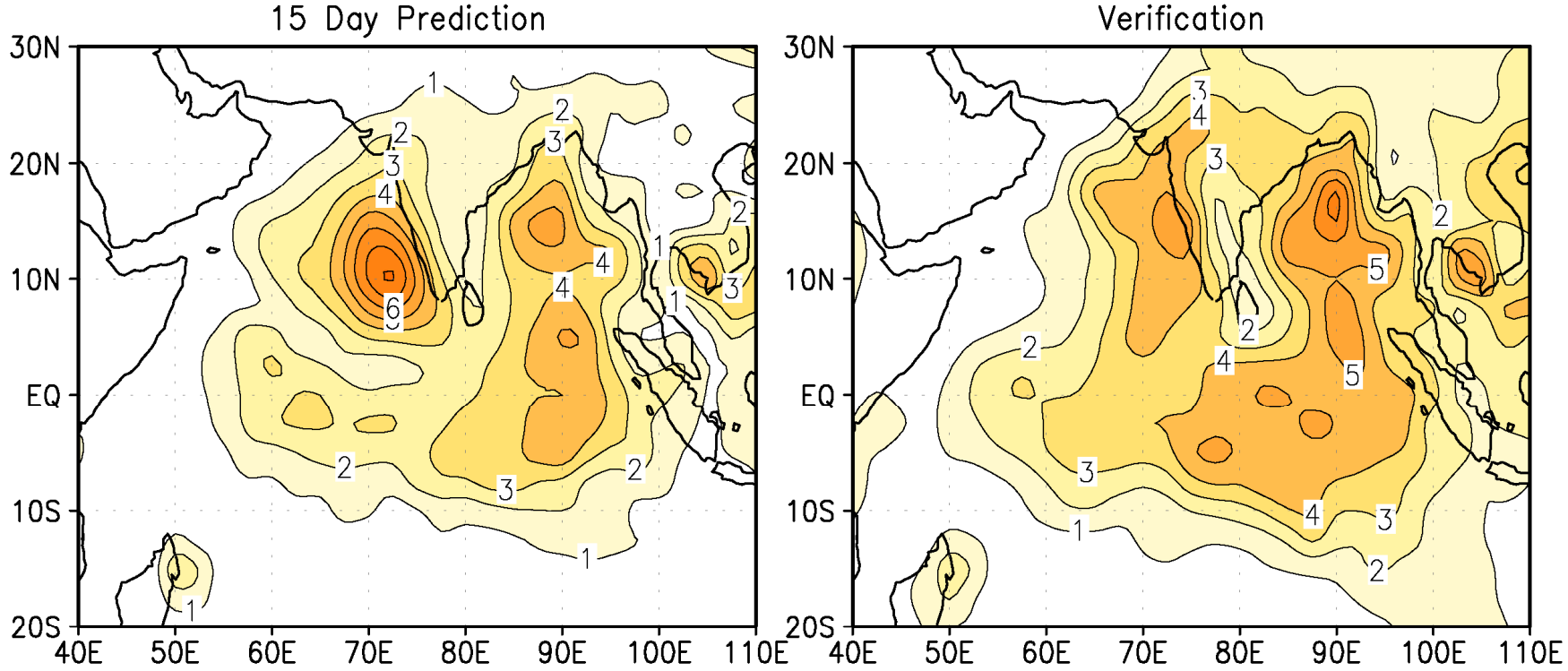

Figure 4.6: The Standard deviation of all 15 day predictions and verifications at all grid points.

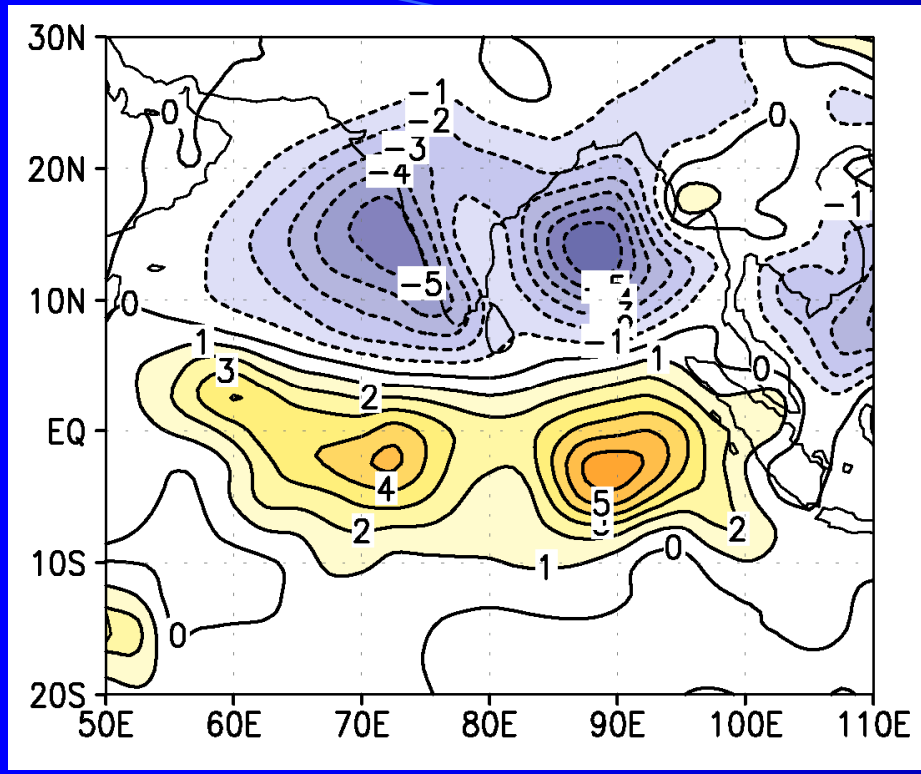

Mean of 18-day predictions of breaks (mm/day)

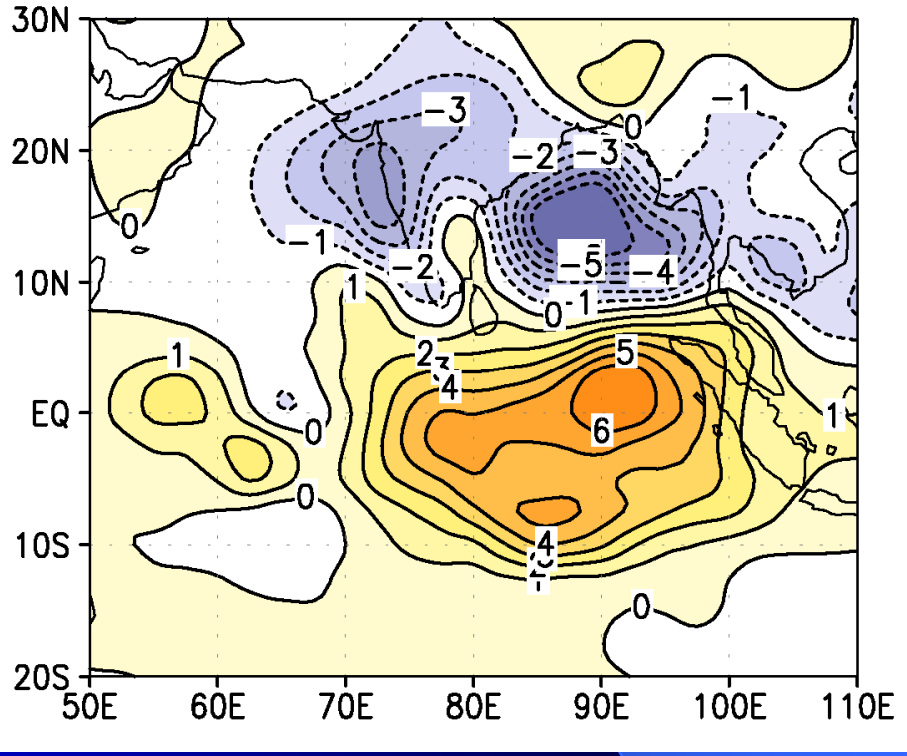

Mean of 57 verifications of the 18-day predictions from CMAP (mm/day)

(Mean of an ensemble of 57 such predictions starting from initial conditions around active conditions)

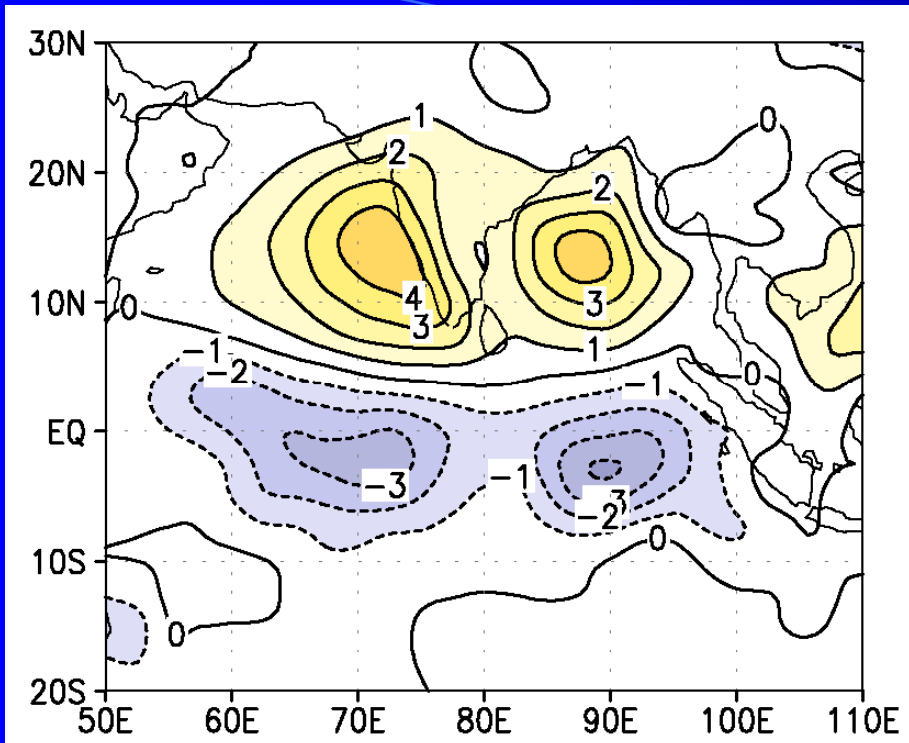

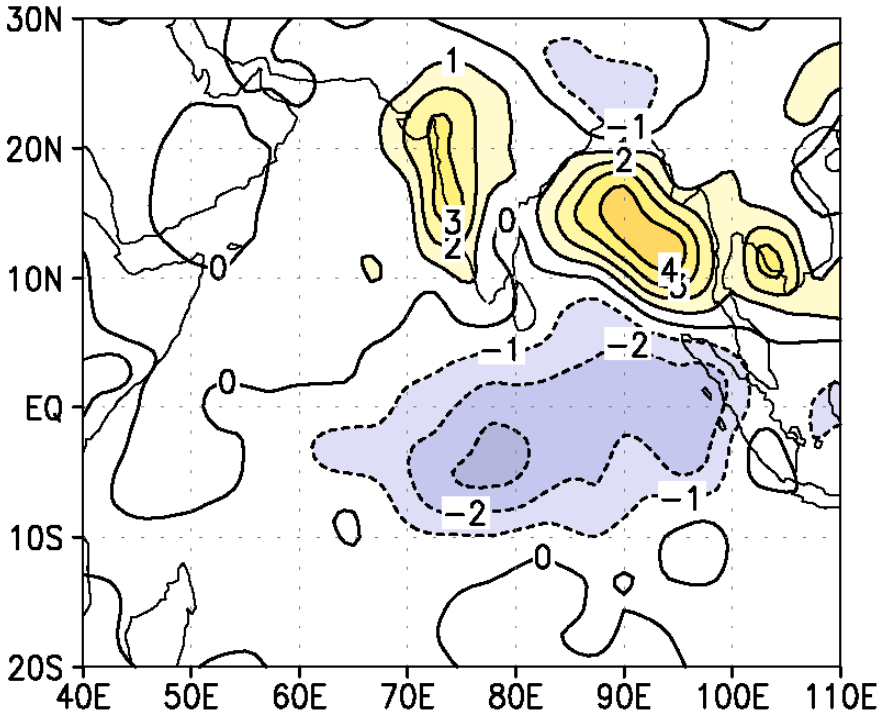

Mean of 18-day predictions of Active conditions (mm/day)

Mean of an ensemble of 54 such predictions starting from initial conditions around break conditions

Mean of 54 verifications of the 18-day predictions from CMAP (mm/day)

Lead Time	Prediction of Breaks	Prediction of Active
15 days	0.65**	0.38*
18 days	0.56**	0.43*

Correlations between predictions and observations of rainfall averaged over the monsoon trough region (70E-85E, 10N-22N)

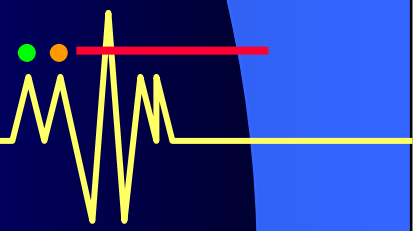

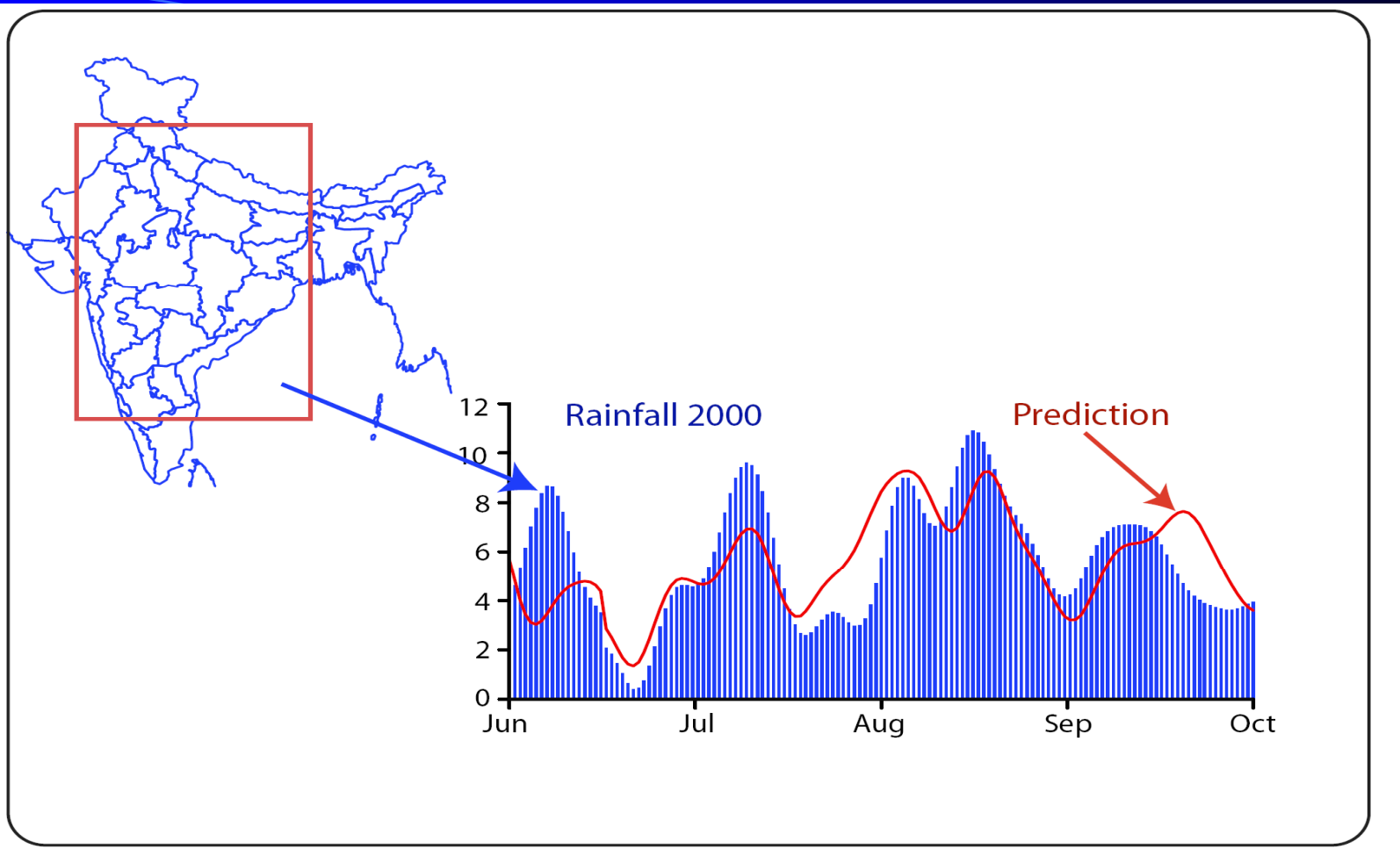

Time series of 18-day predictions (red line) and observations (blue bars) of the rainfall (mm/day) averaged over the monsoon trough region for June to September of (a) year 2000 and (b) year 2001 (Fig.4 of Goswami and Xavier 2003).

Limitations of the old Method and Development of a New Model:

- The CMAP rainfall is not available in near real time. Use of CMAP rainfall made it difficult to extend the method for real time prediction.

- We used 10-90 day filtered data as we were aware of the fact that the 10-20 day mode contributes significantly to ISO variability in the Asian monsoon region. However, it is more difficult to predict the high frequency 10-20 day mode using linear regression technique. Errors in prediction of the 10-20 day mode , then degrades the prediction of even the lower frequency 30-90 day mode.

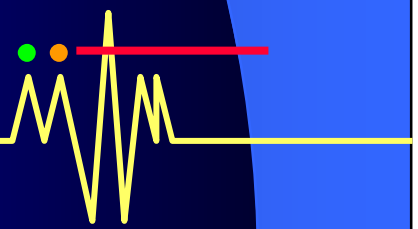

A new Analogue model for Extended Range prediction of the summer Monsoon ISOs useful for real time prediction

(Xavier and Goswami, 2007, MWR , 135, 4149-4160)

- Data Used and methodology:
- Penrad OLR data from 1979 to 2004 are used. No filtering is involved.
- To isolate the ISO, OLR anomalies are reconstructed with the first 10 EOFs
- First spatial analogues are identified and temporal analogue for each PC is found from the cases selected for spatial analogues.

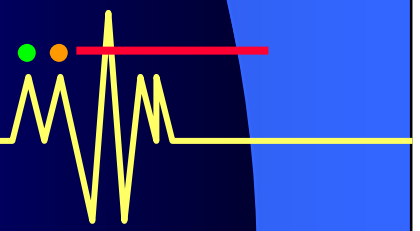

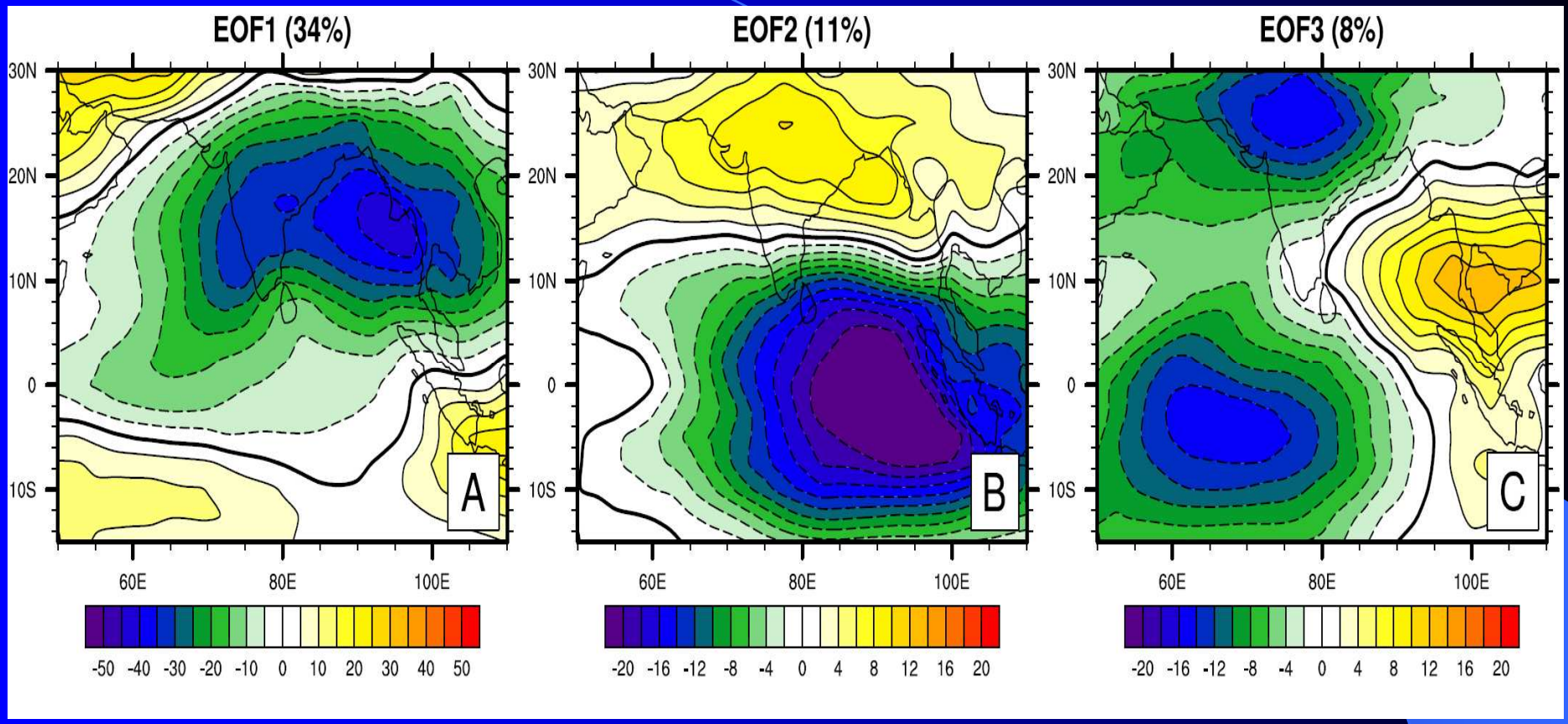

First three EOFs of pentad OLR

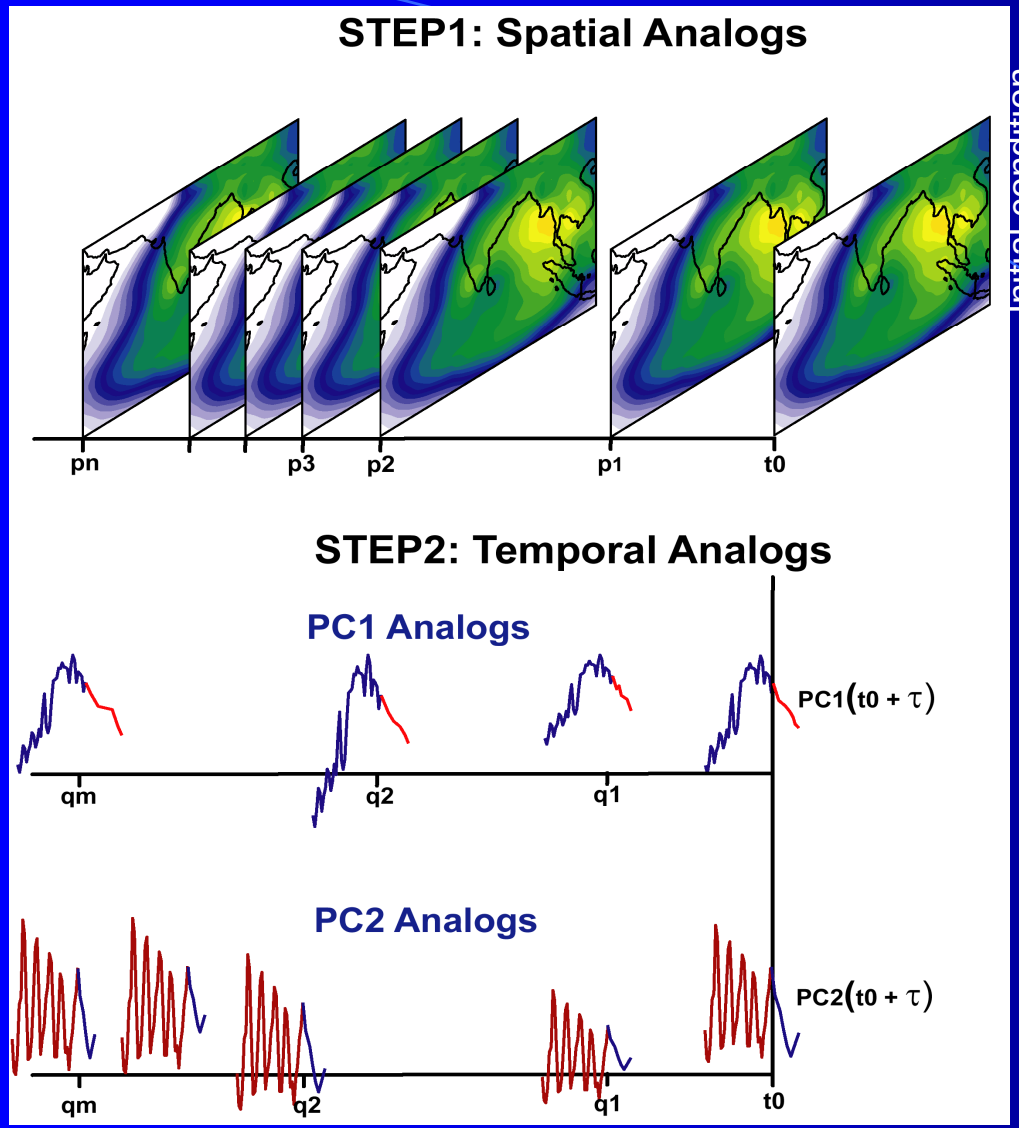

Identify spatial analogues over the entire period (25 years) for the OLR field reconstructed with first 10 EOFs at to

Identify temporal analogues for all 10 PCs going 5 pentads backward from each of the spatial analogues

Prediction → average evolution of the identified temporal analogues

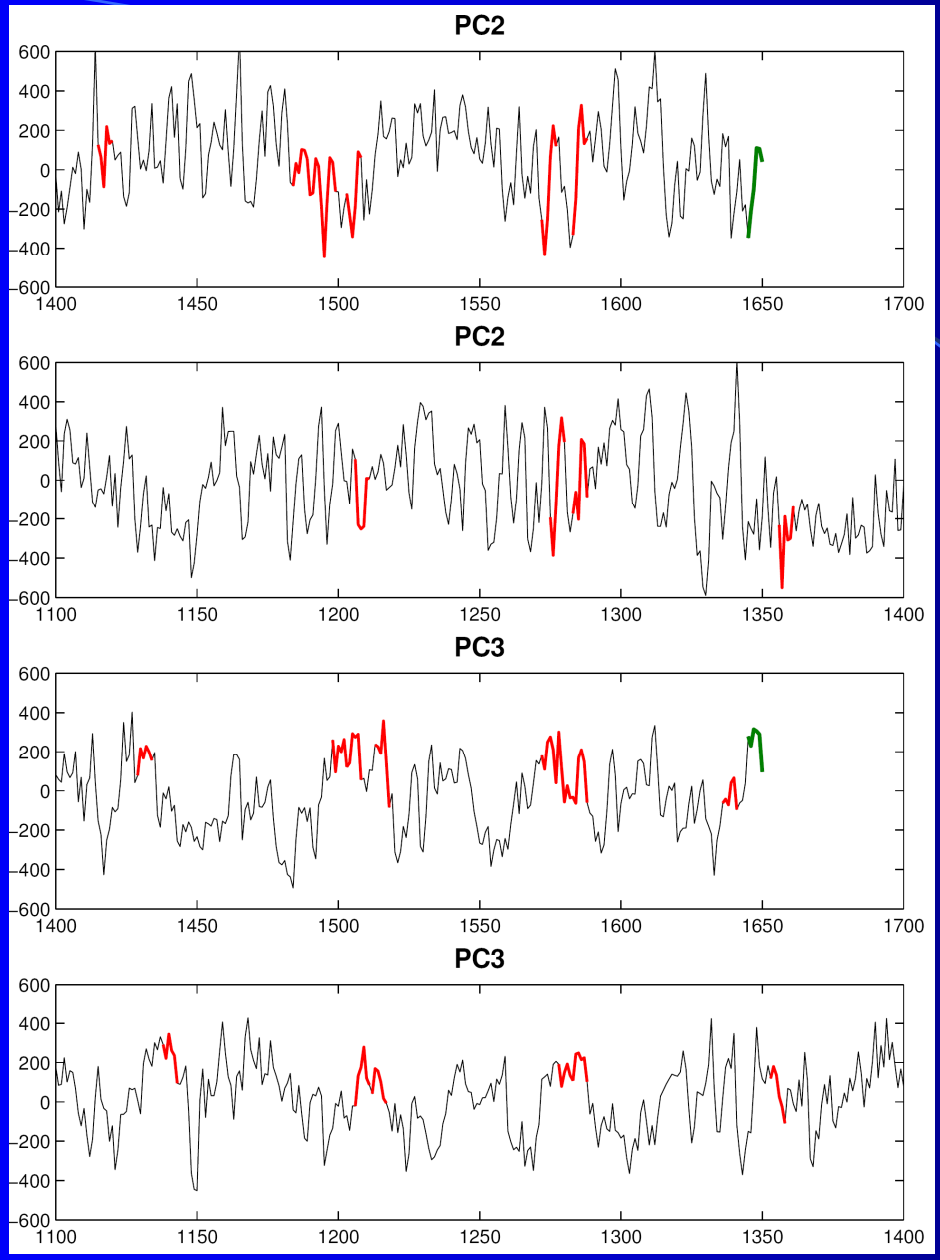

Illustration of a few temporal analogues of PC2 and PC3 for a particular initial condition.

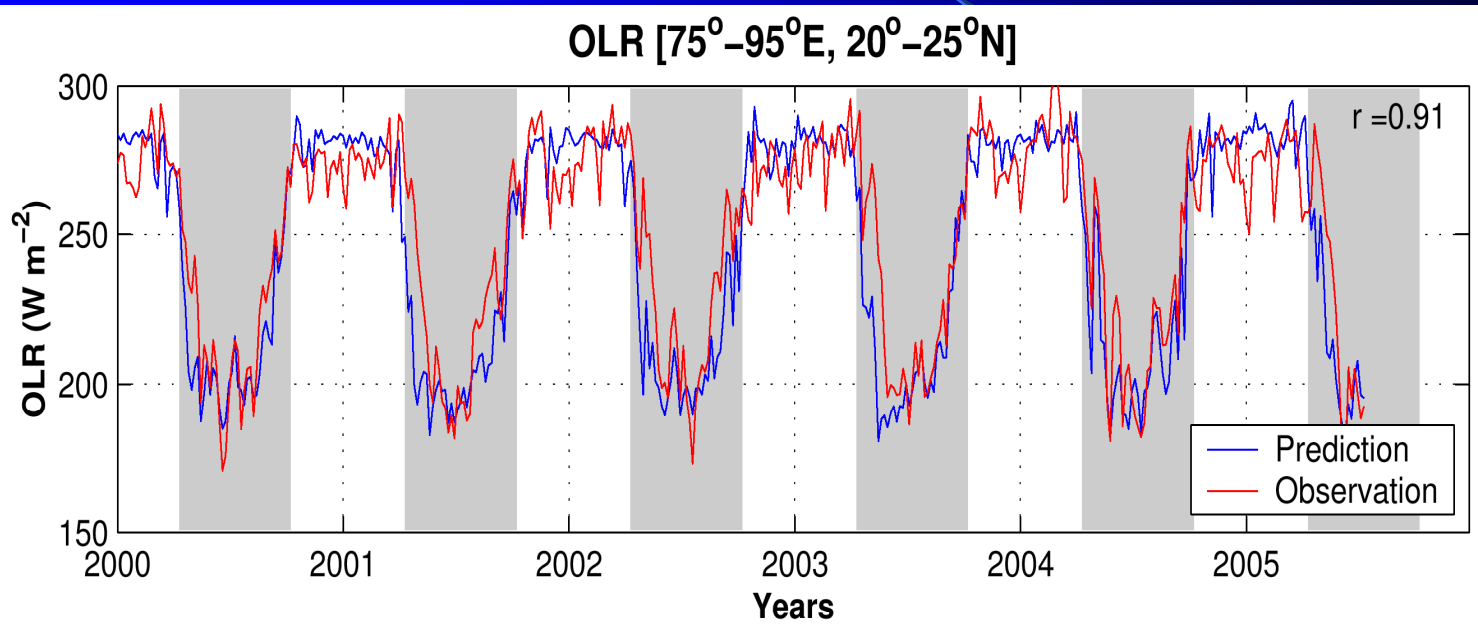

FIGURE 7.8: 4 pentads lead predictions and observations over central India during the hindcast period. Grey shades indicate the summer monsoon season. Correlation coefficient between the two is also shown.

Anomaly hindcasts

- Reconstruct the OLR data with 2-10 EOFs

  (removes the seasonal cycle)

- Look for spatial and temporal analogues as before

- Make predictions based on average evolution of these analogues

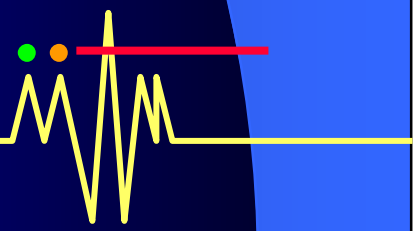

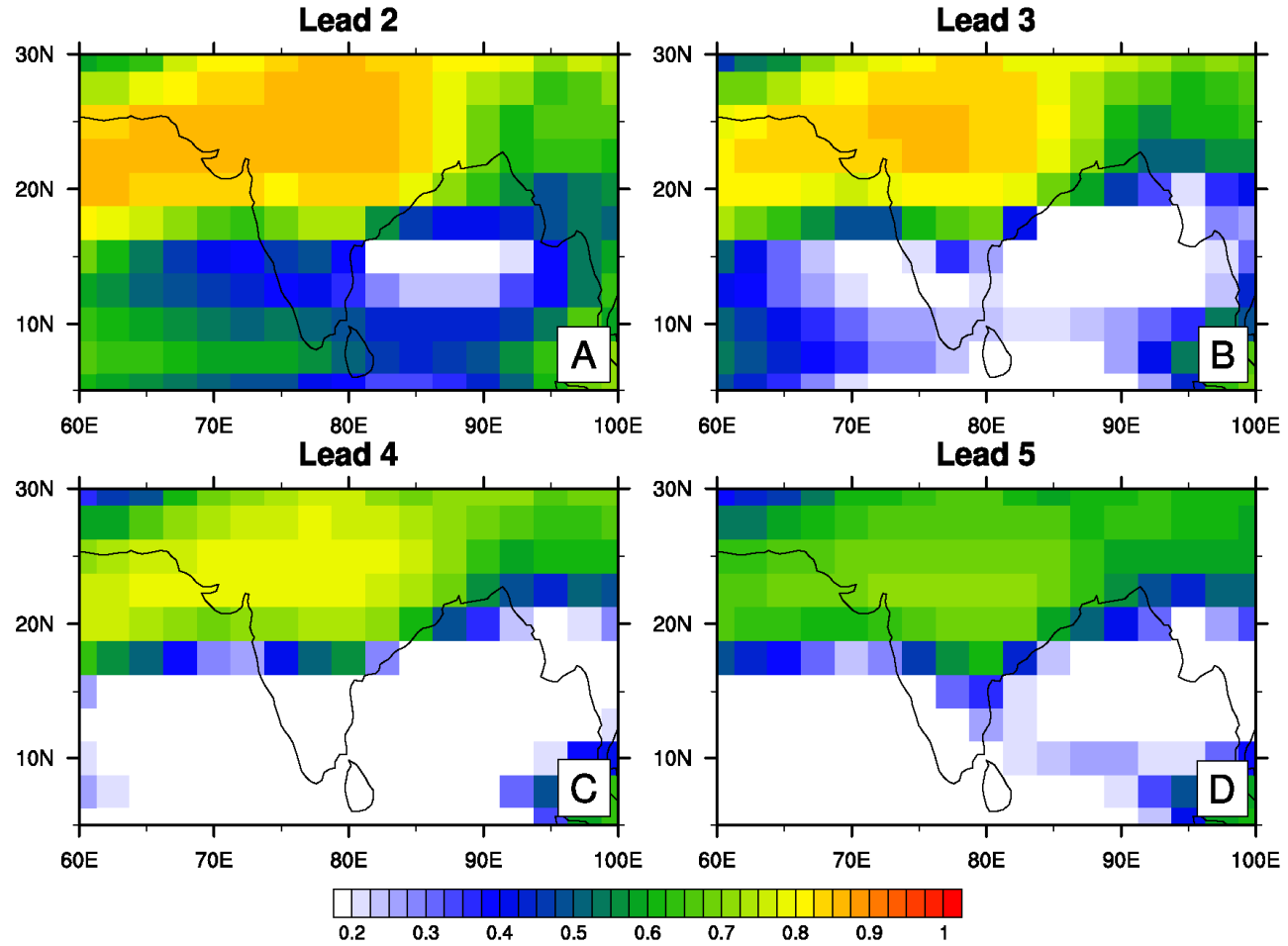

FIGURE 7.11: Temporal correlations between predictions and observations for different lead times during the May-October period in the AH.

Dependency of the forecasts on the state of initial condition

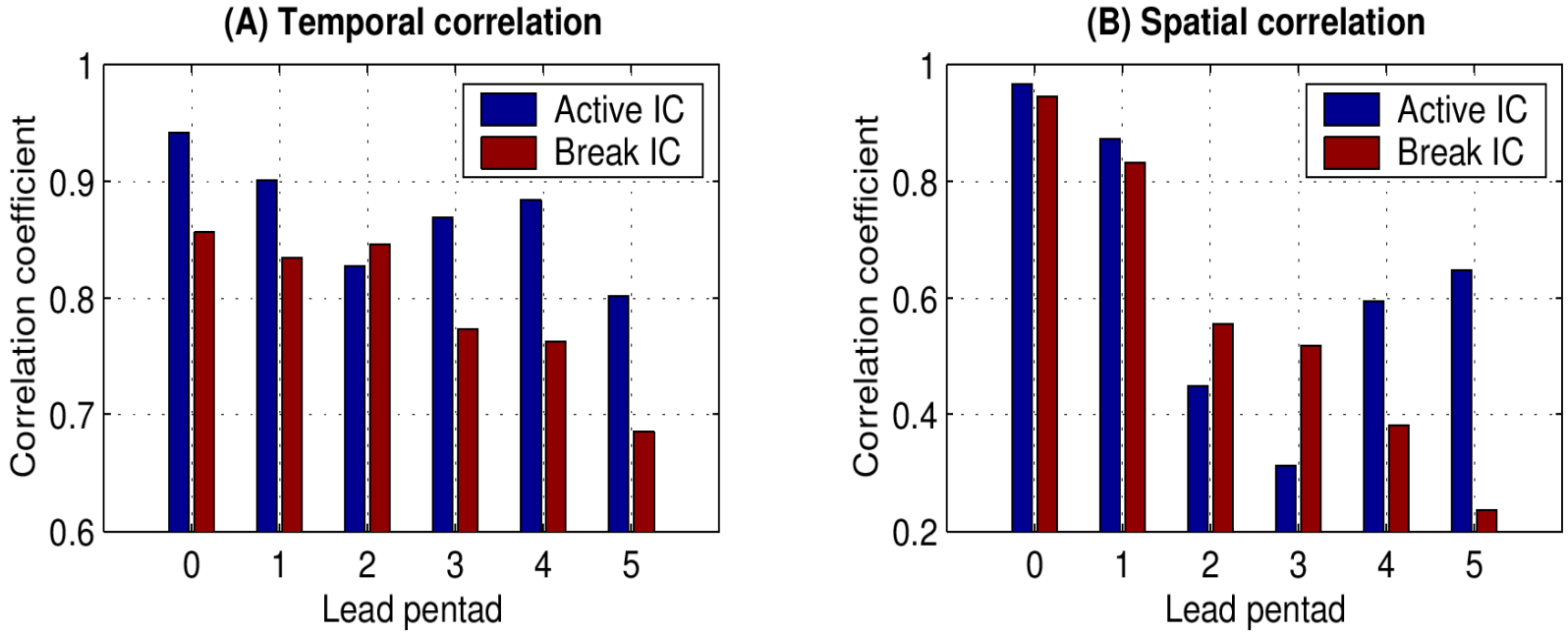

FIGURE 7.14: Temporal and spatial correlations between predictions and observations from active and break initial conditions at different lead times.

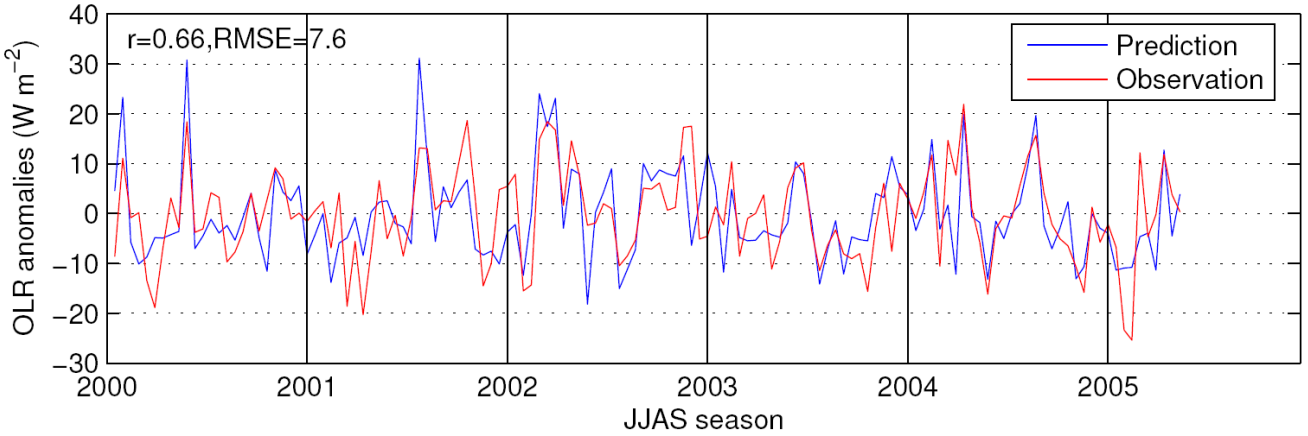

FIGURE 6.11: Prediction of OLR anomalies (W m^{-2}) at 4 pentad lead in comparison with observed values over the region 75°-95°E, 20°-25°N for the JJAS season of the hindcast period.

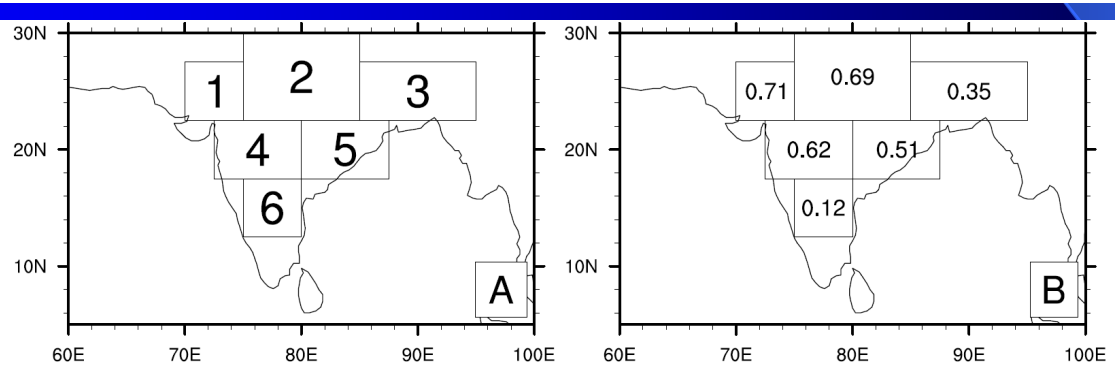

FIGURE 6.13: Regions chosen to evaluate the predictions with observations (A). The correlation coefficient between 4 pentad lead predictions and observations averaged over these regions for the May-October period (B).

This model is currently being used by the India Meteorology Department to make experimental Extended Range prediction of monsoon ISO this year.

Please see the following website

www.imdpune@gov.in

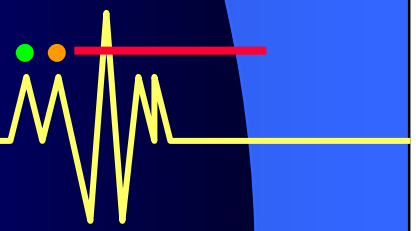

A Nonlinear Model for Real-Time Extended Range Prediction of Active/Break Cycle over Central India

Chattopadhyay,Sahai,Goswami, 2008, JAS
(May Issue)

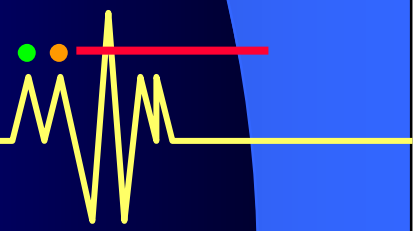

Model 1

1	Precipitation Index **(PR index)*: (*** 70^0E-85^0E, 15^0N-25^0N)
2	Goswami et al. Index **(GO index):** [V850(70^0E-110^0E,10^0S-30^0N) – V200(70^0-110^0E,10^0S-30^0N)]
3	Wang and Fang Index **(WF index):** [U850(40^0 E -80^0E,5^0N-15^0N) - U850(60^0-90^0E,20^0-30^0N)]
4	Webster and Yang Index **(WY index):** [U850(40^0E-110^0E,0^0-20^0N) – U200(40^0-110^0E,0^0-20^0N)] [U850(40^0-110^0E,0^0-20^0N) – U200(40^0-110^0E,0^0-20^0N)]
5	Mean sea level pressure index **(MS index):** msl(65^0E-95^0E,15^0N-25^0N)
6	Specific humidity (850mb) index **(SH index):** Sph850(65^0E-95^0E,15^0N-25^0N)
7	Geopotential Height (500mb) index **(GP index):** Gph500(65^0E-95^0E,10^0N-20^0N)
8	**U-shear index**: [U850(100^0E-140^0E,15^0S-5^0N)-U200(100E-140E,15s-5N)]
9	**Omega** (vertical velocity at 500 mb) index: w500(50^0E-115^0E,0^0N-7.5^0N)-w500(80^0E-150^0E,10^0N-20^0N)
10	**Mean Sea level Pressure shear Index**: msl(110^0E-150^0E,10^0N-20^0N)-msl(40^0E-60^0E,15^0S-5^0N)

RF data used for verification

Model 2

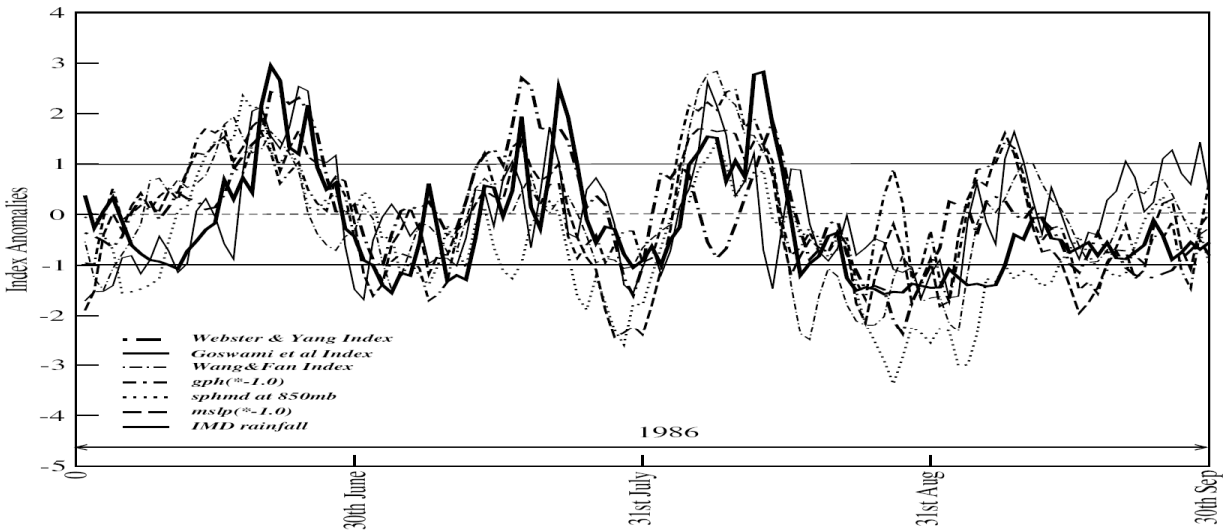

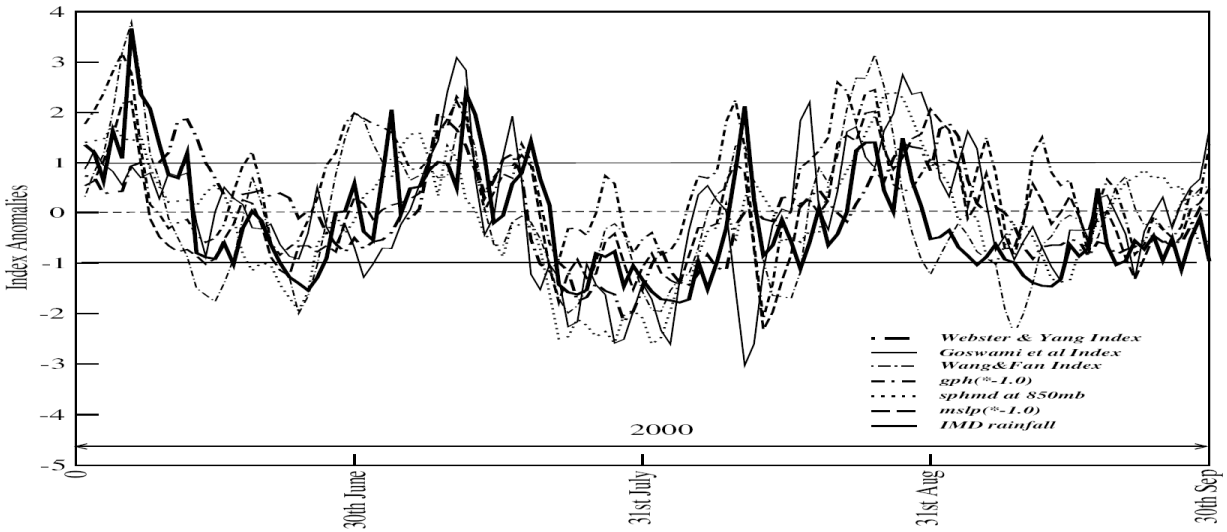

Normalized anomalies of six different indices during June-September of 1986 and 2000

We propose that the dominant monsoon ISO is nonlinear Convectively coupled oscillation

- Thus a unique relationship between a number of dynamical fields representing a nonlinear phase of the oscillation should be uniquely related a phase of the rainfall oscillation

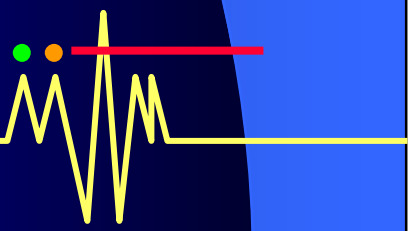

The SOM Algorithm

A non-linear classification scheme using the self-organizing map (SOM) which falls under the category of unsupervised learning neural network technique (i.e. learning without human intervention or any pre-condition)

(Kohenen, 1990; Hewitson and Crane 2002)

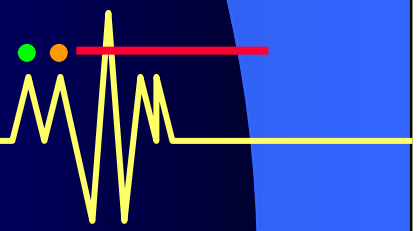

- The SOM consists of a (usually) one or two dimensional array of identical neurons. The input vector is broadcast in parallel to all these neurons.

- For each input vector, the most responsive neuron is located. The weights of this neuron and those within a neighborhood around it are adapted to reduce the distance between its weight vector and the current input vector.

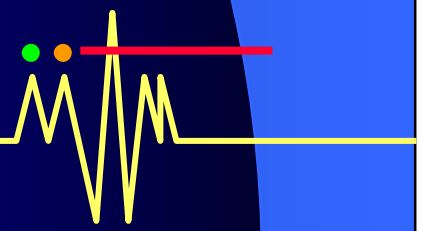

THE SOM NETWORK

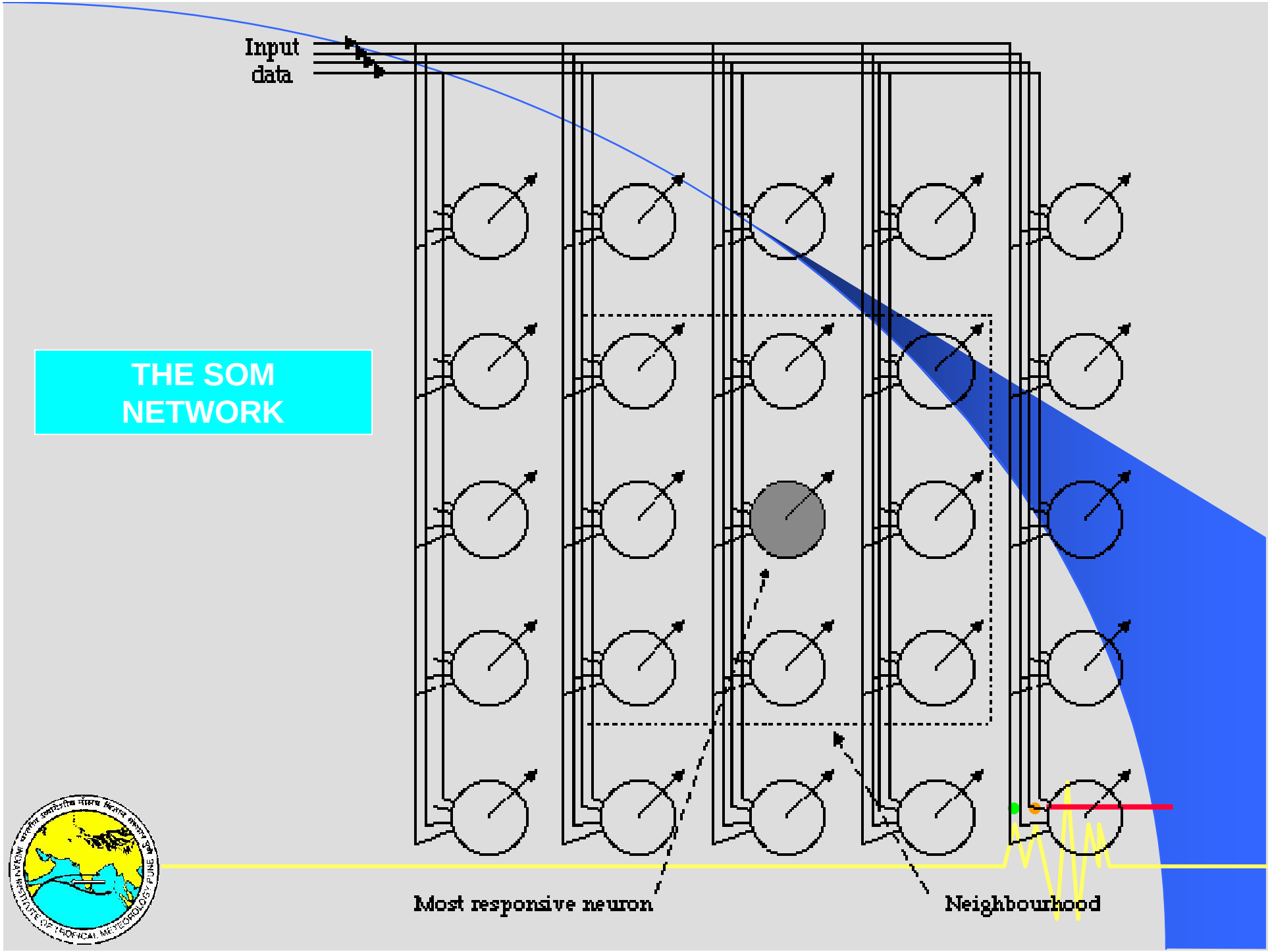

The SOM training for the nth iterative step is given by:

$$W_j(n+1) = W_j(n) + c(n)\{x(n) - W_j(n)\} \quad j \in R(n)$$
$$= 0 \quad \text{otherwise}$$

$W_j(n)$ is the weight vector for the jth node at the nth step of iteration.

$c(n)$ is the learning rate at the nth step.

$R(n)$ is the neighborhood for the nth step.

The inclusion of neighbor hood makes the learning rate non-linear.

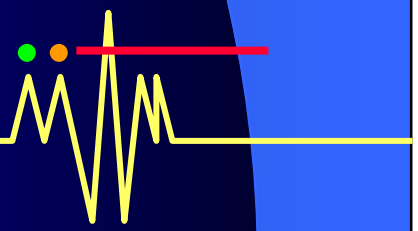

Some application of the SOM algorithm in the study of Indian summer monsoon.

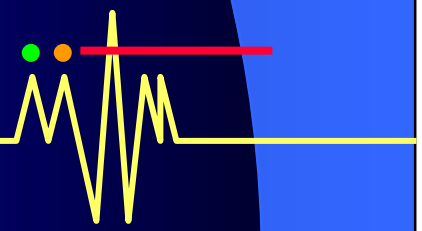

1. **Identification of active and break patterns of Indian summer monsoon using large scale dynamical parameters.**

A. Data Used: ERA-40 data from 1980-2001.NCEP data from 1951-2004. IMD daily gridded rainfall data from 1951-2004.

Parameters: U850,U200,V850,V200,MSLP,Sph850,Gph500 and Rainfall

The large scale indices are constructed based on this data and are used to classify the data using SOM. The data is classified as 3x3 clusters.

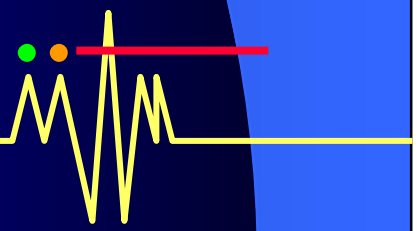

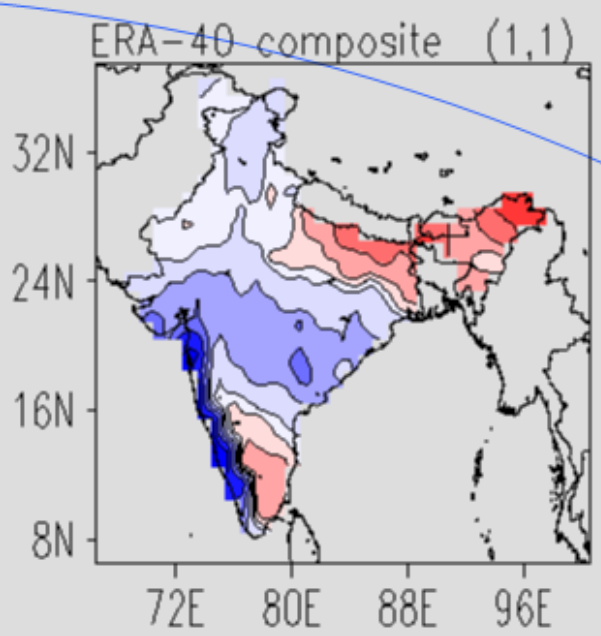

Active SOM

Break SOM

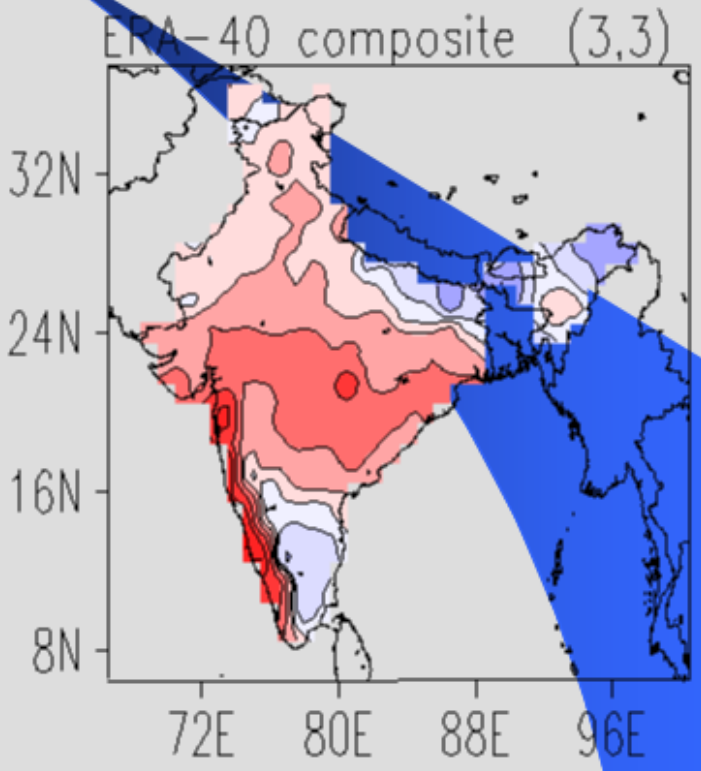

Area averaged rainfall anomaly over central India

(1,3)	(2,3)	(3,3)
-0.32	-1.38	-3.43
(1,2)	(2,2)	(3,2)
1.11	0.09	-1.73
(1,1)	(2,1)	(3,1)
4.14	1.96	-0.59

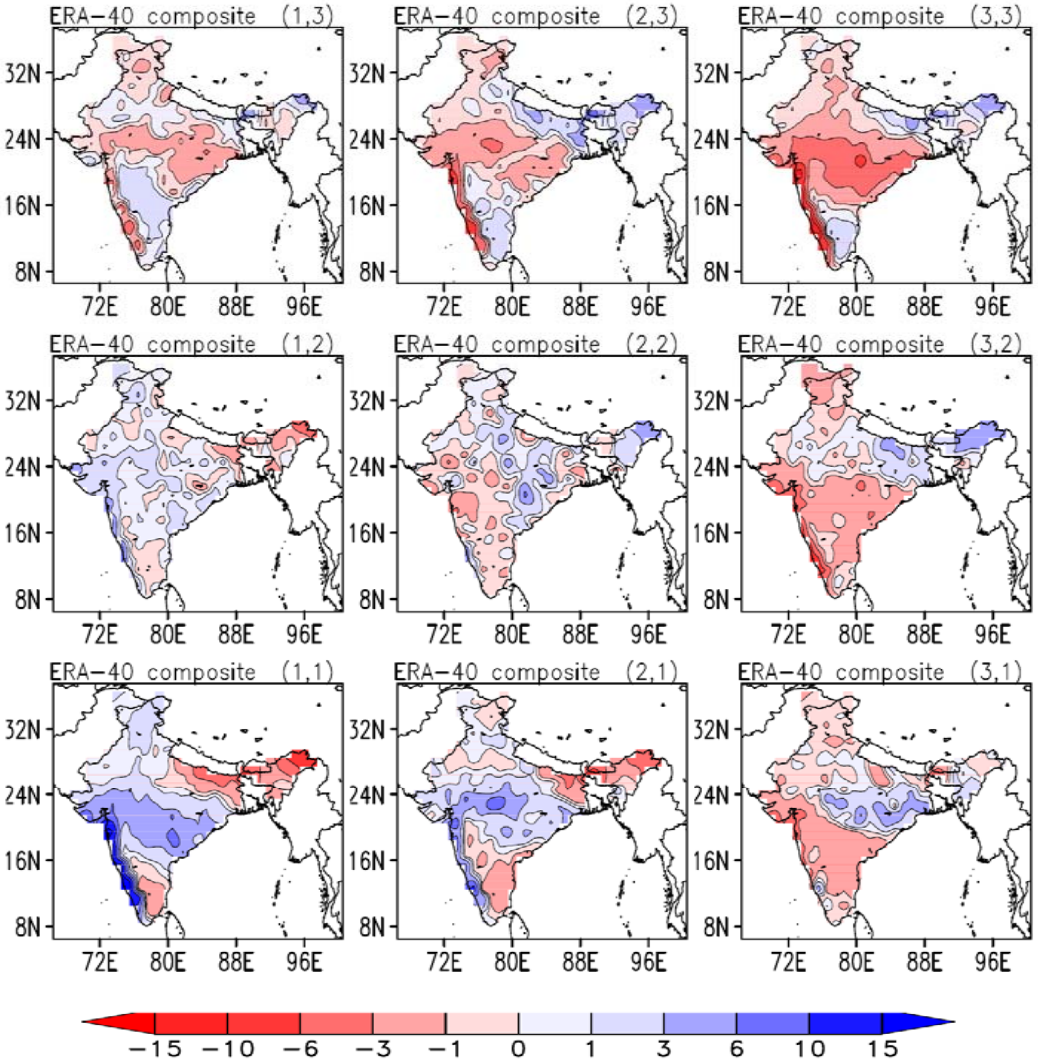

Figure 4: The spatial distribution of anomalous precipitation associated with SOM classified patterns .It is obtained by compositing the IMD daily rainfall anomaly corresponding to the days clustered at the respective SOM nodes. The states (1, 1) and (3, 3) are the most active and break nodes. (units $mm\ day^{-1}$)

The 3x3 SOM clustering.

Plotted here are the composite spatial plot of rainfall anomaly for the dates clustered at each SOM nodes

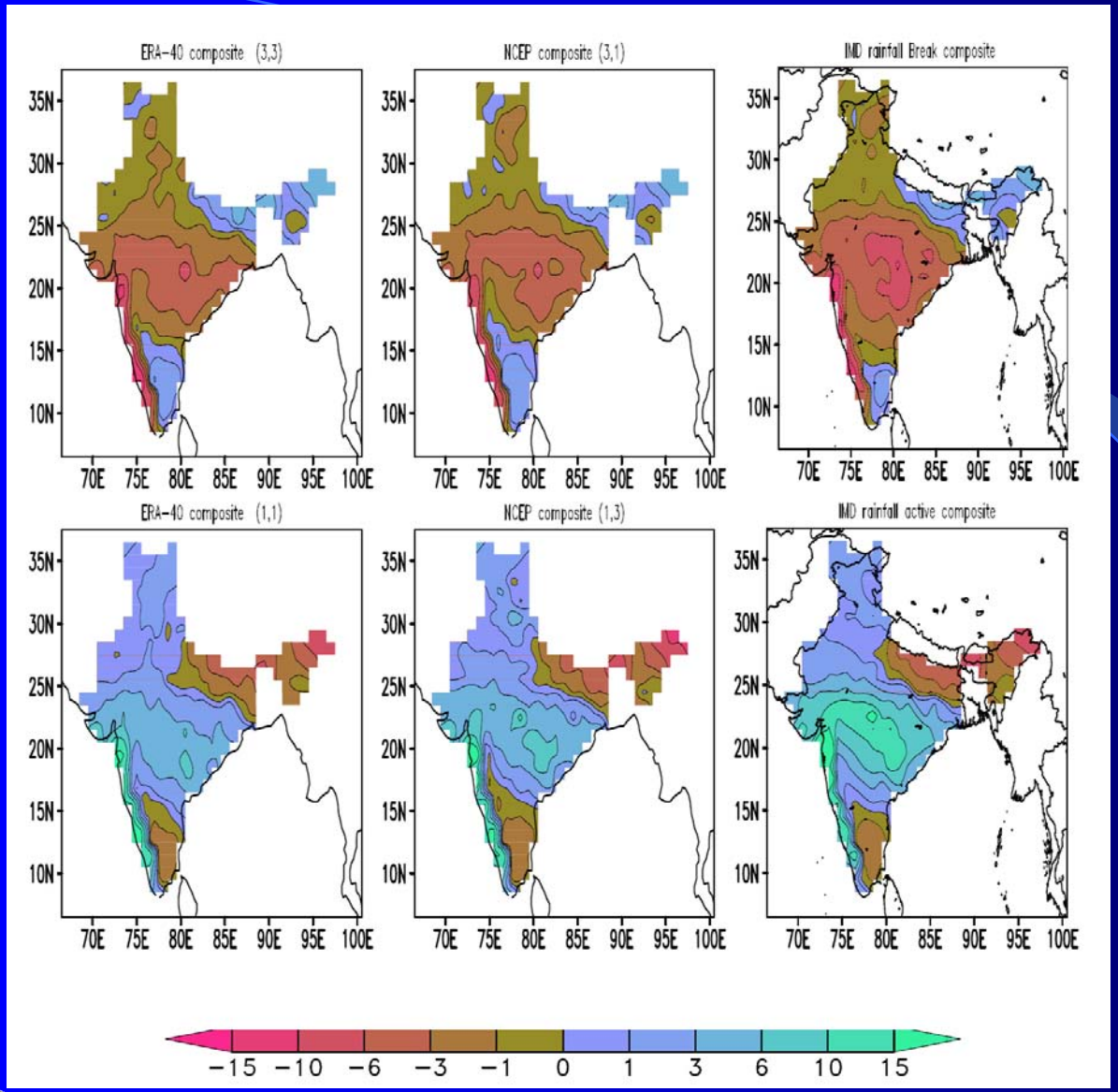

Break (top) and active (bottom) composites through SOM clustering using large scale circulation data from ERA-40 (left), NCEP (middle) and from IMD precip data (right).

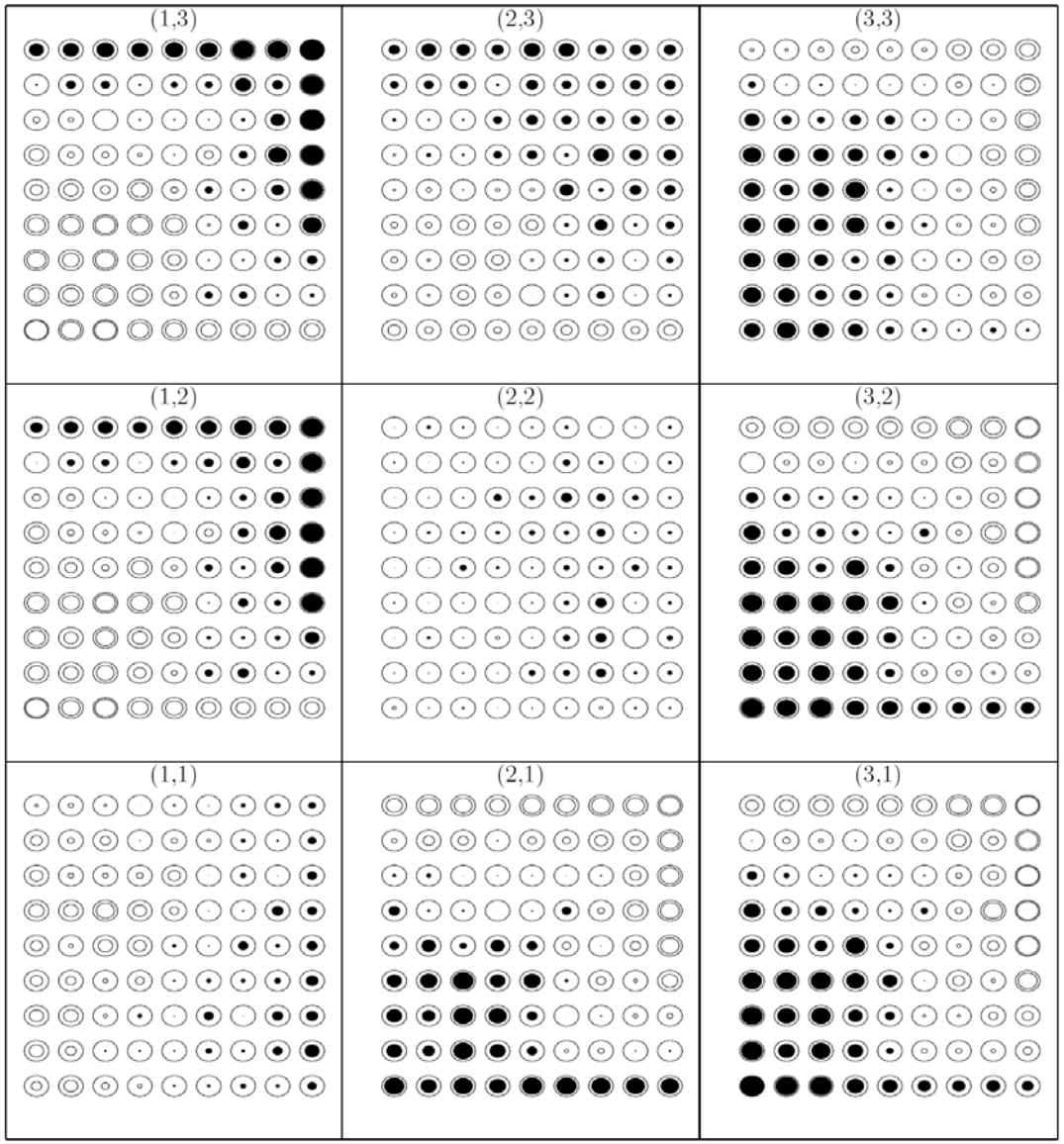

Pattern correlation between each of 3X3 (9) SOM patterns of precipitation and those of 81 patterns associated with 9X9 SOM classification

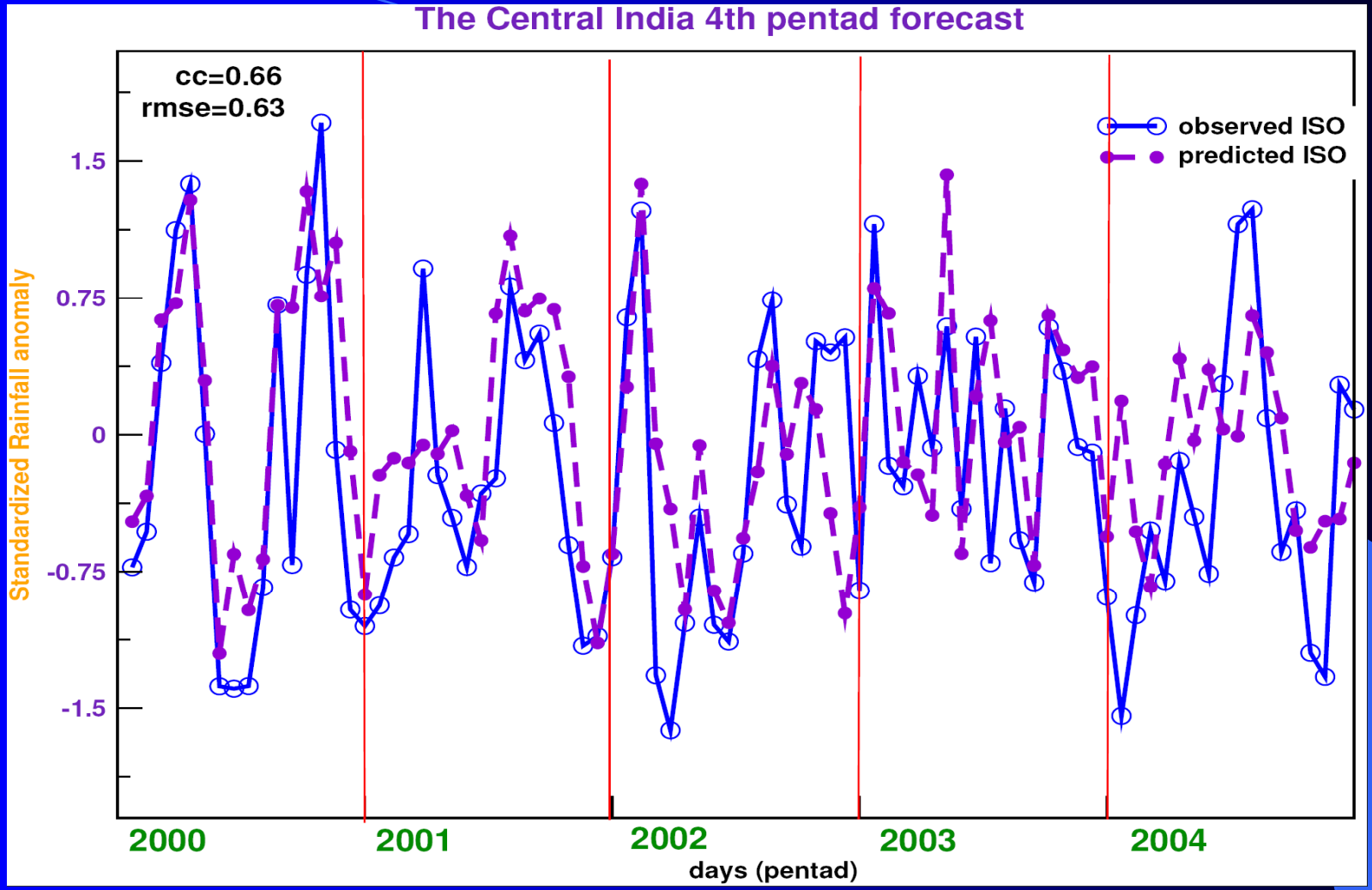
The Central India 4th pentad forecast
cc=0.66
rmse=0.63
observed ISO
predicted ISO
Standardized Rainfall anomaly
1.5
0.75
0
-0.75
-1.5
2000
2001
2002
2003
2004
days (pentad)

CONCLUSION

- Summer monsoon ISOs have large amplitude, as large as the annual cycle and much larger than IAV of seasonal mean.
- On one hand they cluster synoptic activity while on the other they produce internal IAV of seasonal mean. Thus, monsoon ISOs are the building block for monsoon climate
- Quantitative estimate of potential predictability of the summer monsoon ISOs indicate useful prediction of breaks should be possible 20-25 days in advance.
- Summer monsoon ISOs are nonlinear convective coupled oscillations. Large scale circulation may be sufficient to predict Rainfall ISO.
- 'Analogue models' have emerged as useful real time forecasting tool for Extended range prediction (3-4 weeks in advance) of 'active' and 'break' spells

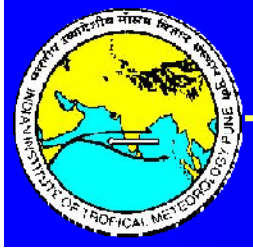

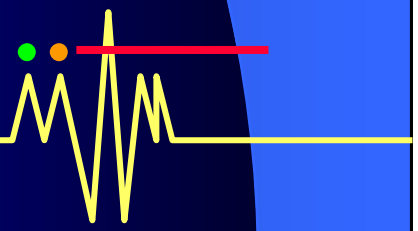

Thank you

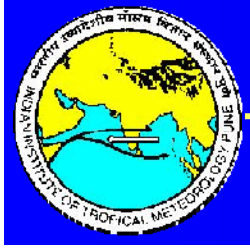

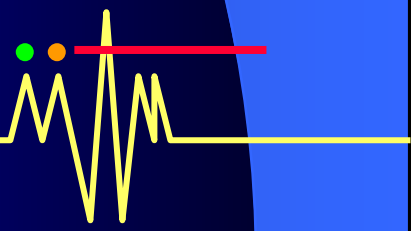

Possible Reasons for Poor Skill of prediction of seasonal mean monsoon precipitation by GCMs.

Model Systematic Bias : All GCMs have significant systematic bias in simulating the climatological seasonal mean Asian monsoon

Simulation of tropical teleconnection : The small predictable signal comes from teleconnections associated with global SST (soil moisture etc) variations. Most models have difficulty in simulating the teleconnection patterns associated with ENSO SST over the Asian monsoon region correctly.

Local Warm Ocean –Atmosphere interactions. Over the Asian monsoon region local air-sea interactions contribute significantly to IAV of the monsoon precipitation. A coupled Ocean-atmosphere model required.

Intrinsic limit on predictability : The predictable signal ('external' var.) is small and unpredictable noise ('internal' var.) is large over the Asian monsoon region.

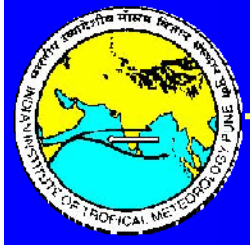

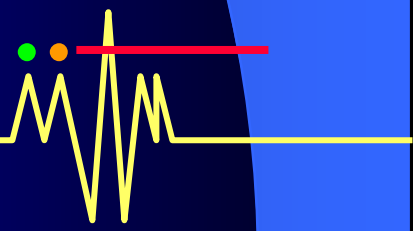

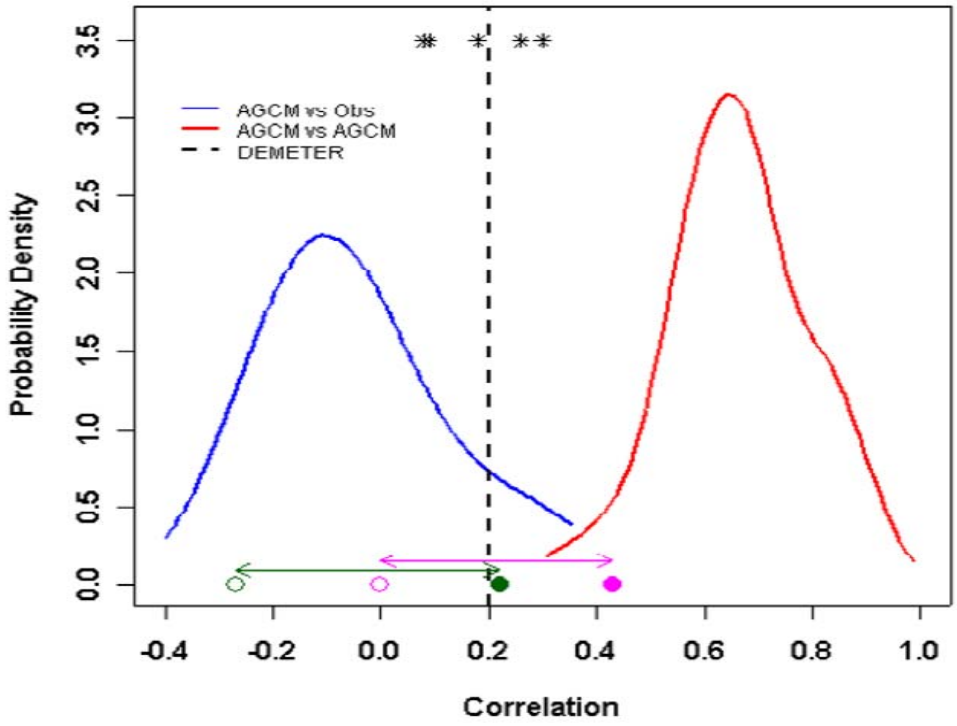

Figure 1. PDFs of correlation skill of June–September Indian monsoon rainfall based on a theoretical 'perfect model' analysis (red curve), and based on the actual skill compared to observed all Indian monsoon rain (blue curve). Analysis is based on 10 AGCMs forced with observed global SSTs of 1950–1999. Closed coloured circles denote the skill of two of the AGCM coupled to a mixed layer model. Arrows denote the change in skill between pairs of uncoupled and coupled GCM simulations. Stars indicate the spread of Indian monsoon rainfall correlation skill of the 7 coupled model hindcasts from DEMETER and the black dashed line is their median skill.

Krishnakumar et al.
2005, GRL

‘Internal’ IAV limits monsoon predictability!

What is responsible for the ‘Internal’ IAV of SAM?

Hypothesis:

Interaction between monsoon ISOs and the slow AC is primarily responsible for the ‘internal’ low frequency variability.

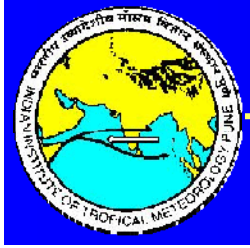

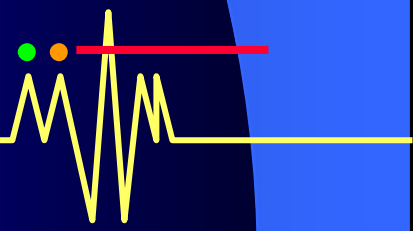

A common mode : Intraseasonal & interannual variability

Structure of dominant ISO mode

Active-Break composite of precipitation from NCEP

From 10-90 day filtered precip. Between 1 June-30 Sept., 1949-2002

Structure of dominant ISV mode

Strong-weak monsoon composite of precipitation from NCEP

From JJAS precip. Between 1949 and 2002, 6 strong and 4 weak monsoon years.

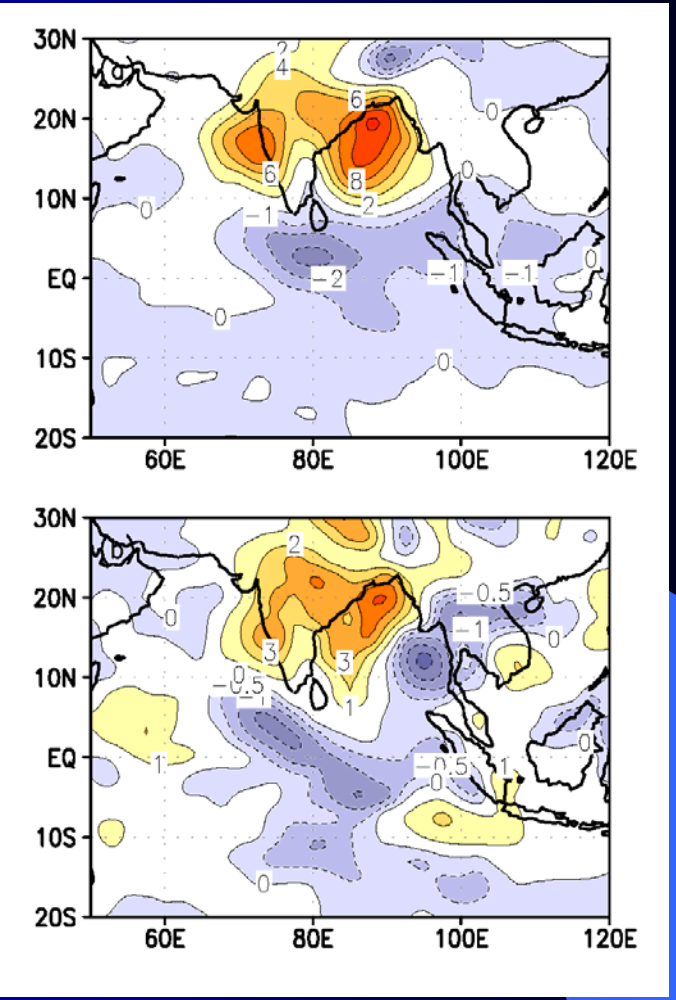

Frequency distribution of ISO anom of P over 70E-90E, 10N-30N

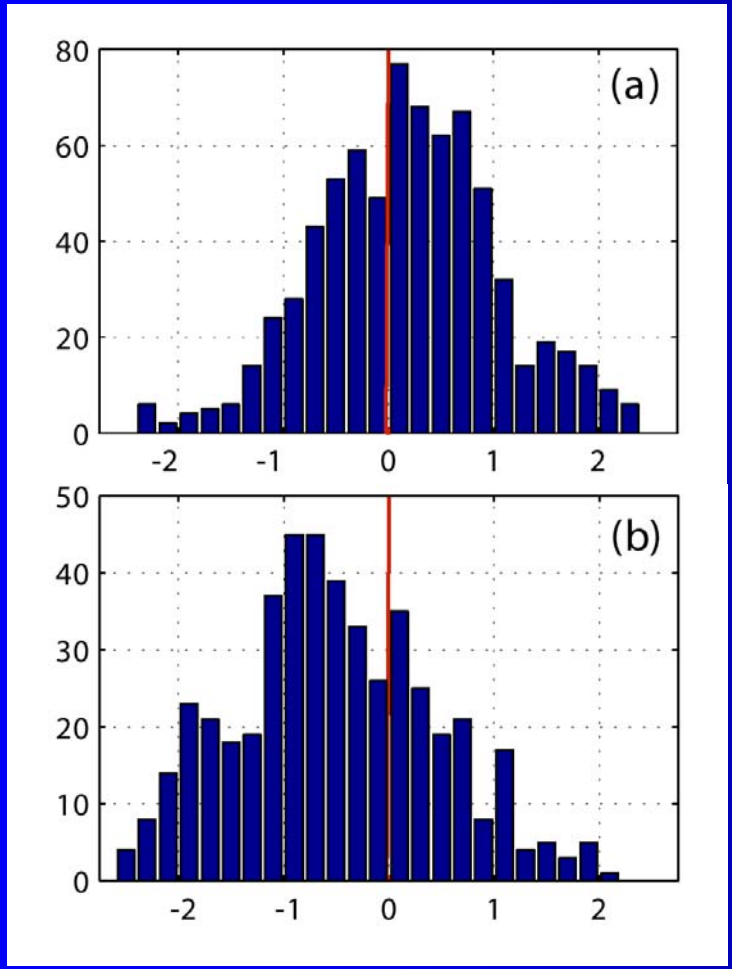

For 6 ‘strong’ Indian monsoon years

For 4 ‘weak’ Indian monsoon years

(from NCEP Reanalysis)

A Hypothesis: Interaction between vigorous ISO's and the Annual Cycle gives rise to 'internal' interannual variability

A Paradigm model for Atmospheric Fluctuations under an Annually varying forcing

$$\dot{X} = -Y^2 - Z^2 - aX + F$$

$$\dot{Y} = XY - bXZ - cY + G$$ ← Solar forcing

$$\dot{Z} = bXY + XZ - cZ$$ ← Land-ocean contrast

$$\dot{F} = F_0 + F_1\cos(\pi t/\tau),$$

X-> Zonal mean , Y,Z-> wave component,a,c-> dissipation

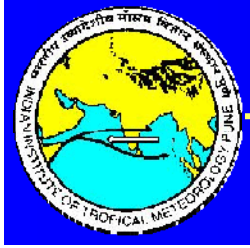

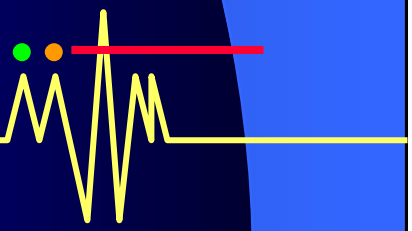

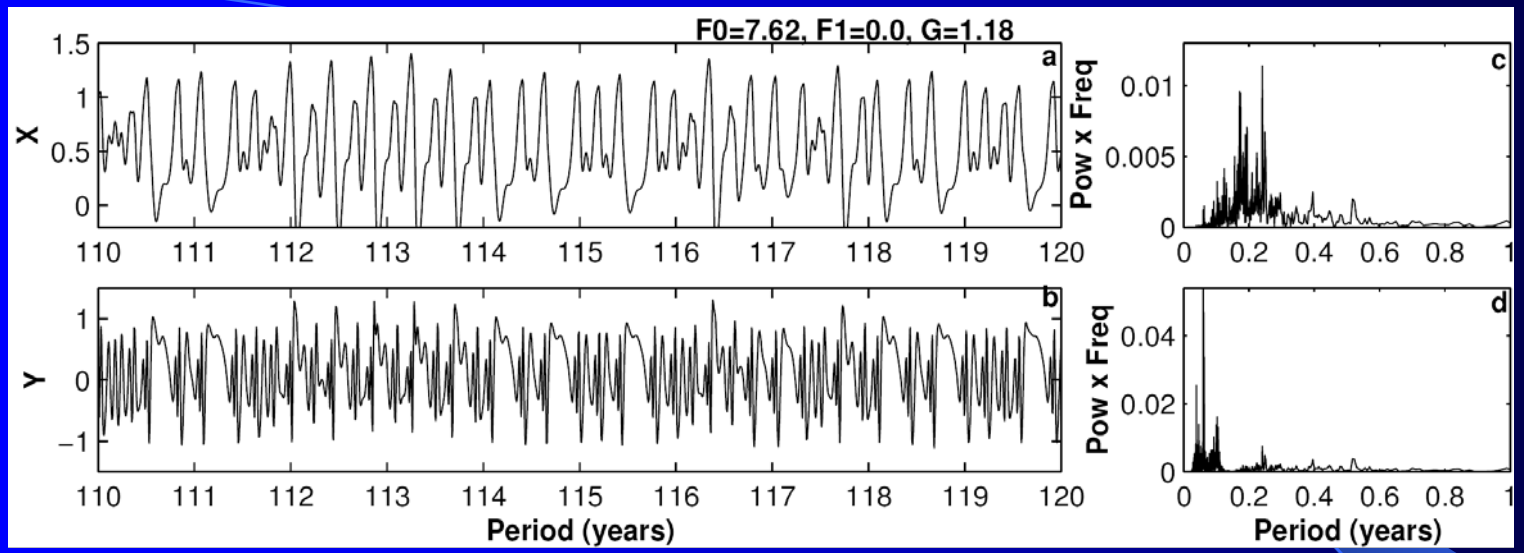

F=const.

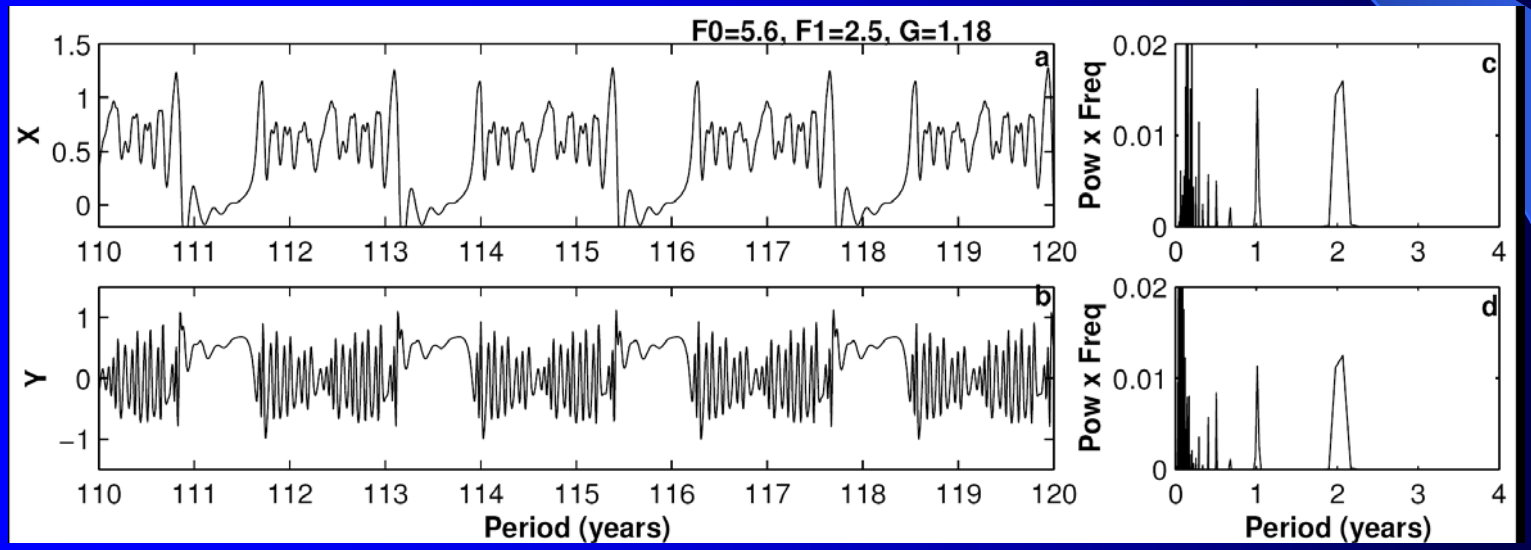

F=ann.cyl

How Does The Tropical Atmosphere Generate nearly Two year oscillation without external Forcing?

Multi year experiments with a state of the Art Mathematical model of the Atmosphere carried out

ANNUAL CYCLE FORCING

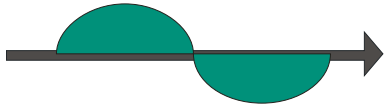

MODULATES

INTERASEASONAL MONSOON OSCILLATIONS 30-50 DAYS

CHAOTIC FOR SOME RANGE OF ANNUAL CYCLE FORCING

TWO STATES WITHIN THE CHAOTIC REGIME

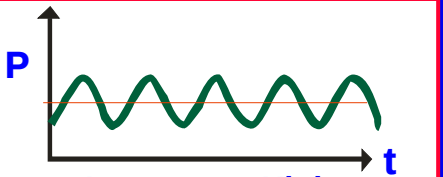

Low mean- High Amplitude State

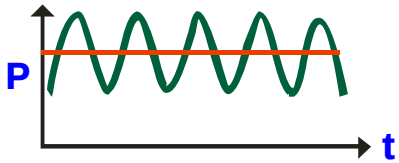

High mean- Low Amplitude State

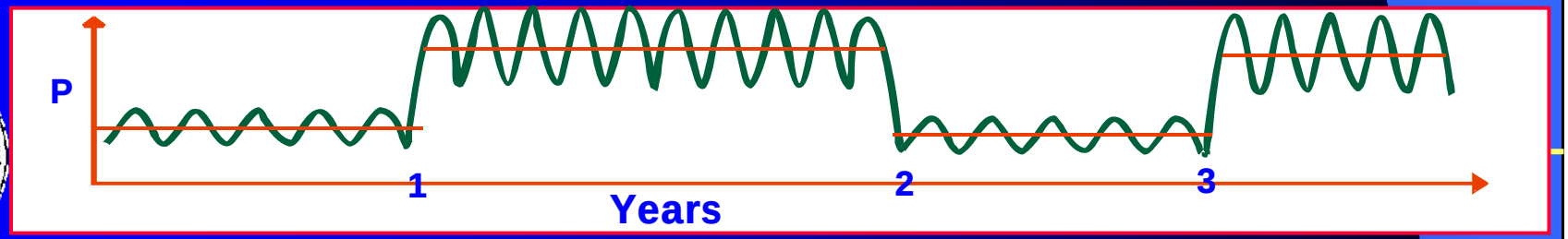

Where do we stand?

- **Most efforts so far has been to predict the seasonal mean**

  No skill so far

  Even with a 'perfect' model , less than 50 % of IAV predictable

  Limited scope

- **An alternative strategy for monsoon prediction is required.**

Extended Range Prediction of Active and Break spells

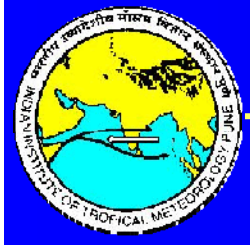

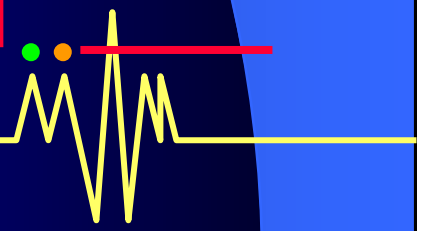

C.

Same as of earlier plot but for CMAP data. Movement of the rainfall Band may be noted

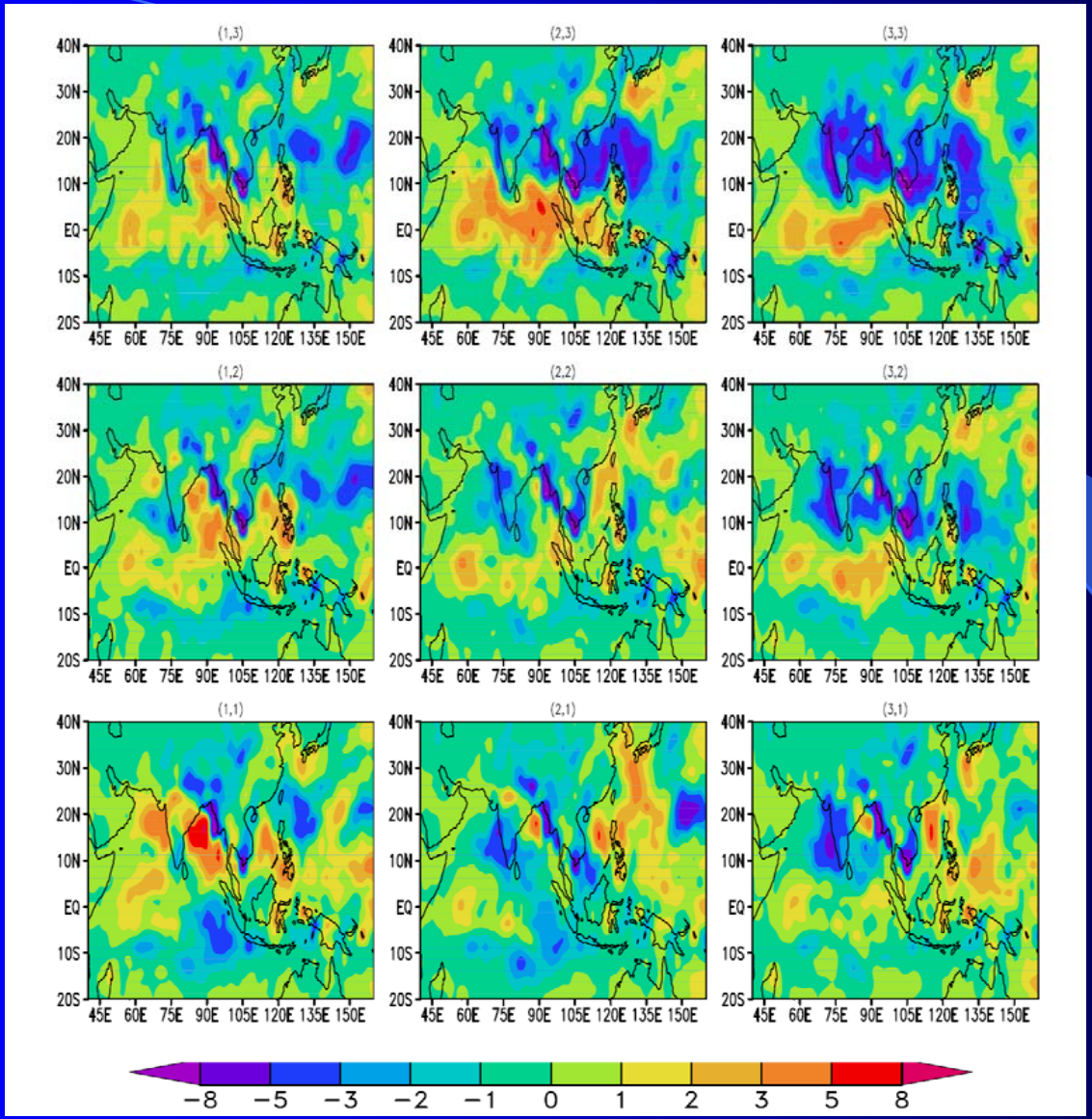

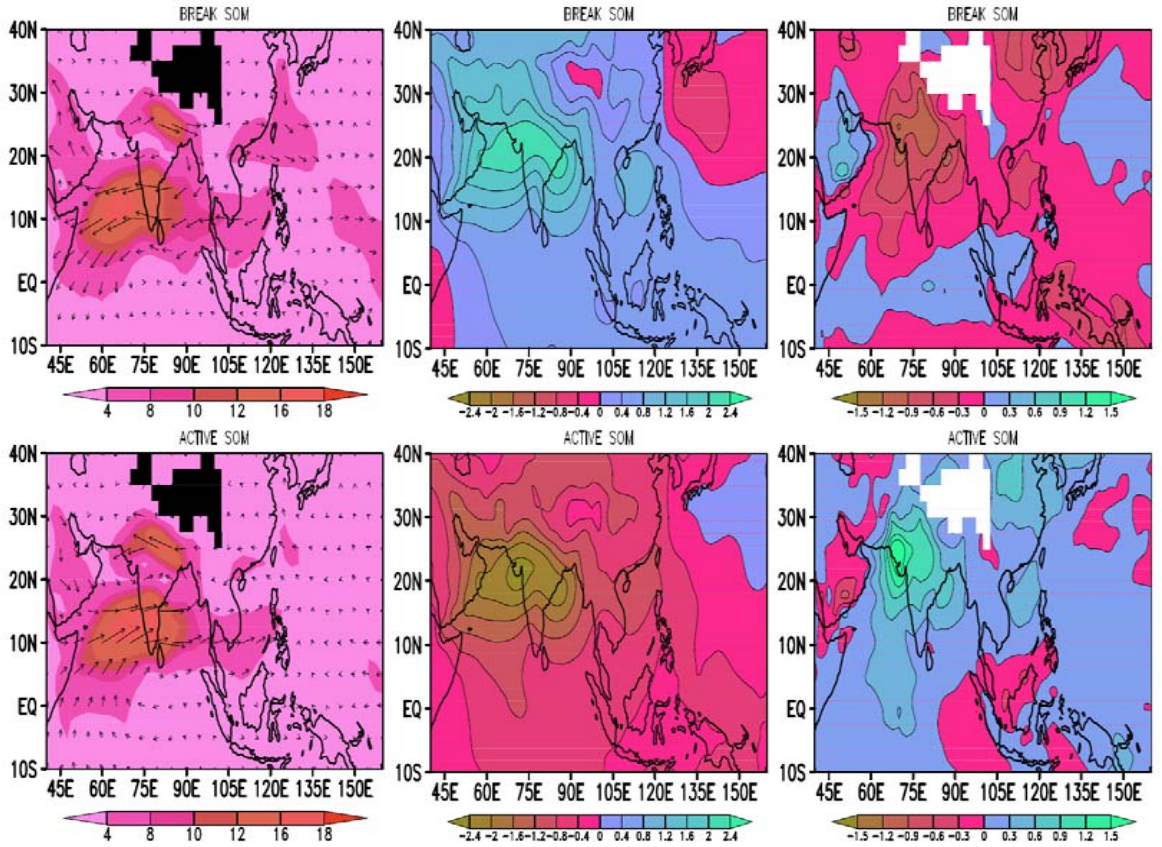

Figure 6: The figure shows the composite plot from ERA-40 data for the break(top panels) and active nodes(bottom panels)for wind 850(left), mean sea level pressure (middle) and speceific humidity at 850mb(right). The composite technique is similar to last figure. The figure shows the composite spatial structure of these parameters during the active or break states. The patterns of rainfall in the earlier figure is well reflected in these parameters

Mean days per ISO event (**Bold**) ,percentage frequency of days (parenthesis) and probability of no transition (curly braces) at each node over central India.

(1,3) **3***(10%)***{**68**}**	(2,3) **3***(9%)*{63}	(3,3) **9***(22%)*{88}
(1,2) **2***(8%)*{57}	(2,2) **2***(5%)*{47}	(3,2) **2***(8%)*{59}
(1,1) **8***(20%)*{87}	(2,1) **3***(8%)*{63}	(3,1) **4***(10%)*{74}

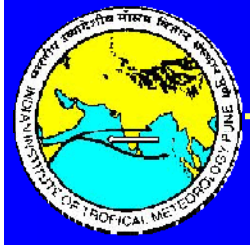

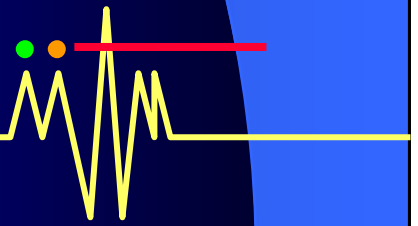

The three values are calculated from the 22 years of ERA-40 data. Here number of “events” is determined by counting the total number of times the data records are mapped consecutively to a particular node without any break.

Mean days per event is defined by dividing the total number of days mapped onto a SOM node by the number of events counted for that node.

Frequency of days is defined as the number of days clustered in a particular node divided by the total number of days used in the classification (22 years *122 days/year).

The probability of “no transition” (also expressed in percentage) is the probability that when an input vector corresponding to a particular day is mapped to a node, the next day will be mapped again to the same node.

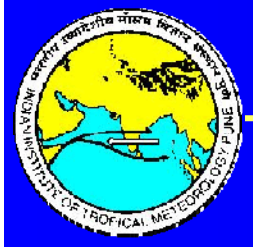

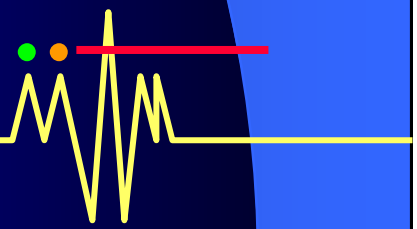

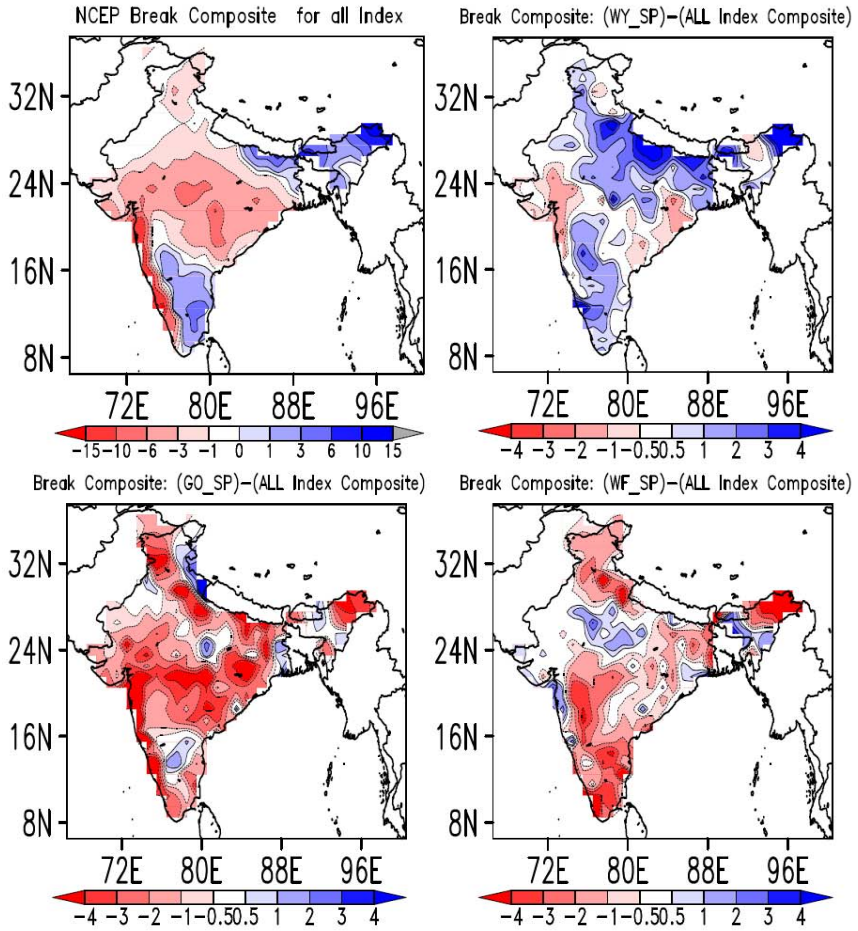

Figure 8: Three different shades (spatial structure) of the break patterns due to the involvement of different circulation indices. The top left panel is the composite break pattern obtained by using the objective criteria defined in Table-1. The other 3 patterns are obtained by subtracting this ensemble mean break composite from the break composite obtained from the days when any two of the indices (shown at the top of the figure) satisfy the specified criteria (see text). (units:$mm\ day^{-1}$)

Two different spatial break pattern.

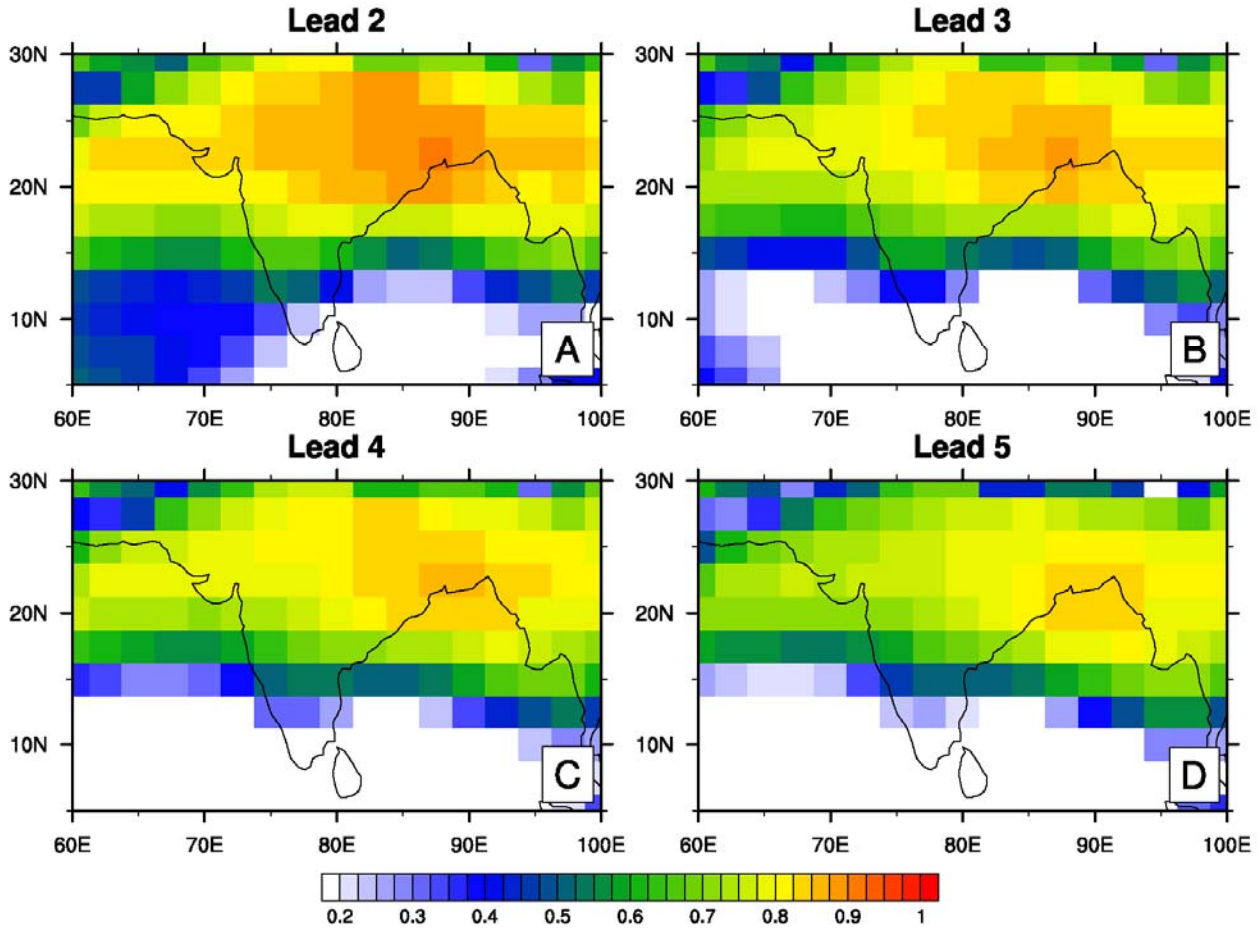

FIGURE 7.9: Temporal correlations between observations and predictions at different lead times during the May-October period.

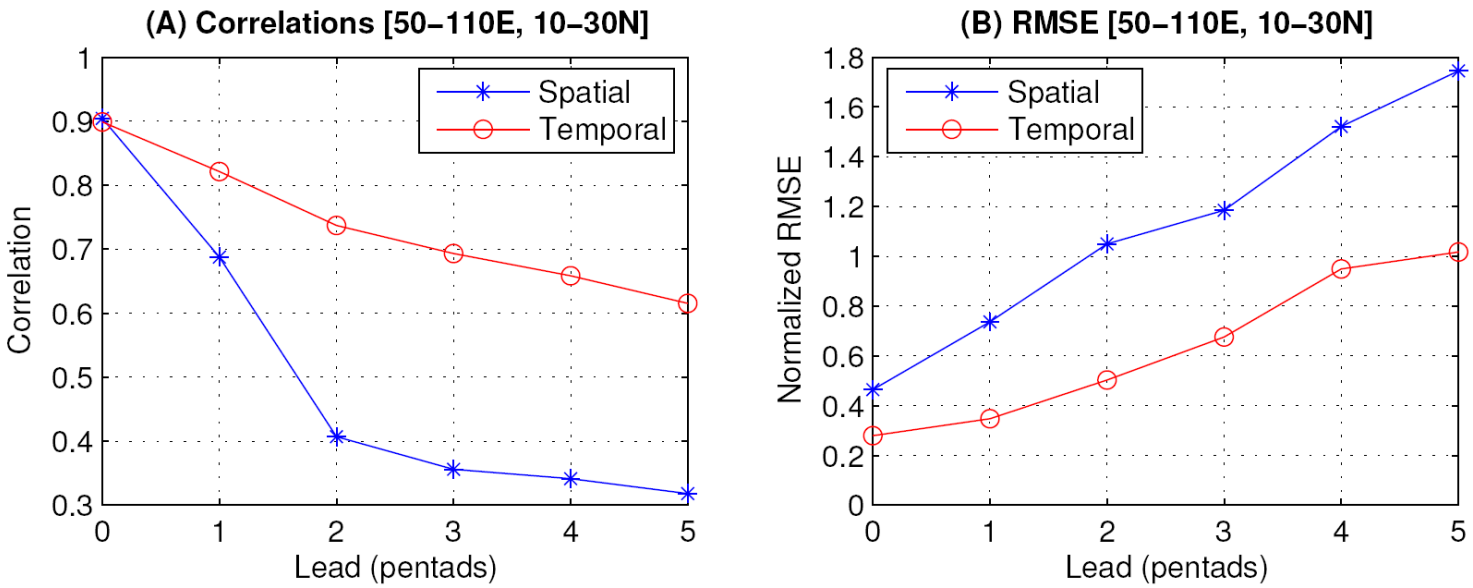

FIGURE 6.10: (A) Spatial and temporal correlations between predictions and observations for JJAS period at different lead times over the region 50°-110°E, 10°-30°N. (B) shows the Spatial and temporal RMSE for the same region. Correlations and RMSE shown are from AH.